Functional Analysis of Cereblon, an Evolutionary Conserved Substrate Receptor of the Cullin4-RING E3 Ubiquitin Ligase, in Mammalian Cells and in *Drosophila melanogaster*

ヒト Cereblon タンパク質と そのキイロショウジョウバエ相同体の機能解析

February 2017

Satoru WAKABAYASHI

若林　慧

Functional Analysis of Cereblon, an Evolutionary Conserved Substrate Receptor of the Cullin4-RING E3 Ubiquitin Ligase, in Mammalian Cells and in *Drosophila melanogaster*

ヒト Cereblon タンパク質と そのキイロショウジョウバエ相同体の機能解析

February 2017

Waseda University

Graduate School of Advanced Science and Engineering

Department of Advanced Science and Engineering

Research on Life Science and Medical Biosciences

Satoru WAKABAYASHI

若林　慧

Table of contents

Chapter 1. Introduction

Cereblon (*CRBN*) is a gene conserved across the animal and plant kingdoms. The *CRBN* family genes encode proteins that contain two conserved domains called the ATP-dependent Lon protease-like domain and the thalidomide-binding domain[1,2] (also known as Cereblon domain of Unknown activity, binding cellular Ligands and Thalidomide (CULT)[3]). CRBN family proteins have been implicated in organismal development[4], metabolism[5,6] and immune system[7,8], and its altered functions are linked to defects in neuronal development[9] and cancer cells survival[8,10,11]. In this chapter, previous studies reporting functions of CRBN family members are summarized.

1.1. Human *Cereblon* gene was identified as a candidate gene for onset of an intellectual disability

Human *CRBN* gene is located on chromosome 3, mapping to 3,148,490-3,179,717 reverse strand. *CRBN* was originally identified as a gene associated with onset of an intellectual disability (ID), a neurodevelopmental disorder characterized by restricted learning capability and adaptive behavior[9]. A homozygous nonsense mutation within the coding region of *CRBN* gene was found from a large kindred in the U.S. associated with a mild type of non-syndromic ID, characterized by IQ scores ranging from 50 to 70 without physical and neuronal anomalies or psychiatric disorders[9]. The mutation forms a putative premature stop codon that leads to either expression of a truncated product (418 amino acid long-protein instead of 442 amino acid long-wild type protein) or transcript degradation by the nonsense-mediated decay, or both.

Another study implicating a link between *CRBN* and ID onset was recently reported[12]. The study reported that three independent ID patients associated with behavior anomalies shared a common duplicated region of 3p26.3-3p26.2, which contains the complete open reading frame of *CRBN*[12]. These clinical genetic studies provide evidence that *CRBN* may play a critical role in learning and memory formation.

1.2. The gene's product CRBN contains two evolutionary conserved domains

Two transcripts of *CRBN* gene have been annotated: one encodes a protein that contains 442 amino acid residues (isoform 1) and the other encodes a protein that does not contain an alanine residue at position 23 of the isoform 1 (isoform 2). Since the isoform 1 has been chosen as the canonical protein, it will be referred as the human CRBN protein in the rest of the thesis.

CRBN protein contains two evolutionary conserved domains: a central ATP-dependent Lon protease-like domain (LON domain; spanning residues 76 to 318 of the human protein) and a C-terminal thalidomide-binding domain (Thal-BD; spanning residues 319 to 428)[2] (Figure1.1A).

The LON domain contains three subregions: two regions whose structures resemble to a bacterial LON N-terminal domain and a non-canonical DNA damage-binding protein 1 (DDB1)-binding motif (spanning residues 188 to 248)[1,2] flanked by the regions (Figure 1.1A). The DDB1-binding motif forms α-helices that are inserted into the cleft formed by the β-propeller A (BPA) and the β-propeller C (BPC) domains of DDB1[1,2], competing with other

interacting proteins such as DDB2[4] (Figure 1.1B). DDB1-mediated functions of CRBN will be discussed later in this chapter.

The Thal-BD is composed of 6 antiparallel β-sheets that are positioned away from the DDB1 interaction interface[1,2] (Figure 1.1B). The domain is responsible for mediating interaction with other proteins[6,8,10,11]. A unique feature of this domain is a hydrophobic pocket (formed by W380, W386, W400, F402) that can be occupied by a class of small molecules[1,2]. The presence of the molecules can alter protein interactions, leading to pleiotropic biological responses. Details of this feature will also be discussed later in the chapter.

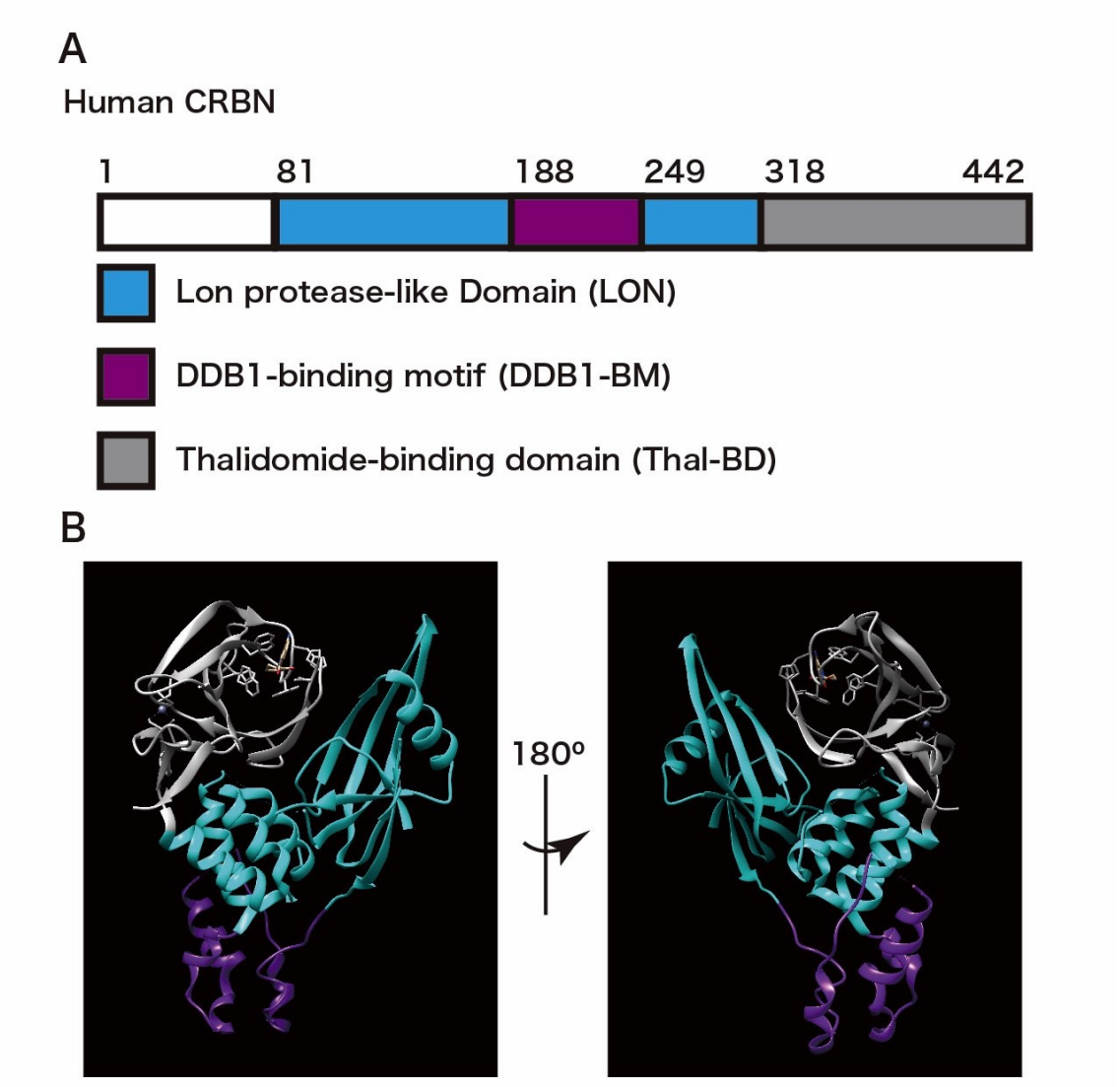

Figure 1.1. Human CRBN protein. (A) A scheme representing the domain structure of the human CRBN. The N-terminal region, the LON domain, the DDB1-binding motif and the Thal-BD are shown in white, cyan, purple and gray, respectively. (B) The structure of the human CRBN is shown in ribbon diagram. The regions are shown in respective colors corresponding to the scheme. Selected amino acid side chains involved in forming a hydrophobic pocket (N351, P352, H378, W380, W386, W400 and F402) are shown as stick models. The crystal structure was determined by Chamberlain and colleagues (PDB ID: 4TZ4)[2].

1.3. CRBN is a substrate receptor of the Cullin4-RING E3 ubiquitin ligase complex

In 2010, CRBN was identified as the substrate receptor of the Cullin4-RING E3 ubiquitin ligase complex[4]. Functions of the CRBN-containing complex have been described in various biological contexts[4,6,8,10,13].

1.3.1. The ubiquitin system

The ubiquitin system is a major post-translational system conserved in eukaryotes[14]. Ubiquitination, a series of biochemical reactions that covalently attaches a ubiquitin molecule to a substrate protein, is performed in combination of 3 enzymes: ubiquitin-activating enzyme (E1), ubiquitin-conjugating enzyme (E2) and ubiquitin ligase (E3). The Figure 1.2 shows a scheme of the reactions. First, the C-terminal glycine residue of a ubiquitin molecule is covalently attached to a cysteine residue of the E1 in a thiolester linkage in ATP-dependent manner. Second, activated ubiquitin molecule is transferred to a cysteine residue of the E2. Finally, E2-E3 complex facilitates an isopeptide bond formation between C-terminus of the ubiquitin molecule and a lysine's ε-amino group of a substrate. Assembly of multiple ubiquitin molecules (polyubiquitin chain) linked via their lysine 48 functions as a signal for recognition and degradation by the 26S proteasome[15]. However, non-proteolytic functions of polyubiquitin chains via different lysines and monoubiquitination have also been identified in past years[16].

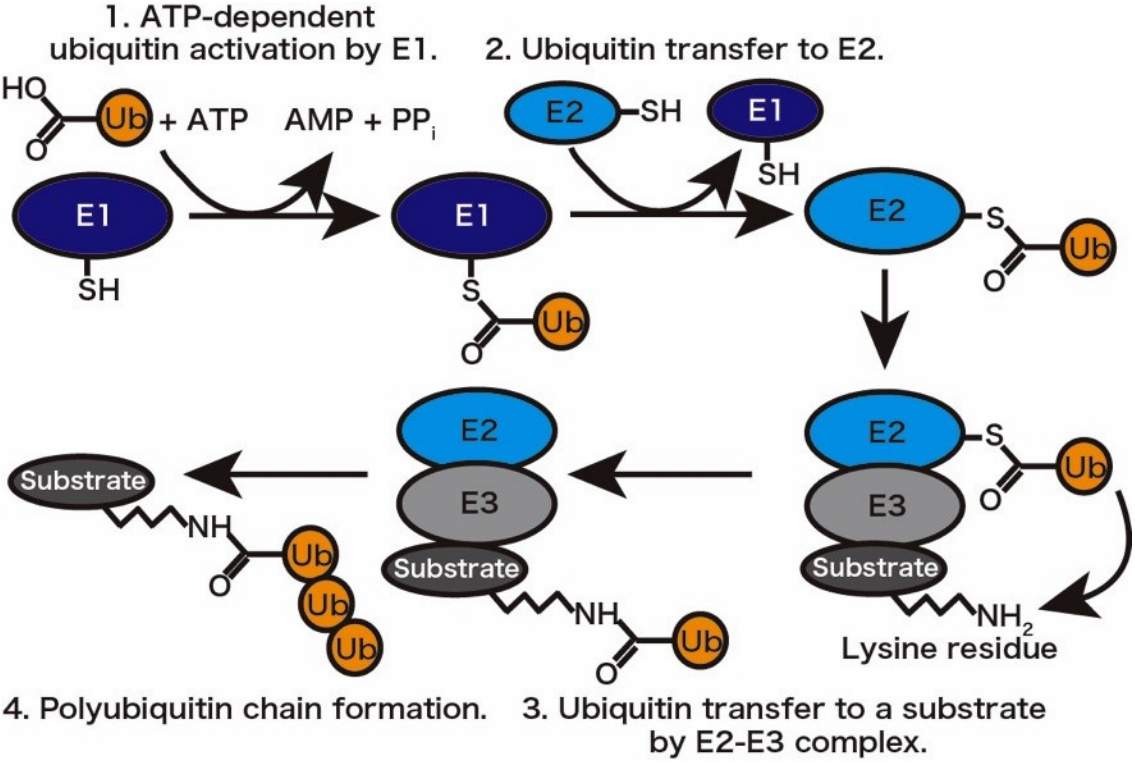

Figure 1.2. The ubiquitin system. The scheme represents four sequential reactions in general ubiquitination. This figure is modified from a figure in the following URL: http://docs.abcam.com/pdf/proteins/Ubiquitylation-system.pdf

1.3.2. The Cullin4-RING E3 ubiquitin ligases

Multi-subunit Cullin-RING E3 ubiquitin ligase complex family is the largest E3 ubiquitin ligase family present in eukaryotes[17]. Members of the Cullin family interact with a small protein with the RING finger domain (RBX1/2) via a highly conserved region called "cullin homology domain" to form a catalytic core[17]. Seven genes encoding the cullin family members have been identified in the mammalian genomes (*CUL1, 2, 3, 4A, 4B, 5, 7*)[18]. The Cullins have been described in numerous biological contexts, including cell cycle, embryogenesis and development[18].

Like other Cullins, Cullin 4 is widely conserved from yeast to human[19]. Single genes encoding Cullin 4 family proteins are found in *S. pombe*, *C. elegans* and *Drosophila*, two closely related paralogs called *Cullin 4A* and *Cullin 4B* are present in vertebrates[19]. Products of the two genes are 83% identical, but Cullin 4B contains an additional 149 amino acids-long N-terminal region with a nuclear localization signal[20]. The *cul4A* and *cul4B* mice show distinct phenotypes[21,22], suggesting that their functions *in vivo* are not entirely redundant.

The Cullin 4A/B proteins is a scaffold protein that assembles RBX1 and DDB1 to form the core catalytic complex[23] (Figure 1.3). Known substrate receptors (called DDB1 and Cullin4-associated factors; DCAFs) of the complex, including CRBN (Figure 1.4), interacts with the complex via the BPA and BPC domains of DDB1[4,24].

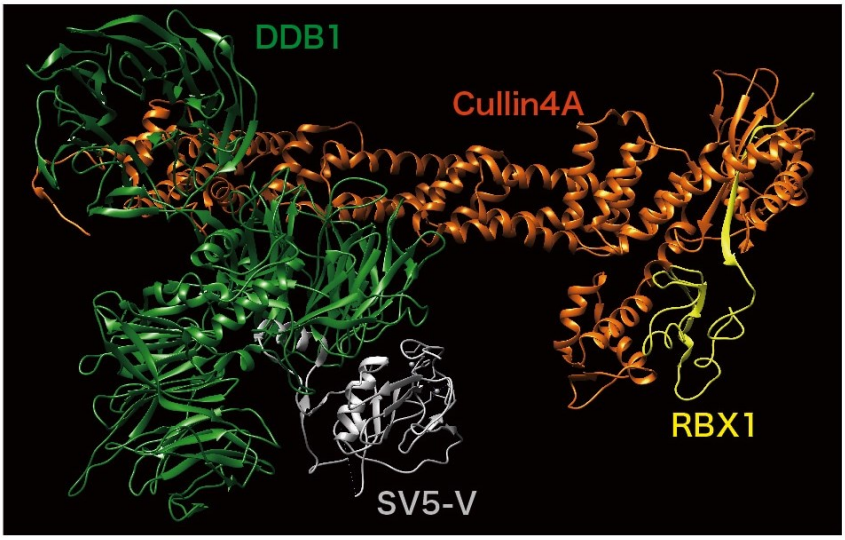

Figure 1.3. The Cullin4-RING E3 ubiquitin ligase complex. The structure of the human Cullin4A-RING E3 ubiquitin ligase complex is shown in ribbon diagram. RBX1, Cullin4A, DDB1 and the V protein of simian virus 5 (SV5-V) are shown in yellow, orange, green and gray, respectively. The crystal structure was determined by Angers and colleagues (PDB ID: 2HYE)[23].

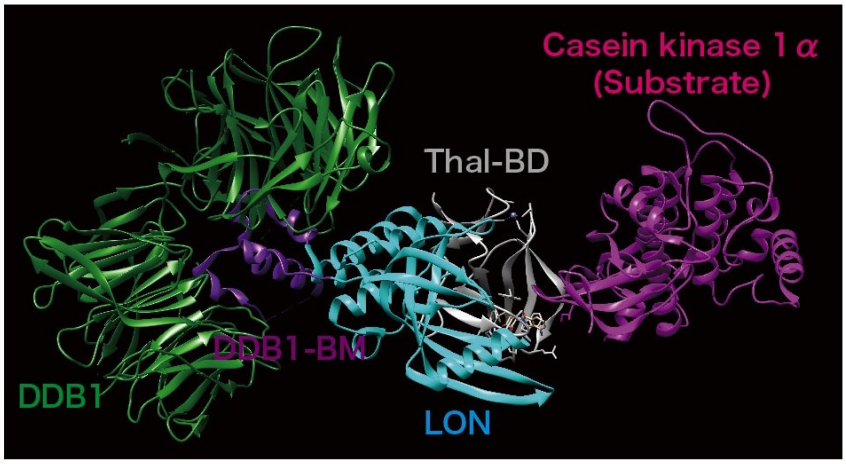

Figure 1.4. CRBN interacts with DDB1 to function as a substrate receptor of the CRL4. The structure of the human DDB1-CRBN-lenalidomide-Casein kinase1α is shown in ribbon diagram. DDB1, DDB1-BM, LON, Thal-BD and Casein kinase 1α is shown in green, purple, cyan, gray and magenta, respectively. The crystal structure was determined by Petzold and colleagues (PDB ID: 5FQD)[25].

1.3.3. Endogenous substrates of the CRBN-containing Cullin4-RING E3 ubiquitin ligase

Four endogenous substrates of the CRBN-containing Cullin4-RING E3 ubiquitin ligase ($CRL4^{CRBN}$) have been identified: large conductance Ca^{2+} and voltage-activated K^+ channels[26,27], CLC-1 Cl^- channels[28], a homeobox protein MEIS2[1] and glutamine synthetase[6].

1.3.3.1. Large conductance $Ca2^+$ and voltage-activated K^+ channels

Large-conductance Ca^{2+} and voltage-activated K^+ (BK_{Ca}) channels are K^+-selective ion channels activated by either membrane depolarization or altered intracellular Ca^{2+} concentration[29]. Mammalian BK_{Ca} channel is a homotetrameric complex of Slo, the protein encoded by a *Slowpoke* gene family member[29]. Studies revealed that the $CRL4^{CRBN}$ directly targets Slo for ubiquitination, subsequently preventing protein's translocation to the plasma membrane, thereby affecting potassium currents upon stimuli[26,27].

1.3.3.2. CLC-1 Cl^- channels

The CLC Cl^- channels are responsible for selective flow of Cl^- ions across the plasma membrane, playing key roles in rest membrane maintenance and electrical excitability regulation of cells[30]. Like Slo, the $CRL4^{CRBN}$ complex ubiquitinates CLC-1, which regulates its stability and subcellular localization[28].

1.3.3.3. MEIS2

MEIS2 is a homeodomain transcription factor essential for proper limb formation in vertebrates[31]. Genomic *MEIS2* disruptions in human are linked to cardiac septal defects, cleft palate and IDs[32,33]. MEIS2 was identified as an endogenous substrate of the human $CRL4^{CRBN}$ by protein microarray analysis[1]. CRBN binds to MEIS2 via the Thal-BD, and thalidomide or its analogs inhibits CRBN-MEIS2 complex formation in mutually exclusive manner[1].

1.3.3.4. Glutamine synthetase

Glutamine synthetase (GS) produces glutamine through catalyzing the condensation of glutamate and ammonia. GS was identified as an endogenous substrate of CRBN through an unbiased proteomics approach[6]. The study showed that upon elevated intracellular glutamine level, CRBN targets GS for polyubiquitination and subsequent proteasomal degradation[6]. The study further identified that diacetylation at lysine residues of GS by the histone acetyltransferase complex p300-CBP is necessary for the $CRL4^{CRBN}$ mediated degradation[6], implicating a putative substrate recognition motif for the $CRL4^{CRBN}$ complex.

1.3.4. Thalidomide and its analogs alter functions of CRBN

CRBN has gained prominence as the direct target of thalidomide and its analogs known as immunomodulatory drugs (IMiDs)[4,34,35]. The presence of these molecules alters functions of CRBN, namely antagonizing endogenous substrates in mutually exclusive manner[1], in parallel enabling CRBN to recruit neomorphic substrates[8,10,11,36].

1.3.4.1. Thalidomide and the immunomodulatory drugs

Thalidomide (α-(N-phthalimido)glutarimide) (Figure 1.5) first appeared in the market in the late 1950s. It was first subscribed as a morning sickness remedy, but its usage was banned after its links to congenital anomalies was reported[37]. Thalidomide came back into focus after its therapeutic effects against leprosy[38] and some antitumor effects[39–41] were identified. At present, IMiDs named lenalidomide and pomalidomide (Figure 1.5) have been demonstrated to be effective against intractable hematological malignancies including multiple myeloma[42] and myelodysplastic syndromes with deletion of chromosome 5q[43]. These drugs have been approved for clinical use against multiple myeloma worldwide.

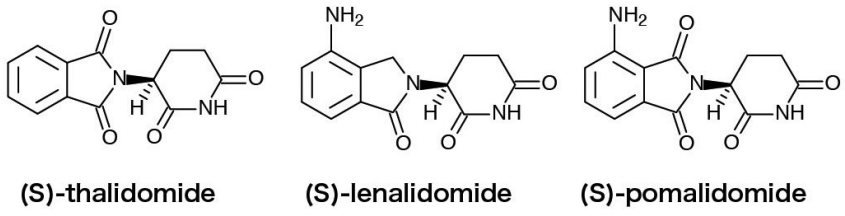

Figure 1.5. Thalidomide and the IMiDs. Structures of (S)-thalidomide (left), (S)-lenalidomide (middle) and (S)-pomalidomide (right) are shown.

1.3.4.2. Identification of CRBN as the primary target of thalidomide

For almost half a century, the molecular target of thalidomide remained elusive. By using a thalidomide derivative-immobilized resins, Ito and colleagues succeeded to purify thalidomide-bound protein complex from human cell lysates, and identified CRBN as the direct target of thalidomide[4]. The group demonstrated that thalidomide modulates ubiquitin ligase activity of the $CRL4^{CRBN}$ complex[4]. The group further showed that CRBN mediates thalidomide-induced teratogenicity in zebrafish and chick, which was associated with altered expression of the gene encoding fibroblast growth factor 8[4]. This landmark study implicated that CRBN may mediate pleiotropic effects of thalidomide and IMiDs.

1.3.4.3. CRBN mediates therapeutic effects of IMiDs against multiple myeloma

After identification of CRBN as the primary target of thalidomide, follow-up studies revealed that CBRN is also responsible for therapeutic effects of IMiDs, namely by promoting cell death in myeloma cells and stimulating interleukin-2 (IL-2) production in T cells[34,35].

Molecular mechanisms of the IMiDs' therapeutic effects against multiple myelomas were unveiled by unbiased screens[8,10]. Two analyses independently identified that protein levels of lymphoid specific transcription factors called Ikaros family zinc-finger protein 1 and 3 (also known as Ikaros and Aiolos, respectively) were reduced upon lenalidomide treatment[8,10]. The studies further showed that in the presence of lenalidomide, the $CRL4^{CRBN}$ complex gains function to target Ikaros and Aiolos for ubiquitination and proteasomal degradation[8,10]. Reduction of Ikaros and Aiolos was associated with altered transcription of genes encoding

interferon regulatory factor 4 (a transcription factor crucial for myelomas' survival) in myeloma cells and IL-2 in T cells, in part explaining anti-myeloma and immunomodulatory effect of lenalidomide[8].

1.3.4.4. CRBN mediates therapeutic effects of lenalidomide against myelodysplastic syndrome with deletion of chromosome 5q

Lenalidomide is also an effective treatment for myelodysplastic syndrome with deletion of chromosome 5q (MDS del(5q))[43]. A group performed a quantitative analysis to investigate changes of proteome and ubiquitome in lenalidomide-treated meyloid leukemia cells and identified decreased protein abundance and increased ubiquitination of casein kinase 1α[11]. The group proved that casein kinase 1α is a neomorphic substrate of the $CRL4^{CRBN}$ that is targeted for ubiquitination only in the presence of lenalidomide, and its reduction results in cell death[11].

1.3.5. Ubiquitin-independent functions of CRBN

Even though many previous studies focused on functions of CRBN in the context of the ubiquitin-proteasome system, its ubiquitin-independent functions have started to emerge.

1.3.5.1. CRBN regulates metabolism via interaction with AMP-activated protein kinase

AMP-activated protein kinase (AMPK) is a heterotrimeric kinase that functions as the master energy sensor by detecting altered ratio of intracellular AMP/ATP and ADP/ATP[44]. Through a yeast two-hybrid screening, the α subunit of AMPK was identified as an interaction partner of mammalian CRBN[45]. The study identified that CRBN suppresses AMPK's activity by competing with the γ subunit in mammalian tissue cell culture[45]. Later, changes in organismal metabolism associated with *crbn* null mice were reported[5]. The *crbn* null mice were more resistant to high-fat diet than control mice, characterized by less accumulation of fats in the epididymal tissues and the liver, improved glucose homeostasis and insulin sensitivity, in part due to hyperactivation of hepatic AMPK[5]. The studies suggest that CRBN may be involved in intracellular and organismal energy sensing.

1.3.5.2. CRBN mediates CD147-MCT1 complex maturation

Recent publication unveiled non-canonical, chaperone-like function of CRBN[46]. CRBN was identified to interact with a transmembrane glycoprotein CD147 and a transmembrane lactate transporter MCT1, promoting maturation and translocation to the plasma membrane of the CD147-MCT1 complex[46]. Either loss of CRBN or lenalidomide treatment led

to destabilization and retention of the complex at the ER[46]. It was also demonstrated that the therapeutic effects of lenalidomide against multiple myeloma and MDS del(5q) as well as their teratogenic effects are in part mediated by CD147-MCT1 complex destabilization[46].

1.3.5.3. CRBN expression in mitochondria results in enhanced resistance against oxidative stress

Previous studies have demonstrated that CRBN is widely distributed in the cellular compartments, including the cytoplasm[4,6], the nucleus[1,8,10] and the endoplasmic reticulum[26]. A group identified that transiently expressed CRBN is also partially localized in mitochondria[47]. To specify CRBN's specific functions in mitochondria, the group established a cell line that stably expresses CRBN with the mitochondrial-targeting signal (MTS-CRBN)[47]. MTS-CRBN expression resulted in enhanced resistance against oxidative stress associated with reduced amount of total carbonylated proteins[47].

1.3.5.4. Regulatory functions of CRBN in immune cells

Identification of CRBN as the primary target of IMiDs[8,10,11] brought focus on its functions in immune cells. A recently published paper uncovered a function of CRBN as a negative regulator of toll-like receptor 4 (TLR4) signaling pathway[7]. A group identified that transient expression of CRBN reduces NF-κB activity upon lipopolysaccharide (LPS) treatment in leukemia monocytic cells[7]. Tumor necrosis factor receptor associated factor 6 (TRAF6), a protein playing the pivotal role in TLR4 signaling pathway, was identified to interact with

CRBN[7]. The presence of CRBN attenuates ubiquitination of TRAF6 and TAB2 (which are required for IKK activation), and subsequently suppresses TRAF6 and TAB2-mediated activation of NF-κB[7].

1.4. Aim of the thesis

Even though diverse functions of CRBN have started to emerge, most of the previous studies shed light on its neomorphic functions in the presence of IMiDs[4,8,10,11,46]. Relatively less is known about CRBN's functions in the absence of the IMiDs and functions *in vivo*. This thesis aims to investigate IMiDs-independent functions of mammalian CRBN and its invertebrate homolog using the fruit fly *Drosophila melanogaster*.

Chapter 2. Human CRBN localizes to aggresome and shows cytoprotective effect against proteasomal dysfunction

2.1. Introduction

Intellectual disability (ID) is a neurodevelopmental disorder that affects approximately 1-3% of the general population[48]. ID patients are associated with learning and adaptive behavior deficits, which restrict them from adapting to the society[49]. Even though socioeconomic burden of ID is significant, measures toward IDs could not be taken for a long time mainly due to lack of understanding towards its molecular mechanisms.

Links between onset of IDs and mutation and altered gene dosage of *CRBN* have been reported. A homozygous nonsense mutation (*R419X*) in the coding region of the gene was associated with a mild type of ID without morphological and neurological anomalies[9]. In addition, microduplications of the genomic region that includes *CRBN* were identified from unrelated ID patients[12]. However, its molecular mechanisms are not known.

Aggresome is a protein inclusion observed in cultured cells upon stress exposure[50]. Aggresome formation has been considered as an active cell response to sequester the toxic misfolded proteins from other organelles and macromolecules[51]. A series of intracellular processes is shown in the Figure 2.1[51]. In brief, regulatory E3 ubiquitin ligases attach Lysine 63-linked polyubiquitin chains to misfolded proteins when their amount exceeds the capacity of the chaperones-mediated folding and the ubiquitin-proteasome system. The polyubiquitinated proteins bind to the dynein motor complex via histone deacetylase 6 (HDAC6) and other accessory proteins. The protein complex is transferred to the microtubule organizing center,

where the aggresome is formed. Once the toxic proteins are concentrated, the aggresomes are cleared by bulk autophagy.

Some E3 ubiquitin ligases are known as a regulatory factor in aggresome formation. Parkin, a RING domain-containing E3 ubiquitin ligase encoded by a familial parkinson's disease causing gene[52,53], targets substrate proteins for polyubiquitination required for transportation to the aggresome[54]. TRIM50, another RING domain-containing E3 ubiquitin ligase, promotes translocation of polyubiquitinated proteins to the aggresome and their elimination[55]. Furthermore, E3 ubiquitin ligases encoded by causal genes of neurodevelopmental disorders are recruited to the aggresome upon extracellular stimuli[55,56], suggesting possible links between the aggresome and onset of the genetic disorders.

In this chapter, a role of CRBN in cytoprotection upon proteasome dysfunction is described. In the presence of a proteasome inhibitor MG132, CRBN was co-localized with aggresome markers at the perinuclear region. The change of its subcellular location was inhibited completely by microtubule disruption and partially by IMiD treatment. Transient expression of CRBN reduced cell death upon MG132 treatment, whereas its reduction by RNAi induction increased cell death, suggesting its role in cytoprotection under altered proteostasis.

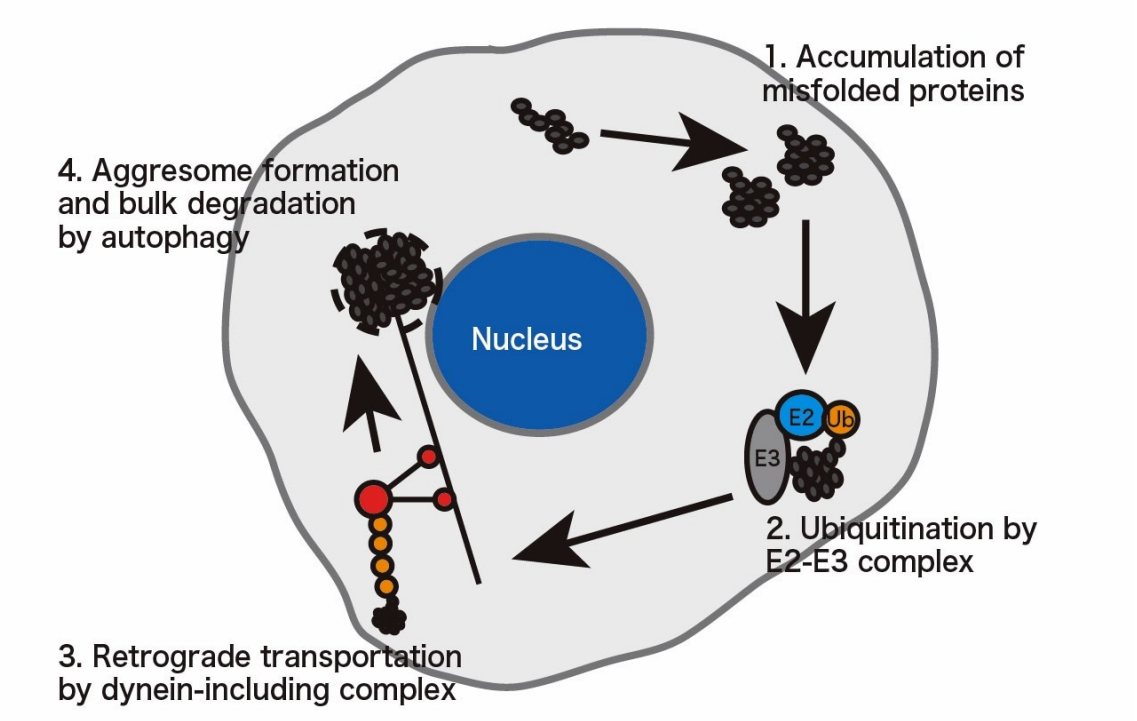

Figure 2.1. Aggresome formation. The scheme represents four sequential biological processes in aggresome formation.

2.2. Materials and methods

2.2.1. Reagents

MG132 (Peptide Institute), nocodazole (Wako) and (RS)-pomalidomide (Sigma Aldrich) were dissolved in dimethyl sulfoxide and stored at -20ºC.

2.2.2. Antibodies

Following antibodies were used in the experiments mentioned in this chapter:

Name	Source	Epitope/Clone	Provider
HA	Mouse	16B12	Covance
HA	Rabbit	YPYDVPDYA-KLH	MBL
CRBN	Rabbit	Details not known(1)	Abnova
Ubiquitin	Mouse	FK2	MBL
HSP70	Rabbit	Details not known(2)	Cell Signaling
γ-tubulin	Mouse	GTU-88	Sigma Aldrich
HRP-conjugated secondary Ab	-	-	GE Healthcare
Fluorophore-cojugated sencondary Ab	-	-	Life technologies

(1). The manufacturer describes as "a synthetic peptide of human CRBN".

(2). The manufacturer describes as "a synthetic peptide corresponding to human HSP70".

2.2.3. Molecular cloning

Human *CRBN* cDNA clone was obtained from Genome Network Project Human cDNA Clones (IRAL038I16, Riken BioResource Center). Coding sequences for full-length CRBN or the putative mutant protein associated with the ID (CRBN R419X) were inserted into a mammalian expression vector pRK5-HA via SalI and NotI sites. A *CRBN* shRNA expresion vector was generated using the pSilencer Vectors (Life Technologies). A rescue construct that expresses a gene encoding wild type CRBN but contains two point mutations to avoid targeting by shRNA was generated by using the KOD Plus mutagenesis kit (TOYOBO). The sequences of all generated plasmid vectors were confirmed by DNA sequencing.

2.2.4. Cell culture

Rat adrenal pheochromocytoma PC12 cells were grown in low-glucose Dulbecco's modified Eagle's medium (Wako) with 5%(v/v) fetal bovine serum, 5% horse serum and 1% penicillin-streptomycin.

2.2.5. Transfection and reagents treatment

The Lipofectamine 2000 reagent (Life Technologies) was used according to the manufacturer's instructions. Cells were cultured in the incubator for 12 to 24 hours after transfection for further use. MG132, nocodazole and (RS)-pomalidomide were treated at final concentration of 10μM, 10μg/mL and 10 or 100μM, respectively.

2.2.6. Protein extraction

Cultured cells were lysed in RIPA buffer (50mM Tris-HCl pH7.5, 150mM NaCl, 1% Nonidet P40, 0.1% sodium dodecyl sulfate (SDS), 0.5% sodium deoxycholate) with the cOmplete Protease Inhibitor Cocktail (Roche). After sonication for further disruption, the lysates were centrifuged at 21,500xg for 5 minutes at 4ºC. Supernatants after centrifugation were recovered and mixed with 2X sample buffer solution (Wako) and 2-mercaptoethanol (Wako).

Immunoprecipitation was performed using nProtein A sepharose 4 Fast Flow (GE) and anti-HA antibody according to manufacturer's instructions.

2.2.7. Western blotting

Western blotting was performed based on the standard protocol. In brief, protein samples were loaded to sodium dodecyl sulfate-polyacrylamide (SDS-PAGE) gels and electrophoresis was performed at 150V. Then, proteins were transferred to a methanol-pretreated polyvinylidene Difluoride (PVDF) membrane at 100V on ice. 5% nonfat milk solution in TBS-T buffer was used for membrane blocking and 2.5% milk solution for antibody incubations. The prepared membranes were treated with Novex ECL Chemiluminescent Substrate Reagent (Thermo Fisher) or ImmunoStar LD (Wako) to detect the signals.

2.2.8. Immunofluorescent microscopy and image acquisition

Cells were seeded on 35mm glass based dish (Iwaki). After brief washing step with PBS, cells were fixed with 4% paraformaldehyde (Wako) in PBS for 15 minutes at room temperature.

Cells were treated with appropriate primary antibody and sencondary antibody. Final samples were mounted with VECTASHIELD mounting medium with DAPI (Vector Laboratories). Cellular images were acquired by using a confocal microscope FV1000 (Olympus).

2.2.9. Cytotoxicity assay

To quantify MG132-induced cell death, lactate dehydrogenase (LDH) activity in culture media was determined using the Cytotox96 Non-Radioactive Cytotoxicity Assay (Promega) according to manufacturer's instructions.

2.3. Results

2.3.1. CRBN is localized at aggresomes under proteasomal inhibition

In previous studies, CRBN was reported to localize in the cytoplasm[4], the nucleus[4], mitochondria[47] and the ER[26]. To investigate whether accumulation of misfolded proteins affects subcellular localization of CRBN, PC12 cells with transiently expressed HA-tagged human CRBN (HA-CRBN) were treated with a proteasome inhibitor MG132. In the absence of MG132, HA-CRBN was predominantly expressed in the cytoplasm and the nucleus (Figure 2.2A), as reported previously[4]. After overnight MG132 treatment, on the other hand, HA-CRBN was almost exclusively localized at the perinuclear region as a spherical structure in most of the HA-CRBN expressing cells (Figure 2.2A). This subcellular localization and structural feature were similar to those of aggresomes reported in the previous studies[54,57]. Therefore, further double immunofluorescence studies were performed to compare localization of CRBN with the known aggresome markers. Three aggresome markers, γ-tubulin, ubiquitin and Hsp70, all co-localized with CRBN in the presence of MG132 (Figure 2.2B-D). Endogenous CRBN also co-localized with ubiquitin at the perinuclear region (Figure 2.2E), suggesting that CRBN is indeed recruited to the aggresome under accumulation of misfolded proteins and protein aggregates.

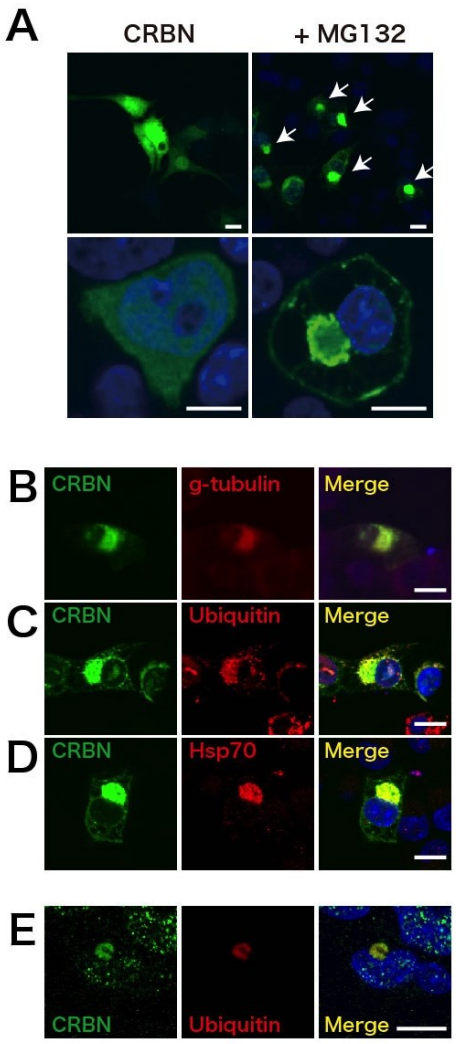

Figure 2.2. CRBN co-localizes with aggresome markers upon MG132 treatment. (A) Immunostaining of HA-CRBN in PC12 cells shows that CRBN is localized in the cytoplasm and the nucleus (left). HA-CRBN was forming spherical structures (white arrows) at the perinuclear region after overnight MG132 treatment (right). (B-D) Co-immunostaining of HA-CRBN with γ-tubulin (B), ubiquitin (C) and Hsp70 (D) after overnight MG132 treatment. (E) Co-immunostaining of Endogenous CRBN with ubiquitin after overnight MG132 treatment. All scale bars represent 10μm. The figures are reprinted from the Figure 1 of Sawamura *et al.,* 2015[58]. The experiments were performed in collaboration with H. Yamada.

2.3.2. A microtubule destabilizer and pomalidomide affects CRBN's localization at aggresomes

Microtubules are essential in aggresome formation, as ubiquitinated proteins are retrogradely transported to the microtubule organizing center by the dynein motor complex and accessory proteins[51]. To confirm whether recruitment of CRBN to the perinuclear region is microtubule-dependent, PC12 cells with transiently expressed HA-CRBN were treated with nocodazole, a microtubule-distabilizing compound, along with MG132. Nocodazole treatment completely abrogated translocation of CRBN to the perinuclear region (Figure 2.3A). This result suggests that CRBN is transported to the aggresome in microtubule-dependent manner, just like other substrates protein and regulatory proteins of the aggresome formation.

Polyubiquitin chain attached to substrate proteins functions as a signal for the transportation to the aggresome[51]. To clarify whether proper E3 ubiquitin ligase activity of CRBN is necessary for its translocation to the aggresome, localization of CRBN was confirmed in the presence of pomalidomide. In the presence of pomalidomide, translocation of CRBN to the aggresome was mildly attenuated, with more CRBN present in the cytoplasm in a diffused state (Figure 2.3B). Number of cells with CRBN in the diffused state increased in a dose-dependent manner (Figure 2.3C), suggesting that the E3 ubiquitin ligase activity of the $CRL4^{CRBN}$ may in part required for the translocation to the aggresome.

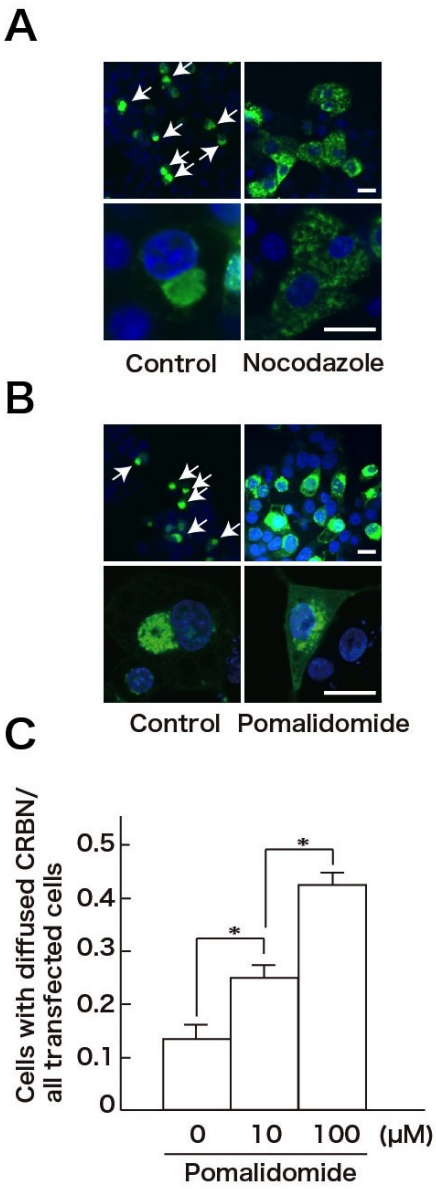

Figure 2.3. Nocodazole or pomalidomide treatment suppress CRBN's recruitment to the aggresome. (A) Immunostaining of HA-CRBN in PC12 cells shows CRBN localized to the aggresome after overnight MG132 treatment (white arrows) (left). Nocodazole treatment completely abolished the translocation of CRBN to the aggresome (right). (B) Immunostaining of HA-CRBN in PC12 cells shows CRBN localized to the aggresome after overnight MG132 treatment (white arrows) (left). Pomalidomide treatment attenuated the translocation of CRBN

to the aggresome, with more diffused state in the cytoplasm (right). (C) Percentage of cells with CRBN in the diffused state after pomalidomide treatment was quantified. * indicates $P<0.05$. P values were calculated by Student's *t*-test. The figures are reprinted from the Figure 2 of Sawamura *et al.,* 2015[58]. The experiments were performed in collaboration with H. Yamada.

2.3.3. CRBN forms ubiquitin-positive, high-molecular weight aggregates under proteasomal inhibition

Previous studies have described biochemical features of the aggresome as a ubiquitin-positive, high-molecular weight protein complex[57]. Biochemical analysis was performed to confirm whether biochemical features of CRBN change upon proteasome dysfunction. Transiently expressed HA-CRBN in PC12 cells was detected as a single band of approximately 55-60kDa (theoretical size of CRBN is 51kDa) (Figure 2.4A). The putative CRBN mutant associated with the ID (HA-CRBN-R419X) was detected as a single band of slightly smaller molecular weight, reflecting the deletion of the C-terminal 24 amino acids (Figure 2.4A). Like wild type CRBN, HA-CRBN-R419X was localized to the perinuclear region after MG132 treatment (Figure 2.4B), suggesting the loss of the C-terminal region does not inhibit recruitment to the aggresome.

Next, either HA-CRBN or HA-CRBN-R419X was purified from the MG132 treated PC12 cells, and samples with the purified immunocomplex were subsequently subjected to western blotting with a ubiquitin-specific antibody. As expected, ubiquitin-positive, high-molecular weight HA-CRBN and HA-CRBN-R419X proteins were detected (Figure 2.4C). The result further reinforced the previous immunofluorescence data that CRBN is a component of the aggresome in the MG132-treated cells.

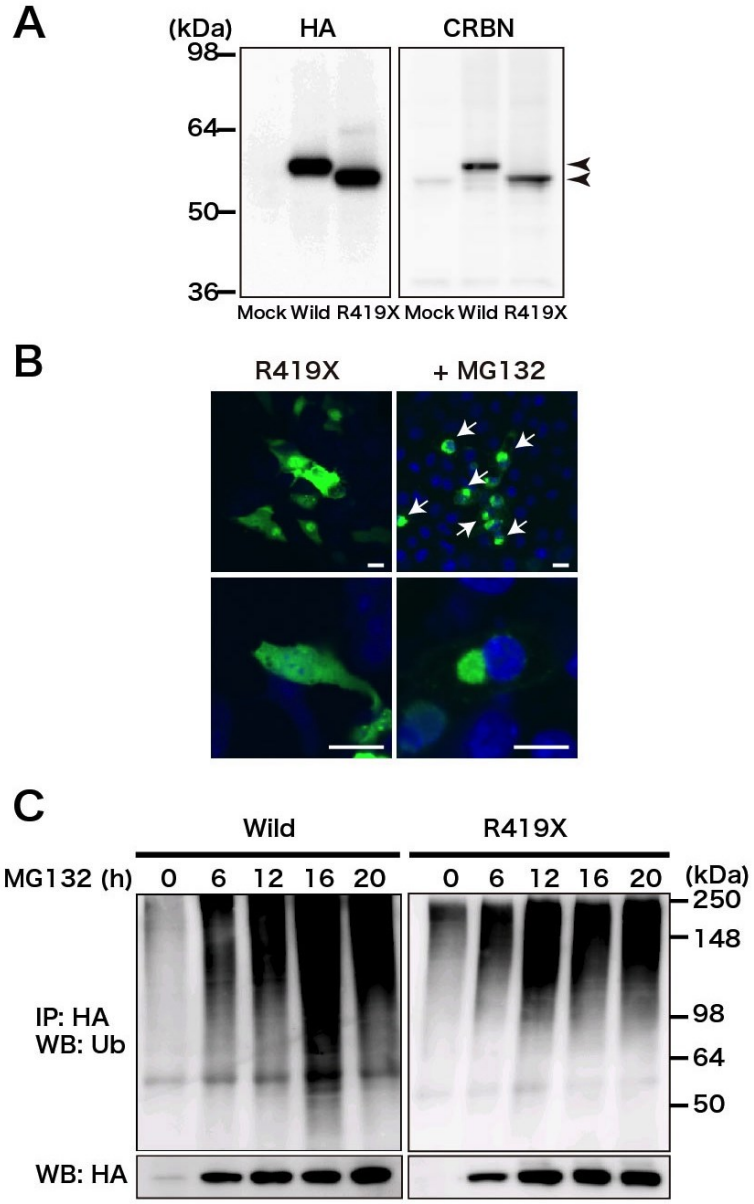

Figure 2.4. CRBN forms ubiquitin-positive, high-molecular weight complexes upon MG132 treatment. (A) Total lysates from PC12 cells expressing either wild type (Wild) or the ID-associated mutant (R419X) were subjected to western blotting with antibodies against indicated proteins. (B) Immunostaining of HA-CRBN-R419X in PC12 cells shows that CRBN is localized in the cytoplasm and the nucleus (left). Immunostaining of HA-CRBN-R419X in PC12 cells shows that HA-CRBN-R419X was forming spherical structures at the perinuclear

region after overnight MG132 treatment (white arrows), just like wild type CRBN (right). (C) Either HA-CRBN or HA-CRBN-R419X was immunopurified from MG132 treated PC12 cells by immunoprecipitation, and the samples containing immunocomplexes were subjected to western blotting with antibodies against indicated proteins. The figures are reprinted from the Figure 3 of Sawamura *et al.,* 2015[58]. The experiments were performed in collaboration with H. Yamada and K. Matsumoto.

2.3.4. CRBN shows cytoprotective effect against proteasomal inhibition

Aggresome formation is considered as an active response to protect cells from accumulation of toxic misfolded proteins[51]. To address whether CRBN plays a role in cytoprotection against proteasomal dysfunction, the lactate dehydrogenase (LDH) cytotoxicity assay was performed to quantify cell death upon MG132 treatment. When either HA-CRBN or HA-CRBN R419X was overexpressed, LDH in culture media was significantly reduced (Figure 2.5A), suggesting that increase of CRBN results in cytoprotective effect against proteasomal dysfuntion and subsequent accumulation of toxic proteins. To further confirm the role of CRBN in cytoprotection, endogenous *CRBN* was knocked down by transfecting shRNAi plasmid (Figure 2.5B). Reduction of *CRBN* led to increase of LDH in media, whereas transient expression of RNAi-resistant CRBN rescued the increase of LDH (Figure 2.5C). These results altogether suggest that CRBN plays a cytoprotective role from misfolded protein-induced cell death.

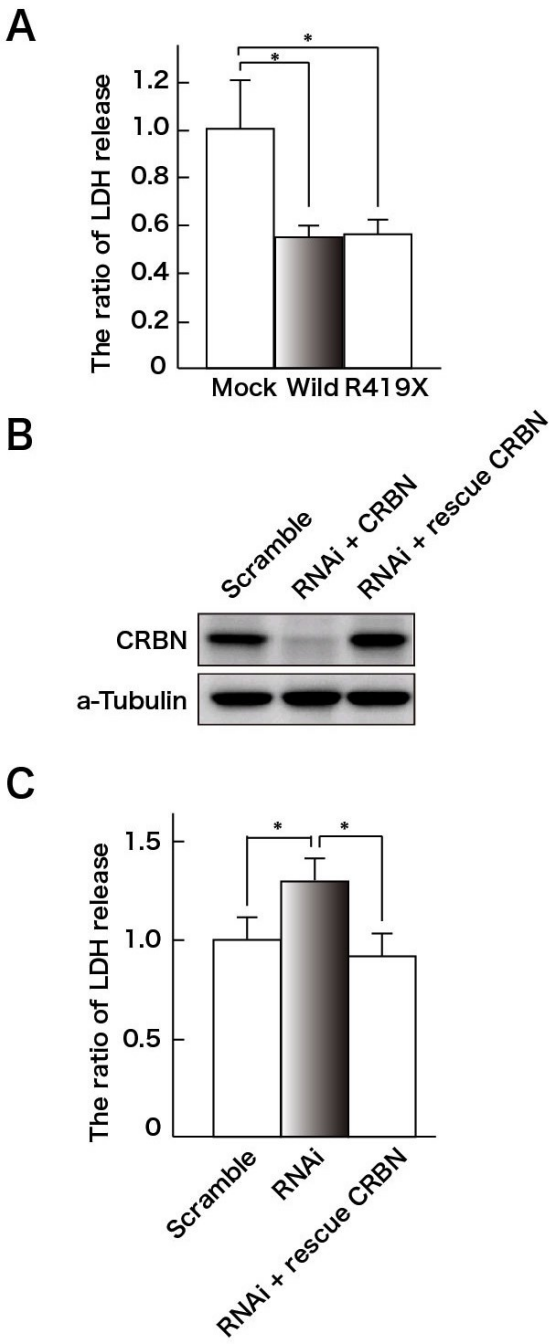

Figure 2.5. Transient expression of CRBN enhances cellular resistance against the proteasomal dysfunction. (A) LDH release from MG132-treated PC12 cells either expressing wild type (Wild) or the ID-associated mutant (R419X) CRBN were quantified. (B) Total lysates from PC12 cells expressing either shRNA against *CRBN* alone or the shRNA with the

RNAi-resistant CRBN were subjected to western blotting with antibodies against indicated proteins. (C) LDH release from MG132-treated PC12 cells expressing either *CRBN* shRNA alone or *CRBN* shRNA with the RNAi-resistant CRBN were quantified. The figures are reprinted from the Figure 4 of Sawamura *et al.,* 2015[58]. The experiments were performed in collaboration with H. Yamada and K. Matsumoto.

2.4. Discussion

The aggresome is an intracellular protein structure formed when protein loads are exceeding the capacity of the protein clearance systems and/or the systems are impaired. To sequester the toxic proteins, cells utilize active response mechanism to concentrate the proteins to the aggresome and eliminate it by autophagy[51].

The cellular biological and biochemical data altogether suggested that CRBN is recruited to the aggresome upon proteasomal dysfunction. Also, transient expression of exogenous CRBN reduced MG132-induced cell death, whereas loss of CRBN enhanced it. As environmental factors are the major causal factors for onset of ID, defects in the cytoprotective system in neuronal cells due to loss of CRBN may be of importance to ID pathogenesis.

From the obtained results, the detailed mechanism of how CRBN protects cells against accumulation of toxic proteins cannot be explained. There are at least 3 possible explanations: 1. CRBN ubiquitinates misfolded proteins. 2. CRBN functions as an accessory protein to promote removal of misfolded proteins from the cytoplasm. 3. CRBN upregulates cytoprotective responses related genes to increase cellular capacity to cope with misfolded proteins.

CRBN is a substrate receptor of the CRL4 complex[4], and several substrate proteins have been identified[1,6,8,10,11,26,28]. Therefore a straightforward explanation is that CRBN targets misfolded proteins for ubiquitination, like other E3 ubiquitin ligases such as Parkin[54] and TRIM50[55].

There were studies showing that CRBN mediates maturation and translocation of

proteins either dependent or independent of ubiquitination[26,46], implicating that CRBN may play roles in intracellular protein trafficking. A previous study identified that an E3 ubiquitin ligase named Carboboxy terminus of Hsp70-interacting protein (CHIP) not only ubiquitinates its substrate, but also mediates its interaction with HDAC6 to promote proper translocation of ubiquitinated proteins to the aggresome[59]. Thus, CRBN could function in similar manner.

Autophagy is a bulk clearance mechanism to eliminate the aggresome. Enhanced activity of autophagy ameliorates cytotoxicity induced by mutant huntingtin and other mutant proteins associated with neurodegenerative diseases[60,61]. One major signal cascade that regulates activity of autophagy is PI3kinase-PKB/Akt-mammalian Target of rapamycin (mTOR) pathway. Of note, FOXO family members, downstream transcription factors of the signal cascade, were identified as a regulator of autophagy. Several studies have shown that activated FOXO can promote autophagy in at least two distinct mechanisms: regulating indirectly by suppressing activity of mTOR[62] and regulating directly by inducing expression of autophagy-related genes[63,64]. Since *Drosophila* homolog of CRBN was identified as a novel regulator of insulin-like signaling[65] and *Drosophila* FOXO could be its potential substrate (for details see chapter 3), it may be intriguing to investigate whether CRBN regulates protective response against accumulation of misfolded proteins via altering functions of FOXO. Further investigations, in particular with neuronal cells, will be necessary to elucidate the functions of CRBN in this context.

Chapter 3. Characterization of Ohgata, the *Drosophila* ortholog of human CRBN

3.1. Introduction

Previous studies have reported that loss of function or misexpression of *CRBN* family members causes wide range of phenotypes in vertebrates. In human, a genetic mutation or altered gene dosage of *CRBN* is associated with IDs[9,12], implicating that CRBN may play roles in neuronal development. In zebrafish, *zcrbn* inhibition by morpholino antisense oligonucleotides leads to morphological defects in limbs and otic vesicles[4]. Unlike zebrafish, morphology of *crbn* null mice is normal throughout development, instead they are resistant against high-fat diet challenge[5], implicating that mice CRBN may play roles in organismal metabolism at least in the pathological metabolic condition. Mechanistic insights of these diverse phenotypes are, however, still lacking.

The fruit fly *Drosophila melanogaster* was chosen to study physiological functions of a CRBN family protein. *Drosophila* is a genetically tractable model organism. With relative ease of obtaining genes' mutants and a number of available genetic tools, *Drosophila* enables to study functions of genes and its products *in vivo* in detail.

In this chapter, a function of Ohgata (OHGT), the *Drosophila* homolog of CRBN, in organismal growth regulation is described. A fly line with a strong allele of *ohgata* (*ohgt*) gene was generated by using an emerging genome editing technology named CRISPR-Cas9 system. Phenotypic analyses identified that this mutant allele is associated with overgrowth phenotype without changes in the body proportion. Immunofluorescence studies showed that OHGT is

expressed in the fat body, an endocrine organ that coordinates nutrient abundance and larval growth. Overexpression of shRNA against *ohgt* in the fat body could phenocopy the overgrowth phenotype of the gene's mutant, suggesting that OHGT in the fat body is in part responsible for the growth phenotype. Biochemical and gene expression analyses identified that insulin-like signaling was elevated in the *ohgt* mutant, probably due to reduction of genes encoding inhibitory cofactors of the circulating insulin-like peptides. Finally, interaction between OHGT and Piccolo, the *Drosophila* homolog of DDB1, was biochemically confirmed, implicating that the $CRL4^{CRBN}$ complex may be conserved in *Drosophila*.

3.2. Materials and methods

3.2.1. Antibodies

Following antibodies were used in the experiments mentioned in this chapter:

Name	Source	Epitope/Clone	Provider
OHGT(1-187)	Rabbit	GST-OHGT(1-187)	Generated in this thesis
OHGT(15-33)	Guinea pig	OHGT(15-33)-Cys-KLH	Generated in this thesis
α-spectrin	Mouse	3A9	DSHB[(1)]
β-tubulin	Mouse	E7	DSHB
Lamin	Mouse	ADL84.12	DSHB
Human DDB1	Goat	C-DLIKVVEELTRIH	Abcam
Ubiquitin	Mouse	VU-1	Life Sensors
GFP	Chicken	Full length GFP	Abcam
HA	Rat	3F10	Roche
Actin	Rabbit	SGPSIVHRKCF	Sigma Aldrich
Actin	Mouse	DDDIAALVIDNGSGK	Abcam
Phospho-Akt	Rabbit	Details not known[(2)]	Cell Signaling
DILP2	Guinea pig	DMKALREYCSVVRN	M. Pankratz[66]
Horseradish peroxidase-cojugated sencondary Ab	-	-	Santa Cruz
fluorophore-cojugated sencondary Ab	-	-	Life technologies

(1). The Developmental Studies Hybridoma Bank, created by the National Institute of Child Health and Human Development of the National Institute of Health, and maintained at the University of Iowa, Department of Biology.

(2). The manufacturer describes as "a synthetic phosphopeptide corresponding to residues around Ser473 of human Akt protein".

3.2.2. cDNA

A cDNA clone containing full-length *CG3925* ORF (LD28592) was obtained from the *Drosophila* Genomic Resource Center (Biology Department, Indiana University).

3.2.3. Molecular cloning

Phusion High-fidelity DNA Polymerase, restriction enzymes (EcoRI, SalI and XhoI), antarctic phosphatase and T4 DNA ligase were all obtained from NEB. DNA purification after reactions was performed using Nucleospin Gel and PCR Clean-up (Macherey Nagel) according to the manufacturer's instructions. Transformation was performed using the *E. coli* DH5α competent cells. Plasmid DNA purification was performed using Nucleobond Midiprep kit (Macherey Nagel) according to manufacturer's instructions. Purified plasmid DNAs were diluted in 1X Tris-EDTA buffer pH8.0 and stored at -20ºC for further use.

3.2.4. Generating OHGT-specific antibodies

Cloning of Glutathione S-transferase-tagged immunogen expression vector

Coding sequence for amino acid 1 to 187 of OHGT protein was amplified using the primer pair shown below (Restriction enzyme sites are underlined and the start/stop codons are shown in red):

F: 5'-ACGCGTCGACATGGACGAAGAGGAGAAC

R: 5'-TATCTCGAGTCATCGAGGTGGCTGCTGT

The digested amplicon was inserted into pGEX-4T3 (GE healthcare) via SalI and XhoI sites. The insertion of the amplicon into the vector was confirmed by DNA sequencing (Seqlab, Göttingen, Germany). The product was named pGEX-OHGT(1-187).

Expression and purification of the recombinant protein

The *E. coli* BL21(DE3) competent cells were freshly transformed with the pGEX-OHGT$^{1\text{-}187}$. A bacterial colony was picked up and was grown overnight in 25mL LB media with Ampicillin to a final concentration of 100µg/mL at 37ºC. The next day, fresh LB media was added up to 1L and further incubated for 1.5 hours at 30ºC. The isopropyl β-D-1-thiogalactopyranoside (IPTG) was added to a final concentration of 0.1mM to induce recombinant protein expression, and the culture media was further incubated for 3 hours at 30ºC.

The bacterial media were centrifuged at 4,000xg for 10 minutes at 4ºC. The cell pellete was resuspended with 50mL glutathione S-transferase (GST)-binding buffer (25mM Tris-HCl pH7.5, 150mM NaCl, 1mM EDTA and the cOmplete Protease Inhibitor Cocktail (Roche)). To lyse the

cells, lysozyme was added to a concentration of 10μg/mL and the mixture was incubated for 30 minutes on ice. After adding glycerol and Triton X-100 to respective final concentrations of 10% and 0.5%, the mixture was sonicated for further cell disruption. The lysate was centrifuged at 15,000xg for 10 minutes at 4ºC, and the soluble fraction was collected and pooled for purification of the GST-tagged OHGT(1-187) (GST-OHGT(1-187)).

Dithiothreitol was added to the soluble fraction to a final concentration of 1mM. 50% slurry of prewashed glutathione sepharose 4B (GE healthcare) was added, and the mixture was incubated for 2 hours at 4ºC. The beads were collected by centrifugation at 500xg for 2 minutes. After supernatant was removed, the beads were washed 4 times with 1% PTX buffer (1% Trition X-100 in 1X PBS), 4 times with 1X PBS and once with the GST-binding buffer. After supernatant was removed, the washed beads were incubated in elution buffer (10mM reduced glutathione in 50mM Tris-HCl pH8.0) for 15 minutes at room temperature. The supernatant that contains the recombinant protein was recovered. Fraction at each process was collected to confirm the protein abundance by SDS-PAGE gel electrophoresis.

Immunization

Stability of purified GST-OHGT(1-187) was confirmed by incubating it overnight at 37ºC. Then the protein solution was sent to Pineda antibody service (Berlin) for injection into rabbits. A synthetic polypeptide corresponding to amino acid 15 to 33 of OHGT with a cysteine residue at the C-terminus (RDEDVQLEDQQSQGLQDRQC; referred to as OHGT(15-33)-Cys) was covalently immobilized to the Keyhole Limpet Hemocyanin (KLH), and the protein complex

was injected into guinea pigs. Sera were collected from the immunized animals at 150 days post immunization.

Affinity purification

To prepare an affinity column for anti-OHGT(1-187) purification, GST-OHGT(1-187)-attached glutathione sepharose 4B was incubated in thrombin solution (1U/20μL of thrombin (GE healthcare) in 1X PBS) for overnight at room temperature with constant rotation. On the following day, thrombin digest flow-through, which contains cleaved OHGT(1-187) and thrombin, was directly transferred to a column containing prewashed benzamidine sepharose 4 fast flow (GE healthcare). The capped column was incubated for 30 minutes at room temperature. The flow-through from the benzamidine column, which contains cleaved OHGT(1-187), was dialyzed using Slide-A-Lyzer G2 Dialysis Cassette (Thermo Fisher) according to manufacturer's instructions. The purified OHGT(1-187) recombinant peptide was immobilized to CNBr-activated sepharose 4B (GE healthcare) according to manufacturer's instructions.

To prepare an affinity column for anti-OHGT(15-33) purification, the OHGT(15-33)-Cys peptide was immobilized to the Sulfolink Coupling Resin (Thermo Fisher) according to manufacturer's instructions.

The prepared columns were stored at 4ºC with 0.02% sodium azide in 1X PBS.

To purify IgGs, 2mL antisera were mixed with 2mL PBS, and the mixture was loaded to the corresponding column. The column with antisera solution was incubated for 2 hours at room

temperature with constant rotation. The column was subsequently washed 3 times with 4mL PBS. The bound proteins were eluted with 500µL 100mM Glycine-HCl pH2.8, and then the eluate was neutralized with 100µL 1M Tris-HCl pH 8.8. 5 fractions were prepared in total. Each fraction was subjected to SDS-PAGE gel electrophoresis to confirm the presence of IgGs. The fraction with the largest amount of IgGs was stored at 4ºC for further use.

Antibody validation

Biochemical analysis was performed to validate OHGT-specific antibodies' specificity. Early 3rd instar larvae of following genotypes were collected: *w** (as a control), homozygous $ohgt^{Ex2}$ and transheterozygous $ohgt^{Ex2}/ohgt^{Df}$. The same number of larvae (5-15) were lysed in RIPA buffer containing the cOmplete protease inhibitor cocktail (10µL/larva). Sample preparation and western blotting were performed as described later in this section.

3.2.5. Fly works

All flies were maintained in standard stock food (11.3L distilled water, 90g agarose, 165g yeast powder, 615g cornmeal, 1L syrup, 200mL 10% methylparaben solution) at 18ºC or 25ºC.

All crosses were performed in the small embryo collection cages. Embryos were collected on an apple agar plate with yeast paste for 4 hours if there is no further indication.

To represent genotypes, semicolon separates chromosomes (unaffected chromosomes are omitted), slash separates different alleles of the same chromosome, plus sign indicates wild type chromosomes, and comma separates different constructs and alleles on the same chromosome.

Name (genotype)	Description	Provider
*w** (*w** ; ;)	Control	Bloomington #5905
$ohgt^{Ex2}$ (w^{1118} ; ; $ohgt^{Ex2}$)	*ohgt* mutant allele	Generated in this thesis
$ohgt^{Df}$ (w^{1118} ; ; *Df(3R)Exel6155, P{XP-U}Exel6155/TM6B, Tb*^{1})	A deficiency line deleting the region containing *ohgt* locus	Bloomington #7634
UAS-ohgt^{RNAiv40486} (w^{1118} ; ; *P{GD11111}v40486*)	*ohgt* RNAi line	VDRC(1) #40486
UAS-ohgt^{RNAiNIG3} (w^{1118} ; ; *P{NIG.3925R}*)	*ohgt* RNAi line	NIG(2) #3925R-3
UAS-dDDB1^{RNAi} (*w** ; *P{UAS-dDDB1.650-dsRNA}23*)	*pic* RNAi line	Kyoto(3) #109605
UAS-dCullin4^{RNAi} (w^{1118} ; ; *P{GD14006}v44829*)	*dCullin4* RNAi line	VDRC #44829
UAS-GFP.nls (w^{1118} ; *P{w[+mC]=UAS-GFP.nls}14*)	Induces expression of GFP	Bloomington #4775
Cg-Gal4 (w^{1118} ; *P{Cg-Gal4.A}2*)	Expresses GAL4 in the fat body and hemocytes	Bloomington #7011
FB-Gal4 (*w** ; *P{w*$^{+mW.hs}$*=GawB}FB/SNS*)	Expresses GAL4 in the fat body	Kühnlein lab(4)
Dilp2-Gal4 (*w** ; *Dilp2-Gal4/Cyo, twi-GFP*)	Expresses GAL4 in the Insulin-producing cells (IPCs)	Bloomington #37516
hs-FLP CD2GFP (*y, hs-FLP* ; *Dicer2* ; *act-FRT-CD2-FRT-Gal4, UAS-GFP/TM6b, Tb, Hu*)	For performing clonal analysis	Hoch lab(5)
vas-Cas9 (y^{1}, w^{1118}, *M{vas-Cas9}ZH-2A/ FM7c*)	For performing CRISPR-Cas9 targeted mutagenesis	Bloomington #51323
Dr^{Mio}*/TM3-GFP* Sb^{1} Ser^{1} (w^{1118} ; ; Dr^{Mio}*/TM3, P{GAL4-twi.G}2.3, P{UAS-2xEGFP}AH2.3,* Sb^{1}, Ser^{1})	For isolating *dCRBN*^{Ex2}	Bloomington #6663

(1). Vienna *Drosophila* Resource Center

(2). National Institute of Genetics

(3). *Drosophila* Genomics and Genetic Resources (Kyoto Stock Center)

(4). A line described in Grönke *et al.,* 2003[67]

(5). The line was established using a line described in Pignoni and Zipursky, 1997[68]

3.2.6. Generating an *ohgata* mutant alleles using the CRISPR-Cas9 genome editing technology

CRISPR-Cas9-mediated mutagenesis and its screening were performed based on the protocols described in the previous studies[69–71].

Designing Cas9 target sites

The CRISPR Optimal Target Finder (tools.flycrispr.molbio.wisc.edu/targetFinder) was used to search for potential target sites within the *ohgt* locus. Since the two evolutionary conserved domains, the LON domain and the Thal-BD, are encoded by exon 3 to 5, genomic sequence containing exon 1, exon 2 and an intron between the exons was used as an input. Following parameters were chosen to look for potential target sites:

1. Length of target site: 20bp

2. Single G at the 5' end (for the efficient transcription from the U6 promoter)

3. Stringency: High

4. PAM: NGG only

From 11 candidates, a sense sequence within exon 2 was chosen as the target site (Figure 3.6).

Cloning guide RNA expression vectors

The molecular cloning of guide RNA expression vectors was performed according to the previous study[70]. In brief, following oligonucleotides were obtained (underlined sequences are complimentary to overhangs generated by BbsI digestion):

F: 5'-CTTCGCAGGACGACACAGCAAGCG

R: 5'-AAACCGCTTGCTGTGTCGTCCTGC

1μmole of each oligonucleotide was used for annealing. After 5'-phosphorylation by using T4 polynucleotide kinase (NEB), oligonucleotides were annealed by following thermal cycler program: 95ºC for 5 minutes, subsequently ramp to 25ºC at the rate of -0.1ºC/sec. The 5'-phosphorylated, annealed oligonucleotides were then inserted into digested pU6-BbsI-chiRNA plasmid vector via BbsI site. The sequences of cloned plasmids were confirmed by DNA sequencing (Seqlab, Göttingen, Germany). The cloned plasmid guide RNA expression vector was named pU6-ohgt^{Ex2}-gRNA.

Screening by High resolution melt analysis and molecular characterization

The Figure 3.7A shows a workflow to isolate an *ohgt* mutant allele. High resolution melt analysis (HRMA) was chosen as a method to screen mutation holders from candidates. HRMA is a simple, rapid and sensitive method for genotyping that utilizes different melting profiles among double stranded DNA fragments[72]. In brief, PCR is performed using genomic DNAs derived from mutant candidates and a primer pair franking the mutation site. Melt curves of the amplicons are obtained through repetitive denaturing and reannealing processes. Presence of

mutations within the amplicon results in heteroduplexes formation, resulting in different melting profiles from wildtypic homoduplexes.

A primer pair was designed based on the following parameters[72]:

1. Size of the amplicons should be 90-120bp long.

2. The mutation site should locate more than 20bp away from both ends.

3. The annealing temperature should be in the range of 59-61ºC.

Based on the parameters, following primer pairs were designed and obtained:

F: 5'-ATGCCTTCCAAGATCCACTG

R: 5'-TGTCACTGCTGGGATGACTG

Efficiency of the primer pair was confirmed with genomic DNAs derived from the flies carrying a GFP-balancer chromosome (*Dr^{Mio}/TM3-GFP Sb^{1} Ser^{1}*; considered as the control in this experiment) prior to use.

The guide RNA expression vectors were injected into *vasa-Cas9* preblastoderm embryos at 250ng/μL. The embryo microinjection was performed according to the standard protocol. On the next day after injection, hatched larvae were collected and raised on standard stock food at 25ºC until eclosion. The eclosed flies were collected and were independently crossed with the flies carrying a GFP-balancer chromosome. After 5-7 days, the injected animals were sacrificed and homogenized in the squishing buffer (10mM Tris-HCl pH8.2, 1mM EDTA, 25mM NaCl and 1X proteinase K) to obtain their genomic DNAs. HRMA was performed using Precision Melt Supermix reagent (Biorad) according to manufacturer's instructions. F_1 progenies from modification-positive parents were further raised until eclosion, and the latter processes were

repeated in the F_1 generation to assess germline transmission of the targeted modification. Amplicons showing different melt profiles from the control were purified after the agarose gel electrophoresis, and they were inserted into pCRII-TOPO vector (Thermo Fisher) for DNA sequencing.

3.2.7. Phenotypic analyses

To quantify average weight of adult flies, 10 staged animals were pooled in a 1.5mL eppendorf tube and weighed. To quantify pupal length and adult wing area, pupae or wings of indicated genotypes were aligned on apple agar plates or glass plates, and their images were obtained using the Olympus SZ12 binocular and the SIS Analysis 2.1 software. Their length or area was quantified using the ImageJ (National Institute of Health). To quantify cell numbers in the posterior compartment of the wing, numbers of hairs in 10,000μm^2 were counted, since each hair is produced from a single epithelial cell. Number of cells in the compartment was calculated by multiplying the area of the compartment with the cell density (cell number/μm^2).

3.2.8. Developmental timing assay

Embryos of indicated genotypes were collected within 2 hours. After 24 hours, 100 larvae were transferred to fresh apple agar plates with yeast paste (25 larvae per plate). Number of pupae on each plate was counted every 12 hours. Pupariation timing was defined as the time point which more than half of final number of pupae had pupated[73].

3.2.9. Immunohistochemistry and image acquisition

Larvae were raised on an apple agar plate with yeast paste until indicated timing. Washed and dissected larvae were fixed with 4% paraformaldehyde/PBS for 40 minutes at room temperature. The fixed samples were blocked in the PTX buffer (0.3% Triton X-100 in 1X PBS) containing 2% donkey serum (D.S.) for 30 minutes at room temperature. Blocked samples were later incubated in the appropriate primary and secondary antibody solutions (antibody solution in the PTX buffer containing 2% D.S.). The final samples were mounted on glass plates with the Fluoromount-G (SouthernBiotech). The confocal microscope LSM710 (Carl Zeiss) was used for images acquisition.

3.2.10. Clonal analysis

Virgin females of the *hs-FLP CD2GFP* and males of the *UAS-ohgt*^{RNAiv40486} were crossed to obtain progenies with following genotype: *y*, *hs-FLP*/+; *Dicer2*/+; *act-FRT-CD2-FRT-Gal4*, *UAS-GFP/ UAS-ohgt*^{RNAiv40486}. At the indicated timing, the larvae were collected and dissected to prepare immunohistochemical samples as described previously.

3.2.11. Protein extraction

RIPA buffer (50mM Tris-HCl pH7.5, 150mM NaCl, 1% IGEPAL CA-630 (Sigma), 0.5% Sodium deoxycholate, 0.1% SDS) with the cOmplete protease inhibitor cocktails was used for protein extraction unless otherwise mentioned. Prewashed Animals were homogenized in ice-cold RIPA buffer with plastic pestles. Supernatants after centrifugation were transferred to

new eppendorf tubes and were mixed with 5X Laemmli buffer with 10% 2-mercaptoethanol. The mixtures were subsequently heated at 95ºC for 7 minutes to denature proteins.

3.2.12. Western blotting

Western blotting was performed based on the standard protocol, as described in the chapter 2. After the final washing step, the PVDF membranes were treated with the Pierce ECL Western Blotting Substrate or the SuperSignal West Femto Maximum Sensitivity Substrate (both Thermo Fisher) for blotting using the CURIX 60 (AGFA healthcare).

3.2.13. Generating tagged OHGT expression vectors

Coding sequence for full length OHGT with a HA tag at the N-terminus was amplified with the following primer pair (restriction enzyme sites are underlined, the start/stop codons are shown in red):

F: 5'-GGAATTCATGTACCCATACGACGTCCCAGACTACGCTGACGAAGAGGAGAAC

R: 5'-CCGCTCGAGTCATTCCATATCGCTTGAGATC

The digested amplicon was inserted into pUASTattB vector via EcoRI and XhoI sites. The generated plasmid vector was named pUASTattB-HA-OHGT.

3.2.14. Cell culture and transfection

Drosophila Schneider 2 cells (S2 cells) were raised at 25ºC in the Schneider's *Drosophila* medium (Thermo Fisher) containing 10% fetal bovine serum and 1% penicillin-streptomycin.

The Effectene Transfection Reagent (Qiagen) was used for transient transfection of S2 cells. Transfection was performed according to the manufacturer's instructions. The pUASTattB-HA-OHGT was co-transfected with pAct-Gal4 vector to induce expression.

3.2.15. Fractionation of S2 cells

Subcellular fractionation of S2 cells was performed using the NE-PER Nuclear and Cytoplasmic Extraction Reagents (Thermo Fisher) according to the manufacturer's instructions. Protein concentration of each fraction was quantified using the Pierce BCA Protein Assay Kit (Thermo Fischer).

3.2.16. Co-immunoprecipitation

S2 Cells were pelleted and lysed in ice-cold lysis buffer (50mM Tris-HCl pH8.0, 150mM NaCl, 1% IGEPAL CA-630 with the cOmplete protease inhibitor cocktail) by incubating on ice for 15 minutes. The cells were further disrupted using a 20G needle. The lysates were centrifuged at 12,000xg for 10 minutes at 4ºC and supernatants were transferred to new eppendorf tubes. Co-IP was performed using the Protein G sepharose 4 Fast Flow (GE healthcare) according to the manufacturer's instructions.

3.2.17. *In vivo* ubiquitination

S2 cells were treated with MG132 for overnight at final concetration of 25μM. The cells were pelleted and lysed in the harsh lysis buffer (50mM Tris-HCl pH8.0, 150mM NaCl, 1% SDS,

1mM DTT and the cOmplete protease inhibitor cocktail). After vigorous vortex and sonication, the cell lysates were incubated for 30 minutes at 4ºC with constant rotation. After centrifugation at 12,000xg for 10 minutes at 4ºC, diluting buffer (50mM Tris-HCl pH8.0, 150mM NaCl) was added to supernatants to dilute SDS. OHGT immunoprecipitation was performed using the Protein G sepharose 4 Fast Flow and anti-OHGT(1-187) according to the manufacturer's instructions.

3.2.18. mRNA extraction

Approximately 10 animals were used for total mRNA extraction and 15-20 animals for tissue specific mRNA extraction, respectively. mRNA extraction was performed using the Nucleospin RNA kit (Macherey-Nagel). Animals were pooled in screw cap microcentrifuge tubes and were snap frozen by using liquid nitrogen. The animals were homogenized using the Precellys 24 Lysis and Homogenization System (Bertin) in lysis buffer RA1 containing 2-mercaptoethanol. The latter processes were performed according to the manufacturer's instructions. After elution, mRNA concentration was measured and the solution was stored at -80ºC for further use.

3.2.19. cDNA synthesis

QuantiTect Reverse Transcription Kit (Qiagen) was used to digest genomic DNA and to synthesize cDNA. 500ng of the extracted mRNAs was used as templates. The reaction mix was diluted into 5X with distilled water to perform quantitave Real-time PCR (qRT-PCR).

3.2.20. Quantitative Real-time PCR

qRT-PCR was performed using the iQ™ SYBR® Green Supermix and the iQ5 Real-Time PCR detection system (both Biorad) according to the manufacturer's instructions. Each reaction mix was loaded in triplicate, and the average C_T value was used to calculate the expression levels of genes of target via the $-2^{\Delta\Delta CT}$ method. The gene encoding Ribosomal protein L32 (*rp49*) was used as a reference gene.Following primer pairs were used in the experiment:

Gene name[Reference number]	Primer pairs
ohgata (ohgt)[65]	F: 5'-AAGATGCCTTCCAAGATCCAC
	R: 5'-TCGCTTGCTGTGTCGTC
Insulin-like receptor (dInR)[74]	F: 5'-AACAGTGGCGGATTCGGTT
	R: 5'-TACTCGGAGCATTGGAGGCAT
Thor (d4EBP)[74]	F: 5'-CATGCAGCAACTGCCAAATC
	R: 5'-CCGAGAGAACAAACAAGGTGG
Lipase 3 (Lip3)[74]	F: 5'-TGAGTACGGCAGCTACTTCCCT
	R: 5'-TCAACTTGCGGACATCGCT
Acid-labile subunit (dALS)[75]	F: 5'-ATGCGGTGGCTGTCATGTC
	R: 5'-GGCAGCTTACCAAAGGCACTT
Imp-L2 (Imp-L2)[76]	F: 5'-AAGAGCCGTGGACCTGGTA
	R: 5'-TTGGTGAACTTGAGCCAGTCG
Unpaired2 (upd2)[77]	F: 5'-CGGAACATCACGATGAGCGAAT
	R: 5'-TCGGCAGGAACTTGTACTCG

Ribosomal protein 49 (Rp49)[74]	F: 5'-GCTAAGCTGTCGCACAAATG
	R: 5'-GTTCGATCCGTAACCGATGT

3.2.21. *In silico* analyses

SWISS-MODEL service[78] (https://swissmodel.expasy.org/) was used to create the OHGT-Piccolo complex 3D model using the human CRBN-DDB1 complex as the template (PDB 4TZ4[2]). UCSF Chimera[79] (a molecular graphics program developed by the Resource for Biocomputing, Visualization, and Informatics at the University of California, San Francisco (supported by NIGMS P41-GM103311)) was used to reposition the created model to the 4TZ4 model and for image acquisition.

The phylogenetic analysis of CRBN family members was carried out by Bayesian inference (Markov chain Monte Carlo method, Jones amino acid model) using MrBayes[80–82]. Analysis was carried out for eight chains until they converged (average standard deviation of split frequencies: 0.004868; potential scale reduction factor: 1.000; average effective sample size: 2432.32).

Following *in silico* tools were used to predict possible post-translational modification sites and sequence motifs: Expasy Scan Prosite tool[83,84] (to predict myristoylation sites, phosphorylation sites and motifs; http://prosite.expasy.org/scanprosite/); iUbiq-Lys[85,86] (to predict lysine ubiquitination sites; http://www.jci-bioinfo.cn/iUbiq-Lys); GPS-SUMO[87,88] (to predict lysine sumoylation sites and SUMO-interaction motifs; http://sumosp.biocuckoo.org/); PSORT II Prediction (to predict subcellular localization; http://psort.hgc.jp/form2.html); NucPred[89] (to

predict nuclear localization of a protein; http://www.sbc.su.se/~maccallr/nucpred/). The latter two programs predict subcellular localization of a protein based on the percentage of basic amino acids and similarity to other known nuclear proteins.

3.2.22. Statistics

Mann-Whitney *U* test was performed to calculate *p* values for (C) to (F) of the Figure 3.11. Student's *t* test was performed to calculate *p* values for other experiments. * indicates $p<0.05$, and ** indicates $p<0.01$.

3.3. Results

3.3.1. The *Drosophila CG3925* gene encodes the putative CRBN family member

CRBN homologs are evolutionary conserved from vertebrates to invertebrates as indicated by phylogenetic analysis (Figure 3.1A). Most proteins are relatively distant from each other, as mammalian proteins seem to have split off early and large set of modification between the protein of *C. elegans* and those of insects exist. Even within the insects, the *Drosophila* proteins are remote from those of other insect species. In particular, N-terminal regions of the proteins differ greatly, suggesting that their functions may differ to some extent.

According to the Flybase, a database of *Drosophila* Genes and Genomes (http://flybase.org/), there is a single annotated homolog of human *CRBN* named *CG3925* in *Drosophila* genome. *CG3925* is located on 85F8, chromosome 3R (10,049,199 to 10,051,527). The gene consists of five exons, which encompasses approximately 2.3kbp (Figure 3.1B). An annotated transcript is expected to encode a putative protein (CG3925-PA) consisting of 585 amino acid residues with a theoretical molecular weight of 66.5kDa.

Protein Sequences alignment by using the Protein Basic Local Alignment Search Tool (Protein BLAST) identified that the two functional domains (a central LON domain and a C-terminal Thal-BD) may be conserved in CG3925-PA (Figure 3.1C; amino acid residues 234 to 414 show 24% identity, and amino acid residues 453 to 555 show 44% identity to corresponding regions in human CRBN, respectively), whereas the N-terminal region show no identity. Further analysis using *in silico* tools identified potential post-translational modification sites for phosphorylation, ubiquitination, myristoylation and sumoylation (Figure 3.1D).

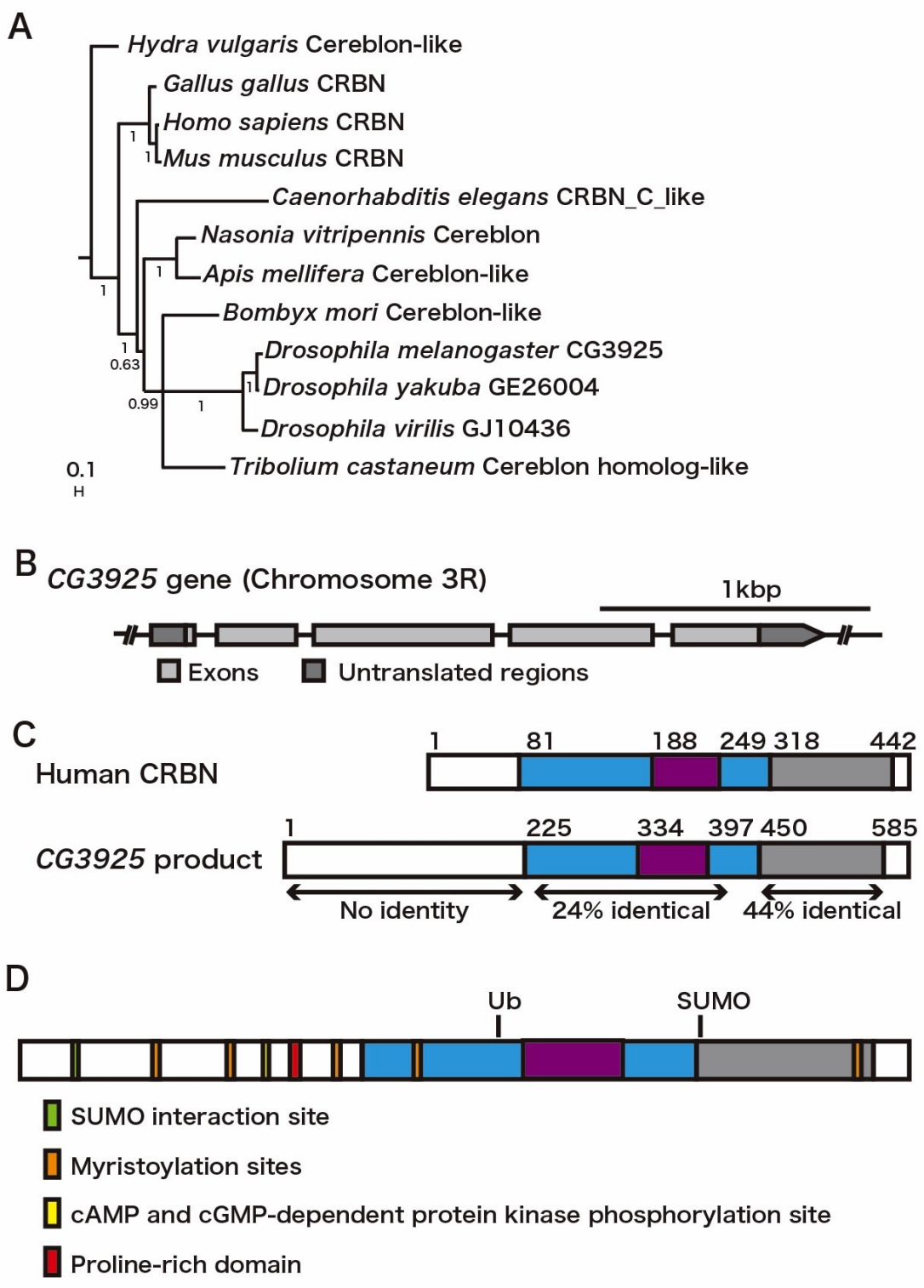

Figure 3.1. The *Drosophila CG3925* gene encodes a putative CRBN homolog.

(A) Phylogenetic tree of CRBN family proteins. Depicted values indicate posterior probabilities.

The scale bar represents branch length. (B) A scheme representing *CG3925* gene locus. Exons and untranslated regions are indicated as filled boxes (light gray and dark gray, respectively). The scale bar represents 1kbp. (C) Schemes representing human CRBN and its *Drosophila* homolog CG3925-PA. The LON domain, the DDB1-binding motif and the Thalidomide-binding domain are indicated as filled boxes (cyan, purple and light gray, respectively). Amino acid identities of the corresponding regions are noted. (D) A scheme representing potential post-translational modification sites identified by *in silico* tools. Following post-translational modification sites and a motif is shown in the figure: a SUMO interaction site (aa34-38); 5 myristoylation sites (aa87-92; 136-141; 206-211; 259-264; 549-544); a cAMP and GMP-dependent protein kinase phosphorylation site (aa160-163); a ubuiquitination site (K315); a sumoylation site (K488); a proline-rich region (aa177-189). A region resembling part of the atrial natriueretic peptide (aa161-192) and a *C. elegans* Her-1-like stretch (aa440-459) were also predicted (not shown in the figure). The figures are reprinted from the Figure 1B and the Figure 2A of Wakabayashi *et al.,* 2016[65]. The phylogenetic tree was generated in collaboration with A. Voelzmann.

3.3.2. Generating antibodies against *Drosophila* CRBN

In order to generate CG3925-PA-specific antibodies, two immunogens were designed (Figure 3.2). One immunogen consists of an N-terminal fragment of the CG3925-PA (amino acid residues 1 to 187) and a GST tag at the N-terminus (referred to as GST-OHGT(1-187)) expressed and purified from BL21(DE3) *E. coli* (Figure 3.3). Another immunogen is a synthetic polypeptide consists of amino acid residues 15 to 33 of the CG3925-PA with KLH protein covalently attached to the C-terminus via a cysteine residue (referred to as OHGT(15-33)-Cys-KLH).

Polyclonal antibodies were affinity purified from antisera using the prepared affinity columns. IgGs were successfully purified from both rabbit and guinea pig antisera (Figure 3.4). Specificity of the affinity purified-antibodies was confirmed by western blotting using mutant flies generated by targeted mutagenesis (see Figure 3.7E,F).

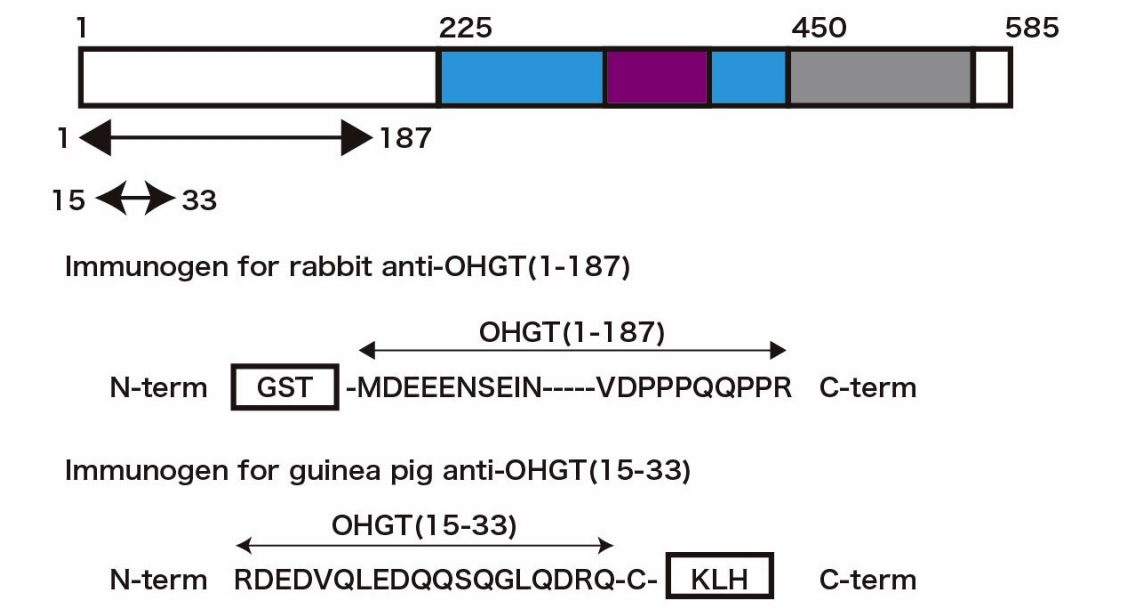

Figure 3.2. Designing immunogens. To generate CG3925-PA-specific antibodies, two immunogens were designed as represented. GST: Glutathione S-transferase; OHGT(1-187): amino acid residues 1 to 187 of CG3925-PA; OHGT(15-33): amino acid residues 15 to 33 of CG3925-PA; KLH: Keyhole Limpet Hemocyanin. The figures are reprinted from the Figure 1B of Wakabayashi *et al.,* 2016[65].

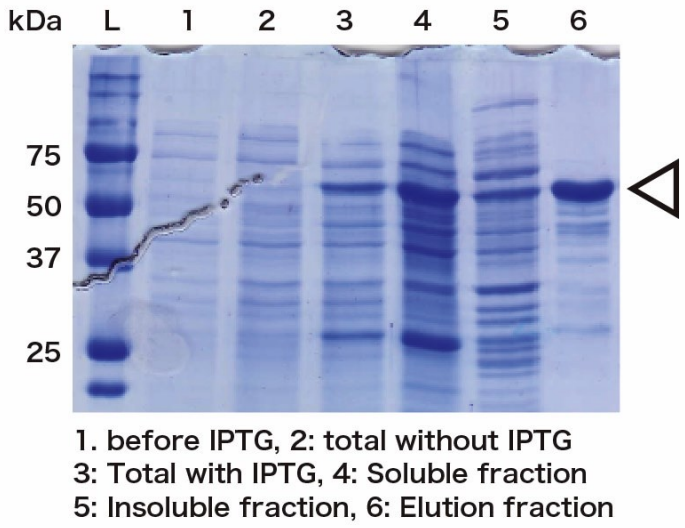

Figure 3.3. Expression and purification of GST-OHGT(1-187). The BL21(DE3) *E. coli* was transformed with pGEX-OHGT(1-187) and GST-OHGT(1-187) expression was induced by IPTG treatment. Each fraction was loaded to SDS-PAGE gel. The expressed protein of approximately 50kDa is indicated with an unfilled triangle.

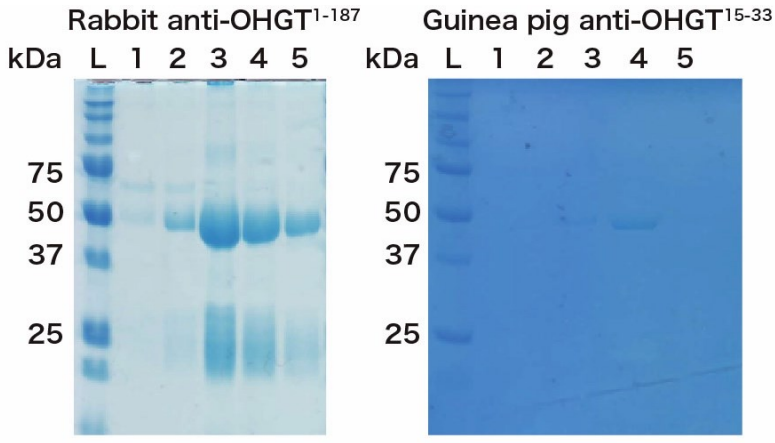

Figure 3.4. Purification of anti-OHGT antibodies. Each eluate fraction was loaded to SDS-PAGE gel to confirm the abundance of IgGs.

3.3.3. Generating a *CG3925* mutant line by CRISPR-Cas9 genome editing technology

To investigate whether loss of *CG3925* affects *Drosophila in vivo*, a genome editing technology called Clustered Regularly Interspaced Short Palindromic Repeats (CRISPR)-Cas9 system was applied. This system utilizes RNA-guided DNA endonuclease Cas9 from the type II bacterial adaptive immune system[90,91]. The Figure 3.5 shows an overview of the CRISPR-Cas9 mediated targeted mutagenesis. In presence of guide RNA (a chimeric RNA consists of a sequence complementary to the genomic target site and a common sequence that is responsible for interaction with Cas9), Cas9 is recruited to the genomic region complementary to the guide RNA sequences. Cas9 induces double-stranded break three nucleotides before a specific motif called protospacer adjacent motif (PAM) sequence. This breakage activates an endogenous repair mechanism called nonhomologous end-joining. Since nonhomologous end joining often causes random indels insertion, leading to cause frameshift mutation or premature stop codon formation.

To utilize CRISPR-Cas9 to generate *CG3925* mutant allele, a 20bp sense sequence within the exon 2 was chosen as the target site (Figure 3.6). Since the putative domains are transcribed by the exon 3 to 5, frameshift or nonsense mutation at the target sequence is expected to result in a strong allele or even a null allele.

Flies with a mutant allele were successfully recovered from the mutagenesis approach (Figure 3.7A-D). Molecular characterization revealed that two nucleotides before the predicted cleavage site by Cas9 were deleted (Figure 3.6). The loss of the nucleotides will cause a frameshift mutation from the exon 2, leading to express a truncated protein with only 15% of

the wild type protein (amino acid residues 1 to 84 of the wild type protein plus 7 amino acid residues caused by the frameshift (RGQSSQQ)). Since animals with this mutant allele showed overgrowth phenotype (see below), the gene was named *ohgata* (meaning "large" in Japanese; abbreviated as *ohgt*), and the generated mutant allele was named $ohgt^{Ex2}$.

Next, expression of the gene's product (Ohgata; abbrevaited as OHGT) was confirmed by western blotting. Total lysates of *w**, homozygous $ohgt^{Ex2}$ ($ohgt^{Ex2/Ex2}$) and transheterozygous $ohgt^{Ex2}/ohgt^{Df}$ ($ohgt^{Ex2}$ over a Deficiency, referred to as $ohgt^{Ex2/Df}$) third instar larvae were subjected to western blotting with the two independent polyclonal antibodies against OHGT. OHGT protein of approximately 75kDa could neither be detected from $ohgt^{Ex2/Ex2}$ nor $ohgt^{Ex2/Df}$ larvae (Figure 3.7E,F), suggesting that endogenous OHGT protein is missing in the $ohgt^{Ex2}$ mutant animals. It is worth noting that the putative mutant protein (theoretical molecular weight: 10kDa) could not be detected from the mutants (Figure 3.7F).

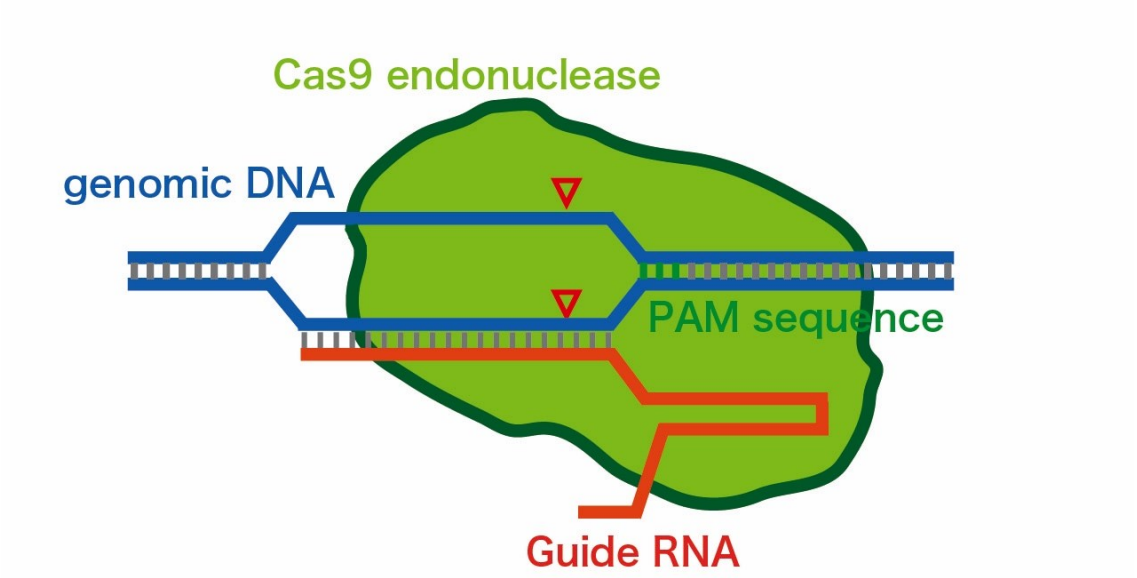

Figure 3.5. CRISPR-Cas9. A scheme represents CRISPR-Cas9-mediated genome editing.

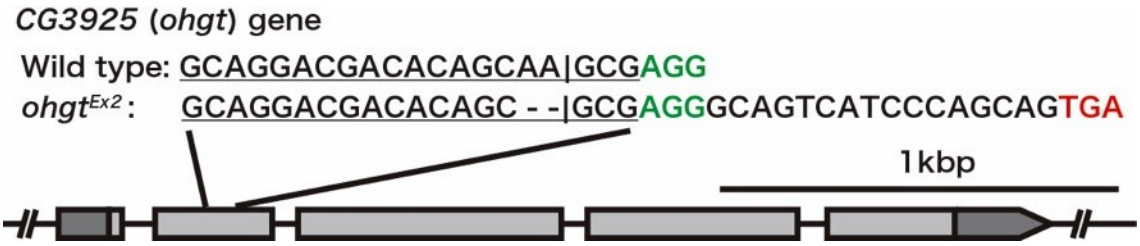

Figure 3.6. Targeting *ohgata* gene by CRISPR-Cas9. The scheme represents *ohgt* gene locus and a target site for CRISPR-Cas9-mediated targeted mutagenesis. A 20bp-long target site (underlined in the figure) was chosen. The vertical bar indicates the expected cleavage site. The protospacer adjacent motif (PAM) sequence and the premature stop codon formed by the mutagenesis are shown in green and red, respectively. The figure is reprinted from the Figure 2A of Wakabayashi *et al.,* 2016[65].

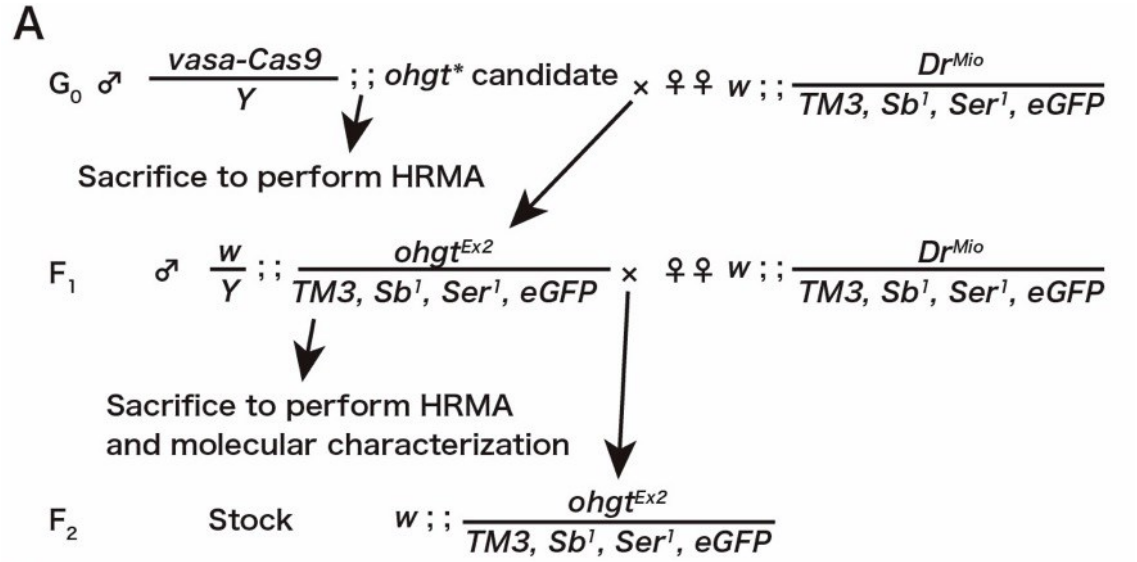

B

Concentration (ng/μL)	Embryos injected	Larvae survived (%)	Flies eclosed (%) (♂,♀)	Candidates (%) (♂,♀)	Germline transmission
250ng/μL	179	7 (3.9%)	2 (1.1%) (2,0)	1 (0.6%) (1,0)	Yes

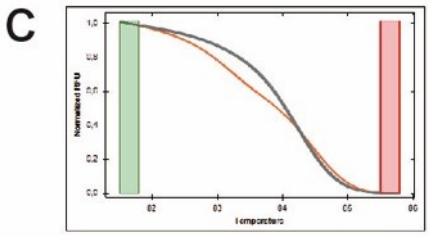

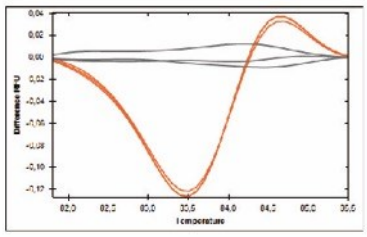

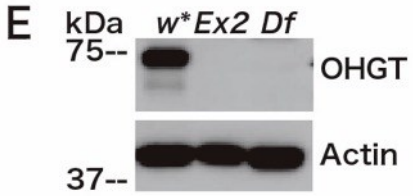

Figure 3.7. Mutagenesis screening by High resolution melt analysis. (A) The diagram

represents a workflow to establish a fly line with the *ohgt*^{Ex2} mutant allele. (B) The table shows an overview of the CRISPR-Cas9 mediated mutagenesis. Concentration of plasmid solution, number of injected embryos, number of survivors after injection, number of eclosed flies and number of the positive candidate after first HRMA screening were noted. (C) The figure shows melting temperatures of a F_1 progeny (orange curve; genotype: *ohgt*^{Ex2}*/TM3,Sb*^{1}*,Ser*^{1}*,eGFP*) and the control (gray curve: genotype: *Dr*^{Mio}*/TM3,Sb*^{1}*,Ser*^{1}*,eGFP*). (D) The figure shows difference in relative fluorescence unit (RFU) between the F_1 progeny and the control shown in (C). (E) Protein lysates from *w**, homozygous *ohgt*^{Ex2} (*Ex2*) and transheterozygous *ohgt*$^{Ex2/Df}$ (*Df*) third larvae were subjected for western blotting with rabbit anti-OHGT(1-187). (F) Western blotting was performed identically as (E) but with guinea pig anti-OHGT(15-33). The figures are reprinted from the Figure 2B-E of Wakabayashi *et al.,* 2016[65].

3.3.4. The *ohgata* mutants show overgrowth phenotype

The $ohgt^{Ex2/Ex2}$ animals were raised to search for associated phenotypes. The $ohgt^{Ex2/Ex2}$ animals were viable, as 79% of the mutants reached to adult stage when raised on standard fly food (83% of *w** reached to adult stage in the same condition). During larval stage, amount of yeast intake was comparable to the control larvae (Figure 3.8A). Even though 30% showed a 12-hour delay to pupate, pupariation timing of majority of the mutant animals was comparable to the control animals (Figure 3.8B). Moreover, both $ohgt^{Ex2/Ex2}$ males and females were fertile, indicating that altered *ohgt* expression does not perturb reproduction. In all developmental stages, the body proportions of the mutant animals looked normal.

Surprisingly, the adult $ohgt^{Ex2/Ex2}$ flies were larger than the control flies (Figure 3.9A). The $ohgt^{Ex2/Ex2}$ male flies were significantly heavier (Figure 3.9B) and the wing area was significantly larger (Figure 3.9C) compared to the control. Significant increase of cell number in the posterior compartment of the wing was also observed (Figure 3.9D), suggesting that the growth phenotypes is in part due to increase in cell number. Female flies exhibited similar phenotypes (data not shown), suggesting that the growth phenotype is independent of gender. The $ohgt^{Ex2/Df}$ animals showed a slightly enhanced phenotype, indicating that the $ohgt^{Ex2}$ is a strong allele (although probably not a null) and the phenotype is not due to off-target effects of the CRISPR-Cas9 mediated mutagenesis. The enlarging phenotype was already obvious in pupal stage, as length of the two mutants were significantly longer compared to the control pupae (Figure 3.9E,F). Altogether, these results suggest that impairment of *ohgt* results in larger body and organ size associated with increased cell number.

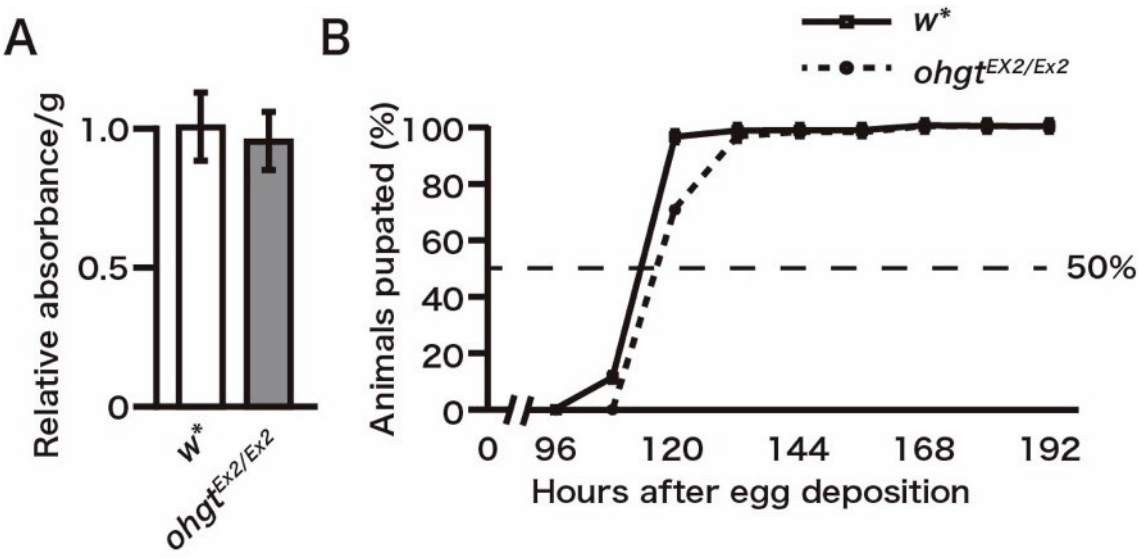

Figure 3.8. Feeding behavior and develop timing of the *ohgt* mutants are comparable to the control. (A) Relative yeast intake of *w** and $ohgt^{Ex2/Ex2}$ 3rd instar larvae. (B) Number of pupae of each genotype was counted every 12 hours. The experiment was repeated for five times (100 larvae for each genotype per experiment). The figures are reprinted from the Figure 3A and C of Wakabayashi *et al.,* 2016[65].

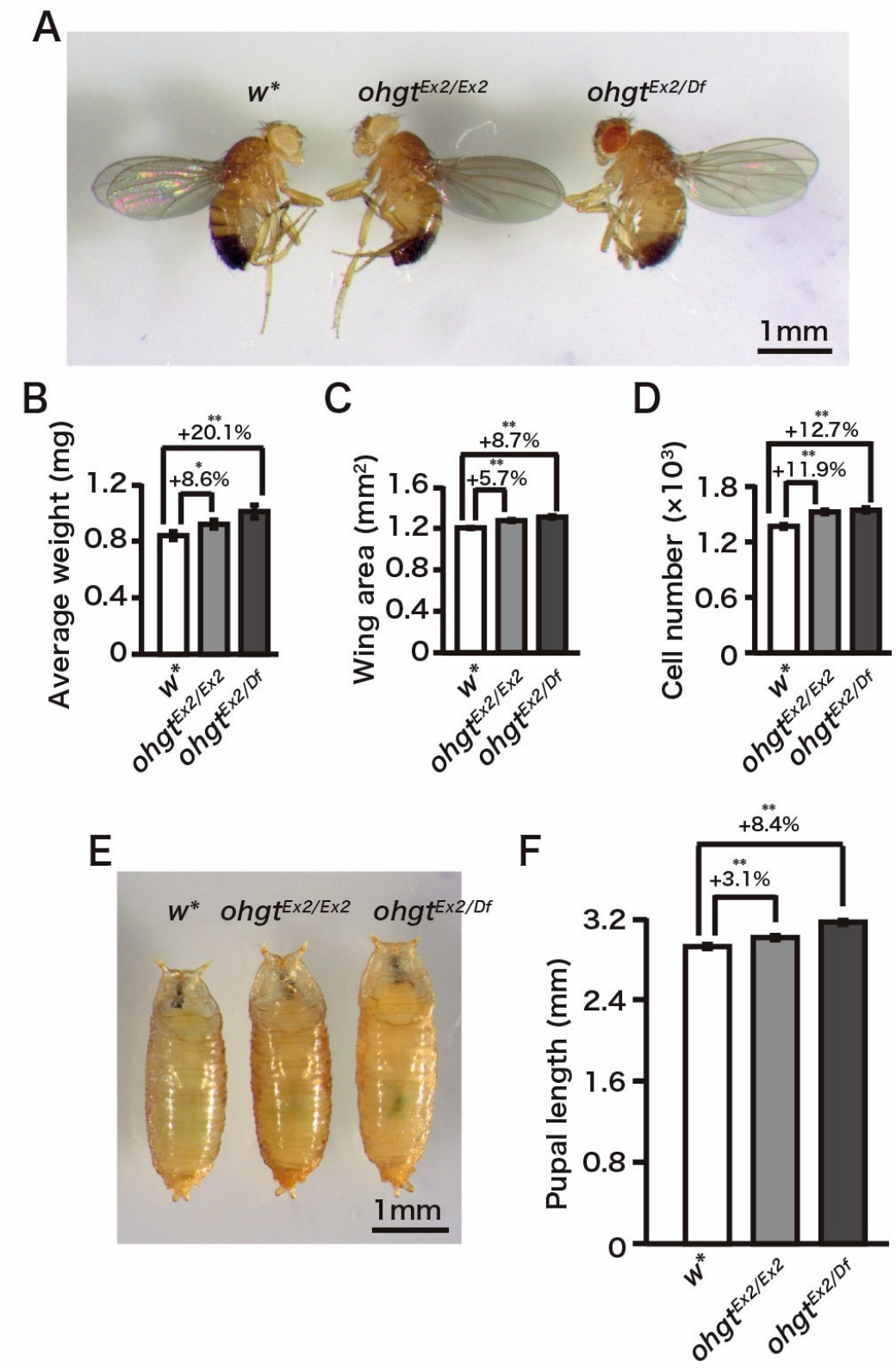

Figure 3.9. The *ohgt* mutants show overgrowth phenotype associated with increased cell

number. (A) *w**, $ohgt^{Ex2/Ex2}$ and $ohgt^{Ex2/Df}$ adult male flies. The scale bar represents 1mm. (B) Average weights of 3-7 days old *w**, $ohgt^{Ex2/Ex2}$ and $ohgt^{Ex2/Df}$ adult male flies. Flies were weighed in batch of 10 (n=10). (C) Average wing areas of *w**, $ohgt^{Ex2/Ex2}$ and $ohgt^{Ex2/Df}$ adult male flies (n=30). (D) Average cell number in the posterior compartment of the wing of *w**, $ohgt^{Ex2/Ex2}$ and $ohgt^{Ex2/Df}$ adult male flies (n=30). (E) *w**, $ohgt^{Ex2/Ex2}$ and $ohgt^{Ex2/Df}$ pupae. The scale bar represents 1mm. Animals whose length is the closest to the average was chosen from each genotype. (F) Average body length of *w** (n=66), $ohgt^{Ex2}$ (n=80) and $ohgt^{Ex2/Df}$ (n=73) pupae. The figures are reprinted from the Figure 3B, D-H of Wakabayashi *et al.,* 2016[65].

3.3.5. The gene's product OHGT is expressed in the larval fat body

Body size and its proportion are determined by genetic factors, as well as environmental factors during development such as nutrients, temperature, population density and presence of pathogens. Metazoans utilize the conserved insulin/insulin-like growth factor signaling (IIS) pathway to couple body size with extrinsic cues[92].

Genetic studies using *Drosophila* made significant contributions to understand a genetic program growth in multicellular organism including insulin-like signaling (ILS)[93,94]. *Drosophila* genome contains eight genes encoding insulin-like peptides (DILPs) that function as ligands of a common Insulin-like receptor (dInR). Activation of dInR by DILPs initiates a signal cascade that resembles the mammalian IIS pathway, consists of components such as phosphoinositide 3-kinase (dPI3K), serine-threonine kinase dAkt, and forkhead transcription factor dFOXO[93,94]. Genetic defects or manipulation of the pathway's component results in altered cell size and cell number, leading to altered body and organ size[74,95–97].

The insulin-producing cells (IPCs) are the major production and secretion sites of DILPs. The IPCs are the symmetric clusters of seven neurosecretory cells located in each brain hemispheres[96,98]. The IPCs produce and secrete at least four DILPs (DILP1, 2, 3 and 5), and ablation of these cells results in small adults, just like mutants of genes encoding ILS components[98].

The fat body, the functional analog of mammalian liver and adipose tissue, is another organ that plays versatile roles in systemic ILS regulation[94]. The larval fat body produces DILP6, the *Drosophila* homolog of mammalian IGF1, to regulate post-feeding growth[99,100]. Also the

organ was identified as the primary nutrient sensor, which produces and secretes numerous humoral factors into haemolymph (circulating fluid in *Drosophila*) upon changes in nutrient conditions[101,102]. Fat body-derived factors with variety of functions in the context of ILS regulation have been described[75,77,99,100,103–107].

To confirm whether the product of *ohgt* (Ohgata; OHGT) is expressed in the major growth regulating sites, immunohistochemical analysis was performed using the OHGT-specific antibody. First the IPCs were visualized using an IPCs-specific *Gal4* driver line (*dilp2-Gal4*) and a line that expresses GFP under the control of the upstream activating sequence (UAS) (*UAS-GFP.nls*). OHGT was not detected from the GFP positive cells (Figure 3.10A,B), suggesting that it is not expressed in the larval IPCs. On the other hand, OHGT was prominently expressed in the fat body (Figure 3.10C,D). The signal observed in the wildtypic fat body was strongly reduced in those of the $ohgt^{Ex2/Df}$ (Figure 3.10E,F) and *ohgt* RNAi-induced clones (Figure 3.11A-F). These results indicate that endogenous OHGT protein is indeed localized in fat body cells. Of note, OHGT was almost exclusively present in the nucleus (Figure 3.10C,D), which is consistent with results from subcellular fractionation of S2 cells (Figure 3.12) and bioinformatic prediction algorithms for proteins subcellular localization including the Reinhardt NCNN algorithm and NucPred (data not shown). The subcellular location of OHGT was not dramatically changed either in nutrient scarce condition or in other developmental timings (data not shown). These results indicate that OHGT is a nuclear protein in fat body cells.

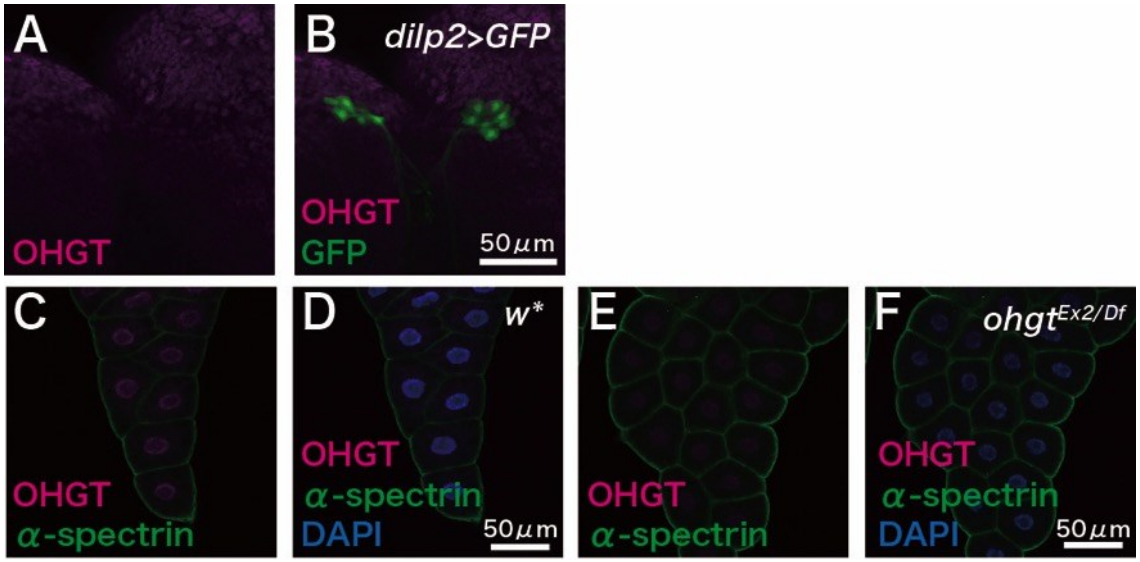

Figure 3.10. OHGT is expressed in larval fat body cells but not in the IPCs. (A,B) OHGT was co-immunostained along with GFP expressed in the IPCs of *dilp2>GFP* third instar larvae. (C,D) OHGT was co-immunostained along with a plasma membrane marker α-spectrin in the fat body of *w** third instar larvae. (E,F) OHGT was co-immunostained along α-spectrin in the fat body of $ohgt^{Ex2/Df}$ third instar larvae. All scale bars represent 50μm. Rabbit anti-OHGT(1-187) was used in all experiments. The figures are reprinted from the Figure 4A-F of Wakabayashi *et al.,* 2016[65].

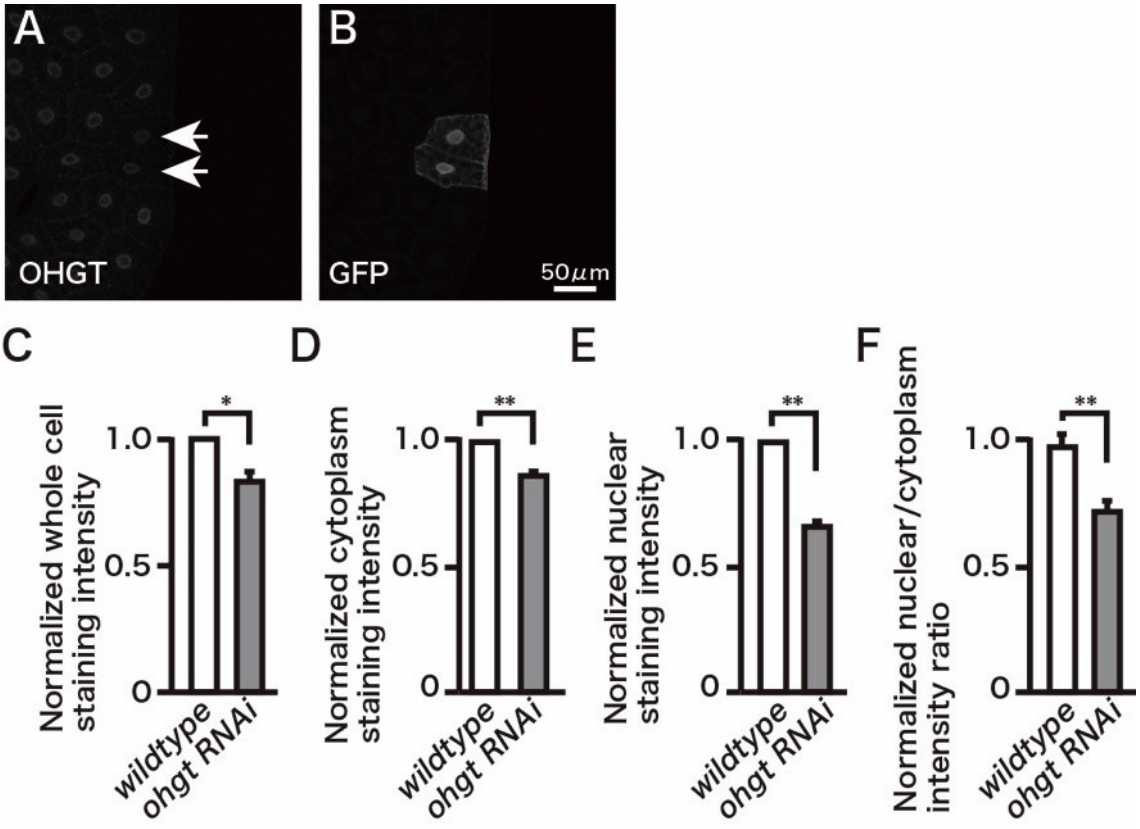

Figure 3.11. Expression of OHGT is reduced upon *ohgt* RNAi induction. (A,B) Co-immunostiaining of OHGT and GFP after clonal *ohgt* RNAi induction in fat body cells of third instar larvae. GFP-positive cells (pointed by the arrows in the panel A) are *ohgt* RNAi induced clonal cells and GFP-negative cells are wild type clonal cells. The scale bar represents 50μm. Rabbit anti-OHGT(1-187) was used in this experiment. (C-F) Normalized staining intensities of OHGT in whole cell (C), the cytoplasm (D), the nucleus (E) as well as nuclear to cytoplasm ratio of wild type clonal cells (n=34) and *ohgt* RNAi induced clonal cells (n=17). Error bars indicate S.E.M. * indicates $p<0.05$ and ** indicates $p<0.01$, respectively. *P* values were calculated by Man-Whitney *U* test. The figures are reprinted from the Figure 4G-L of Wakabayashi *et al.,* 2016[65].

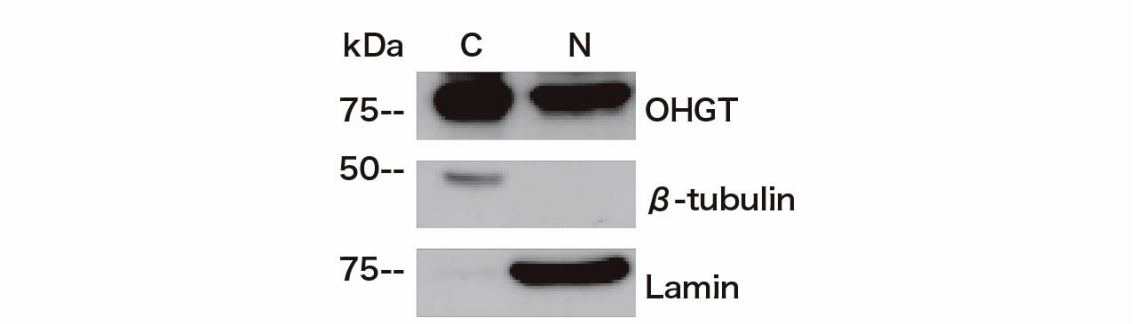

Figure 3.12. Subcellular fractionation of S2 cells. S2 cells were fractionated into the cytoplasmic and the nuclear fractions. Equal amounts of proteins from the cytoplasmic (C) and the nuclear (N) fractions were subjected to western blotting with antibodies against the indicated proteins.

3.3.6. Loss of *ohgata* in the fat body is sufficient to phenocopy the growth phenotype of the mutants

To address whether OHGT in the fat body is involved in growth regulation, males of an *ohgt* RNAi line (v40486 from the Vienna *Drosophila* Resource center; referred to as *UAS-ohgt*^{RNAiv40486}) were crossed with virgin females of a fat body *Gal4* driver line (*Cg-Gal4*) to obtain progenies with reduced *ohgt* expression in the fat body (referred to as *Cg>ohgt*^{RNAiv40486}). First, *ohgt* transcript level in the *Cg>ohgt*^{RNAiv40486} third instar larvae were quantified by qRT-PCR. In the fat body, *ohgt* transcript was reduced by about 80%, whereas it was not altered in the carcass (larval bodies after fat body removal) (Figure 3.13). This result indicates that *ohgt* expression is strongly reduced only in the fat body of *Cg>ohgt*^{RNAiv40486} larvae.

Next, *Cg>ohgt*^{RNAiv40486} animals were raised along with the control animals (*Cg>w**). As expected, *Cg>ohgt*^{RNAiv40486} animals showed overgrowth phenotype similar to those of the *ohgt* mutants. They showed significant increase in pupal length (Figure 3.14A,B), as well as in adult weight (Figure3.14D) and in wing area (Figure3.14E). Increase of wing area suggests that OHGT in the fat body regulates size of other organs non-cell autonomously to some extent. Using another *ohgt* RNAi line (NIG3925R-3 from National Institute of Genetics; referred to as *UAS-ohgt*^{RNAiNIG3}) or a different fat body *Gal4* driver line (*FB-gal4*) resulted in larger pupae (Figure 3.14B), suggesting that the observed growth phenotypes are in part due to the reduction of *ohgt* in the fat body. These results point out an organ-specific function of OHGT to regulate organismal growth.

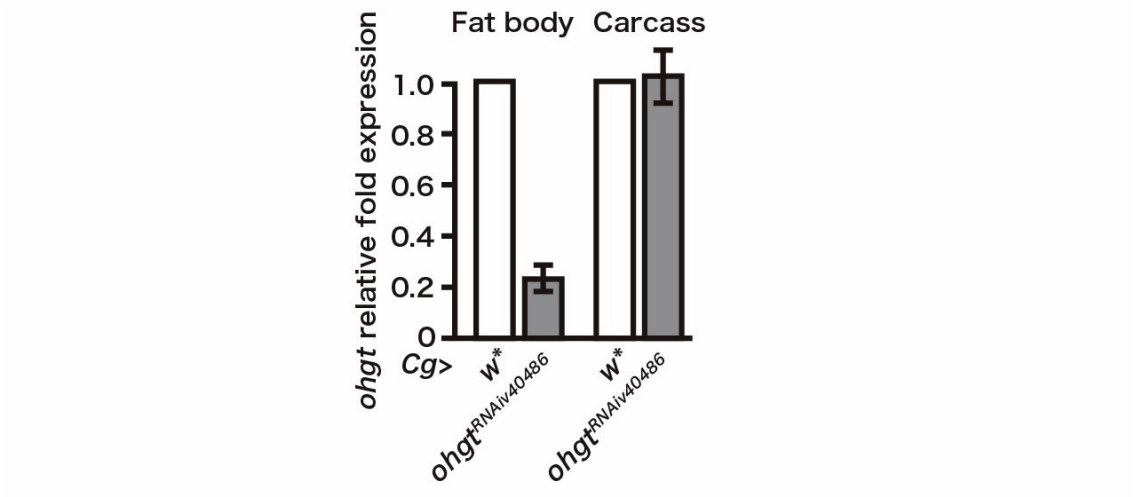

Figure 3.13. *ohgt* is reduced upon RNAi induction in the fat body. Transcript level of *ohgt* in the fat body and the carcass of 72h AED *Cg>w** and *Cg>ohgt*^{RNAiv40486} larvae (n=4). The figures are reprinted from the Figure 5A of Wakabayashi *et al.,* 2016[65].

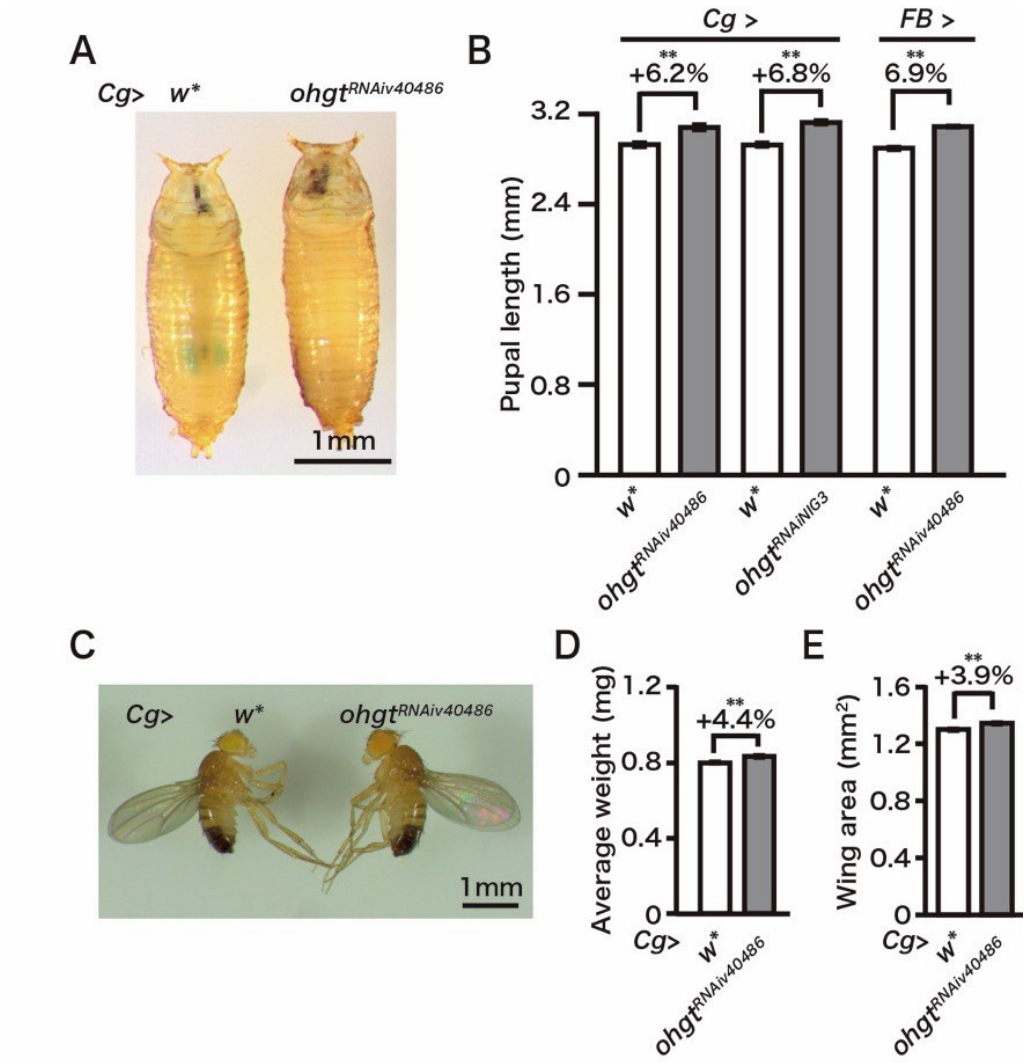

Figure 3.14. *Cg>ohgt*^{RNAiv40486} animals phenocopy the *ohgt* mutant phenotypes. (A) *Cg>w** and *Cg>ohgt*^{RNAiv40486} pupae. An animal whose body length is closest to the average was used for image acquisition. The scale bar represents 1mm. (B) Average body length of *Cg>w** (n=48) versus *Cg>ohgt*^{RNAiv40486} (n=66); *Cg>w** (n=40) versus *Cg>ohgt*^{RNAiNIG3} (n=48); *FB>w** (n=48) versus *FB>ohgt*^{RNAiv40486} (n=52). (C) *Cg>w** and *Cg>ohgt*^{RNAiv40486} adult male flies. The scale bar represents 1mm. (D) Average weight of *Cg>w** and *Cg>ohgt*^{RNAiv40486} adult male flies (n=8). (E) Average wing area of *Cg>w** and *Cg>ohgt*^{RNAiv40486} adult male flies (n=20). The figures are reprinted from the Figure 5B-F of Wakabayashi *et al.,* 2016[65].

3.3.7. Loss of *ohgata* leads to elevated insulin-like signaling

The observed phenotypes of $ohgt^{Ex2}$ mutants were reminiscent to animals associated with high ILS activity[75,95,104]. In order to investigate whether altered loss of *ohgt* is associated with altered ILS activity, expression level of phosphorylated dAkt was analyzed. Since Akt gets phosphorylated under high ILS activity[108] (Figure 3.15), level of phosphorylated Akt is an experimental readout for activity of the signaling pathway. Total protein lysate of $ohgt^{Ex2/Ex2}$ third instar larvae was subjected to western blotting with phsopho-Akt specific antibody and found that phospho-dAkt level in the $ohgt^{Ex2/Ex2}$ larvae was indeed higher than in control larvae (Figure 3.16A), suggesting that ILS is elevated in the *ohgt* mutants. The major role of Akt is to phosphorylate transcription factor FOXO, resulting in its retention in the cytoplasm[109]. Downregulation of ILS allows dFOXO to shuttle into the nucleus, promoting expression of its target genes[97] (Figure 3.15). To confirm dFOXO's activity in the $ohgt^{Ex2/Ex2}$ mutants, expression levels of two dFOXO target genes, *d4EBP* and *dInR*, were quantified by qRT-PCR. Consistent with increased phospho-dAkt level, the two target genes were downregulated in $ohgt^{Ex2/Ex2}$ mutant larvae compared to the control animals (Figure 3.16B). Increased level of phospho-dAkt and downregulated *d4EBP* (but not *dInR*) were also observed upon *ohgt* inhibition in the fat body (Figure 3.16C,D). Along with the previous phenotypic data, these results lead to a conclusion that OHGT in the fat body negatively regulates organismal growth via ILS.

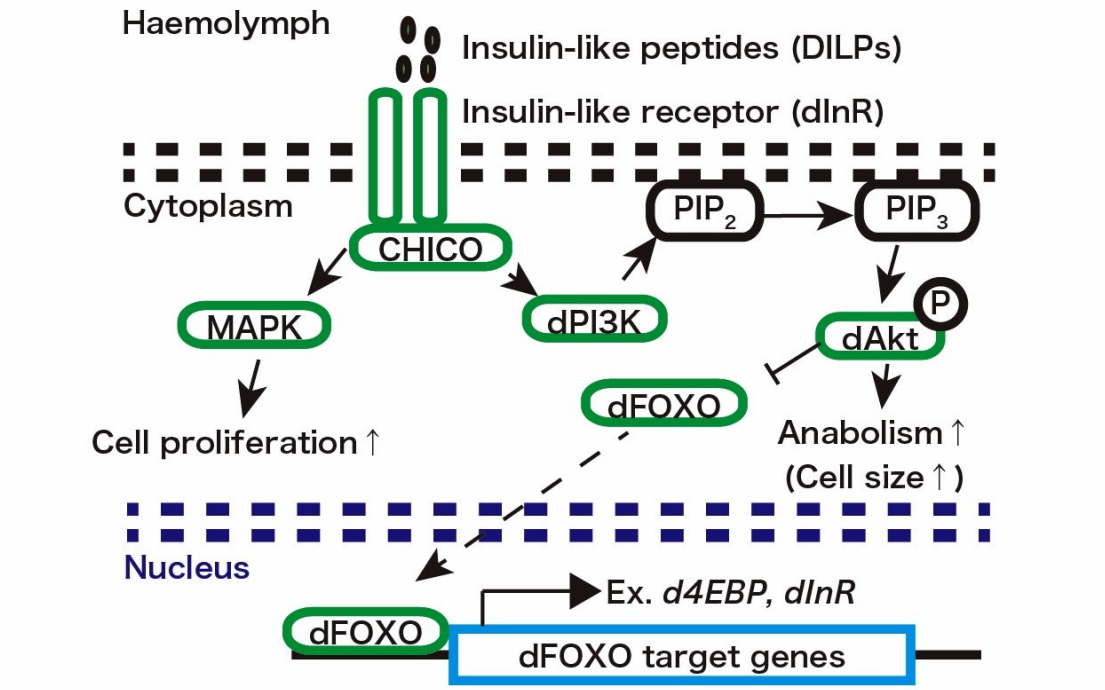

Figure 3.15. *Drosophila* insulin-like signaling. The diagram shows a simplified signal cascade of *Drosophila* ILS. Circulating DILPs interacts with a common dInR to stimulate downstream components including dPI3K, dAkt and dFOXO. Activated dInR also stimulates MAPK pathway in distinct manner.

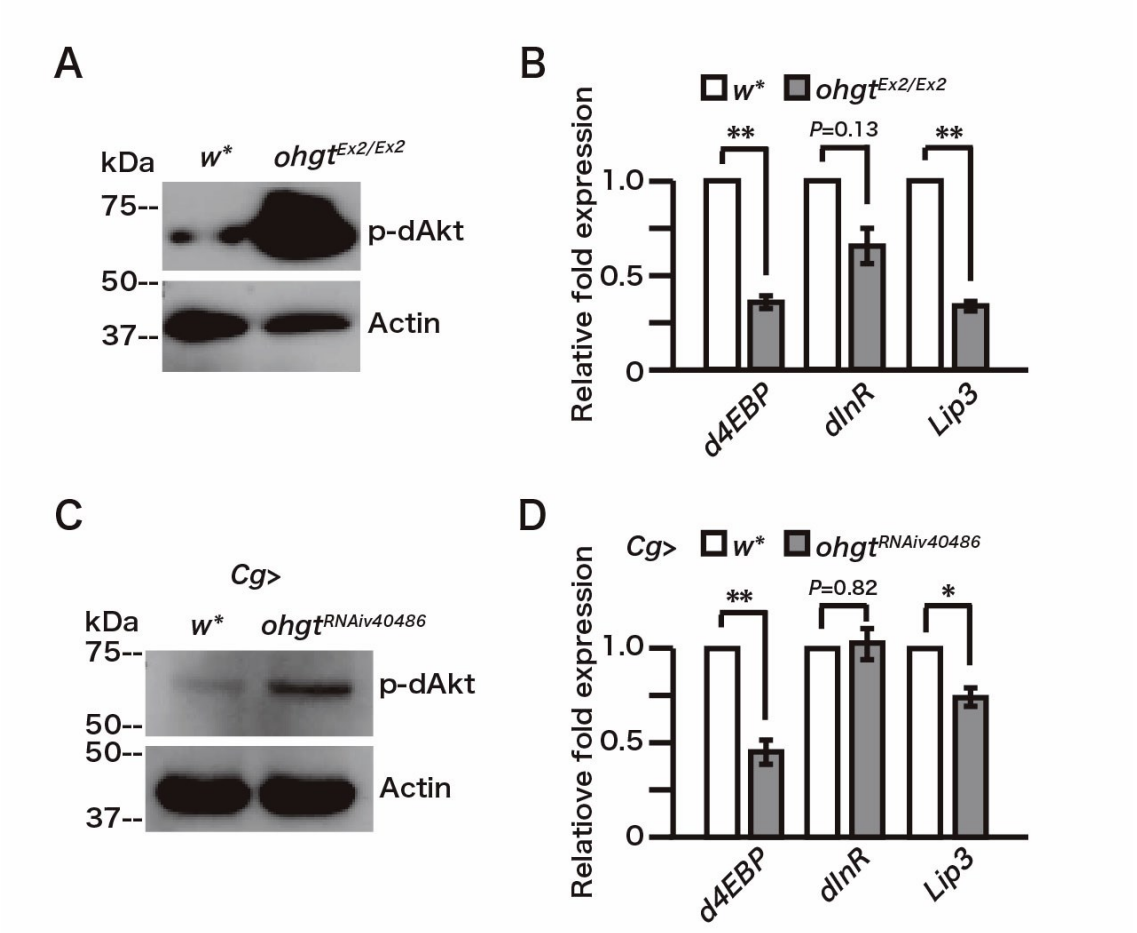

Figure 3.16. Loss of *ohgt* is associated with elevated ILS. (A) Total protein lysates of *w** and $ohgt^{Ex2/Ex2}$ 72h AED larvae were subjected to western blotting with phospho-Akt specific antibody (the experiment was performed more than three times). (B) Transcript levels of two dFOXO target genes, *d4EBP* and *dInR*, in *w** and $ohgt^{Ex2}$ 72h AED larvae (n=4). (C) Protein lysates of *Cg>w** and *Cg>*$ohgt^{RNAiv40486}$ 72h AED larval carcasses were subjected to western blotting with phospho-Akt specific antibody (the experiment was performed in triplicate). (D) Transcript levels of *d4EBP* and *dInR*, in *Cg>w** and *Cg>*$ohgt^{RNAiv40486}$ 72h AED larval carcasses (n=4). The figures are modified from the Figure 6A-D of Wakabayashi *et al.,* 2016[65].

3.3.8. Loss of *ohgata* alters expression of genes encoding DILPs' cofactors

The fat body is an endocrine organ that produces and secretes humoral proteins in response to changes in nutrient conditions[101,102] (Figure 3.17). Among those, there are some proteins that interact with DILPs after their release into haemolymph. Acid labile subunit (dALS)[75] and Imaginal morphogenesis protein-Late 2 (IMP-L2)[104] are the two DILPs-interacting proteins that have been described in *Drosophila*. In circulation, dALS and IMP-L2 forms a heterotrimeric complex with DILP2 or DILP5 to suppress them from interacting with peripheral dInR[75,104]. During larval stage, dALS is produced in the IPCs and in the fat body, thereby antagonizing DILPs in growth control as well as carbohydrates and lipids metabolism[75]. IMP-L2 is already present in the cellular blastoderm stage and can be observed in several cell types throughout development[110]. It was identified as a protein counteracting hyperplasia induced by *dInR* overexpression, and its loss results in larger body size and enhanced vulnerability to starvation[104]. Another studies demonstrated that IMP-L2 is secreted from malignant tumors to reduce ILS in proximal tissues, resulting in loss of the organs known as organ-wasting[76,111]. Thus, these two proteins are proposed as circulating DILPs antagonists in *Drosophila*.

To investigate whether reduction of *ohgt* affects expression levels of genes encoding the DILPs cofactors, qRT-PCR was performed using cDNAs synthesized from total $ohgt^{Ex2/Ex2}$ third instar larvae and cDNAs synthesized from the fat body of $Cg>ohgt^{RNAiv40486}$ third instar larvae. Intriguingly, *Imp-L2* was reduced only in the total fraction, whereas *dALS* was reduced in both total and the fat body specific fractions (Figure 3.18A,B). *unpaired 2* (*upd2*), one of

the genes encoding DILPs secretion promoting factors, was not altered in both genetic conditions (Figure 3.18A,B). These results are consistent with the previous study showing that the fat body is the major production site of dALS, and its fat body-specific knock down leads to increased final body weight[75].

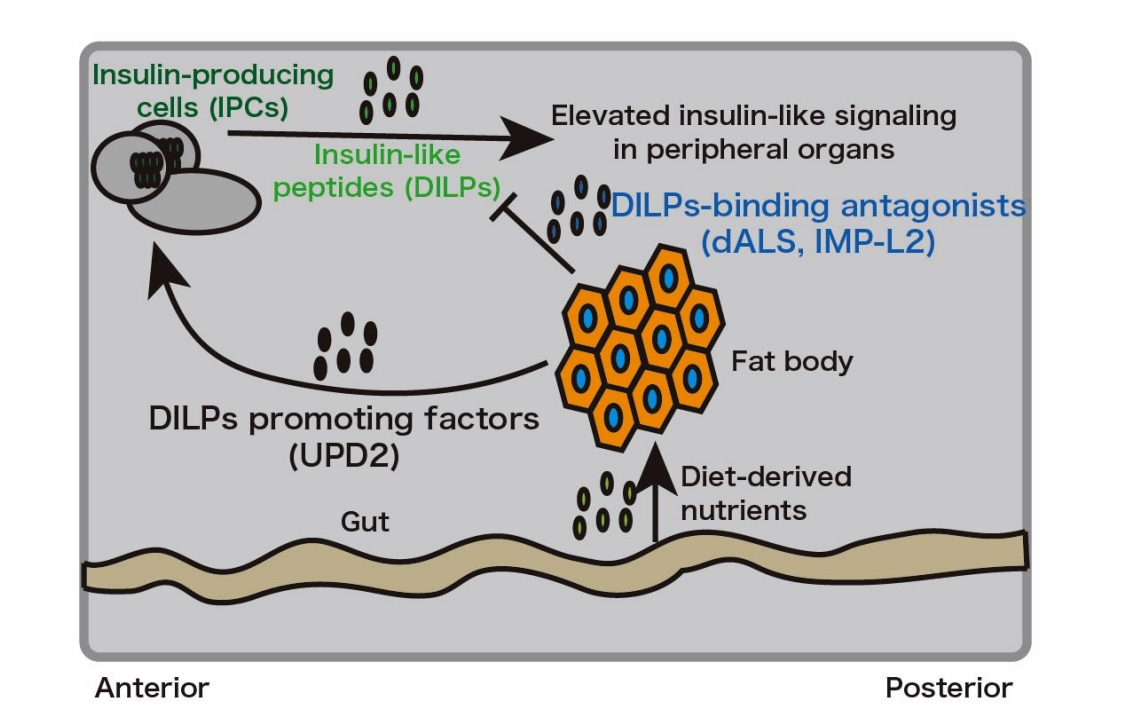

Figure 3.17. The larval fat body coordinates nutrient abundance and growth. The scheme showing a part of humoral relay mechanisms for systemic ILS regulation. The fat body produces and secretes both DILPs secretion-promoting factors (ex. UPD2) and DILPs inhibitory cofactors (dALS and IMP-L2) in response to changes in nutrient condition.

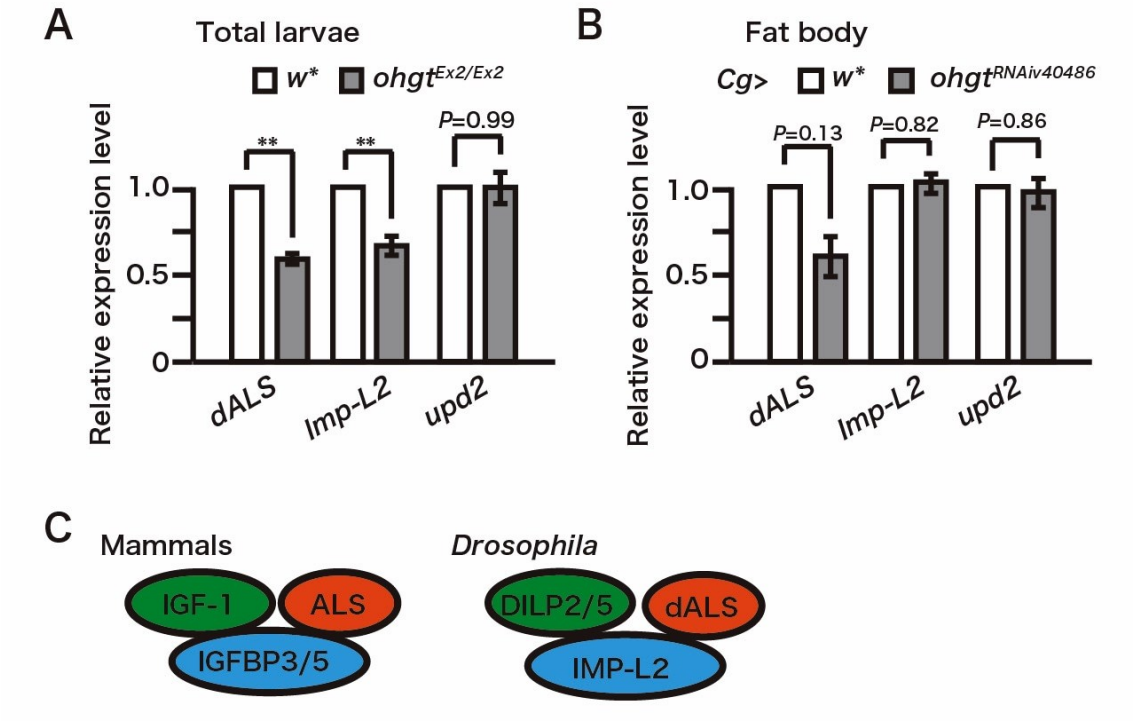

Figure 3.18. Genes encoding DILPs cofactor were downregulated under genetic inhibition of *ohgt*. (A) Transcript levels of genes encoding Acid labile subunit (*dALS*), Imaginal-morphogenesis Late 2 (*Imp-L2*), and unpaired 2 (*upd2*) in *w** and $ohgt^{Ex2}$ 72hAED larvae (n=4). (B) Transcript levels of *dALS*, *Imp-L2*, and *upd2* in *Cg>w** and $Cg>ohgt^{RNAiv40486}$ 72h AED larval carcasses (n=4). The figures are modified from the Figure 6E,F of Wakabayashi *et al.,* 2016[65].

3.3.9. OHGT interacts with Piccolo, the *Drosophila* ortholog of DDB1

Previous studies have demonstrated that vertebrate CRBN family members is a substrate receptor of the CRL4 complex to regulate stability and turnover of substrate proteins via ubiquitination[4]. Crystallographic studies have identified that the structural feature of the DDB1-binding motif is conserved among vertebrates[1,2].

The *Drosophila* homolog of DDB1 has been identified by sequence comparison[112]. The gene encoding the protein was later determined to be allelic to a previously defined locus called *piccolo* (*pic*)[113]. Previous genetic studies revealed its putative roles in development and genome stability maintenance[113–115]. The *pic* gene consists of seven exons (Figure 3.19A), which encodes a protein consisting of 1140 amino acid residues with a theoretical molecular weight of 126kDa. The protein (PIC) shows 61% sequence identity with human DDB1 throughout the sequence, and three domains (WD repeat β-propeller A, B and C) are well conserved (Figure 3.19B).

To investigate whether OHGT interacts with PIC in a manner similar to the human CRBN-DDB1 interaction, a 3D structure model for the OHGT-PIC complex was created using the crystallization data (PDB 4TZ4) as a template (Figure 3.20A,B). The OHGT-PIC complex model showed that the interaction interface may be similar to that of the human complex (Figure 3.20C,D).

Next, biochemical experiments were performed to confirm the interaction between OHGT and PIC. A commercial polyclonal antibody against human DDB1 could detect a protein of the expected size from total S2 lysate (Figure 3.21A).

Using this antibody, co-immunoprecipitation experiments in Schneider 2 (S2) tissue cell culture were performed. PIC was detected from both HA-OHGT-containing immunocomplex (Figure 3.21B) and endogenous OHGT-containing immunocomplex (Figure 3.21C), suggesting that OHGT and PIC indeed form a complex in S2 cells (Figure 3.21C).

Mammalian CRBN and other CRL4 components are known to undergo autoubiquitination under certain conditions, including absence of specific substrate proteins or the presence of MG132[4,116,117]. Therefore, ubiquitination assay was performed by purifying endogenous OHGT in the presence of MG132. Endogenous OHGT was indeed polyubiquitinated after overnight MG132 treatment (Figure 3.21D), similar to human CRBN (chapter 2 of this thesis). These results altogether suggest that OHGT may also be a substrate receptor of the CRL4 in *Drosophila*. Unfortunately, genetic interaction between *ohgt* and genes encoding other CRL4 components could not be proved because both *pic* and *dCullin4* RNAi induction in the fat body using the *Cg-Gal4* resulted in complete lethality during larval stage (data not shown). Also, attempts to purify endogenous or tagged-OHGT from larval lysates were unsuccessful (data not shown). Therefore, biochemical analysis using S2 cells could not be extended towards functional experiments with putative interaction partners *in vivo*.

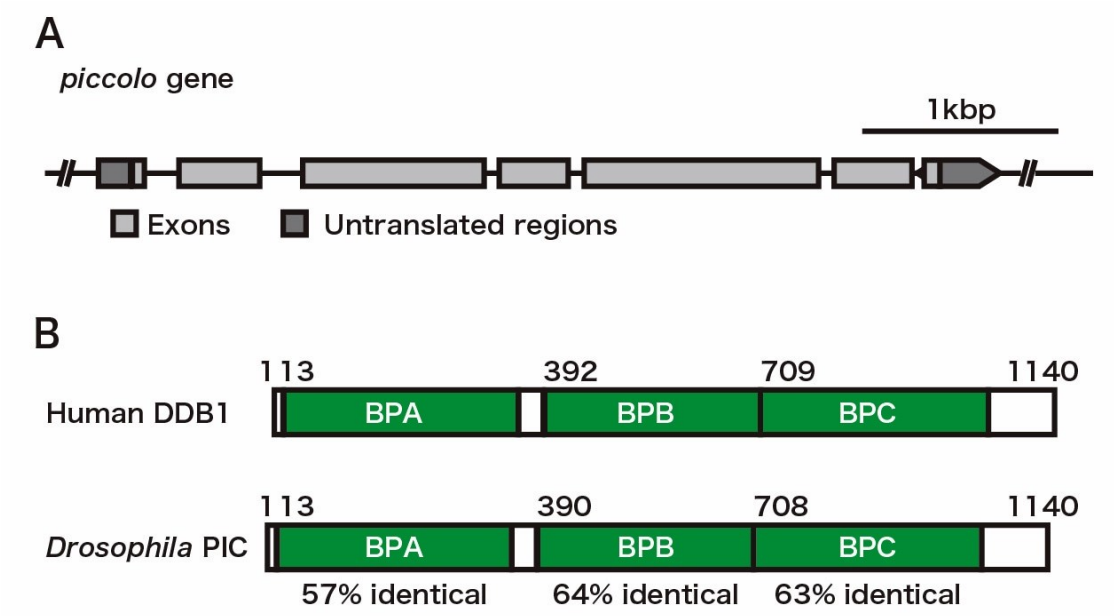

Figure 3.19. The *piccolo* gene encodes the *Drosophila* homolog of human DDB1. (A) A scheme representing *pic* gene locus. Exons and untranslated regions are indicated as filled boxes (light gray and dark gray, respectively). The scale bar represents 1kbp. (B) Schemes representing human DDB1 and *Drosophila* PIC. Evolutionary conserved WD repeat β-propeller A, B and C domains (BPA, BPB, BPC) are indicated as filled boxes (green). Amino acid identities of the corresponding regions are noted.

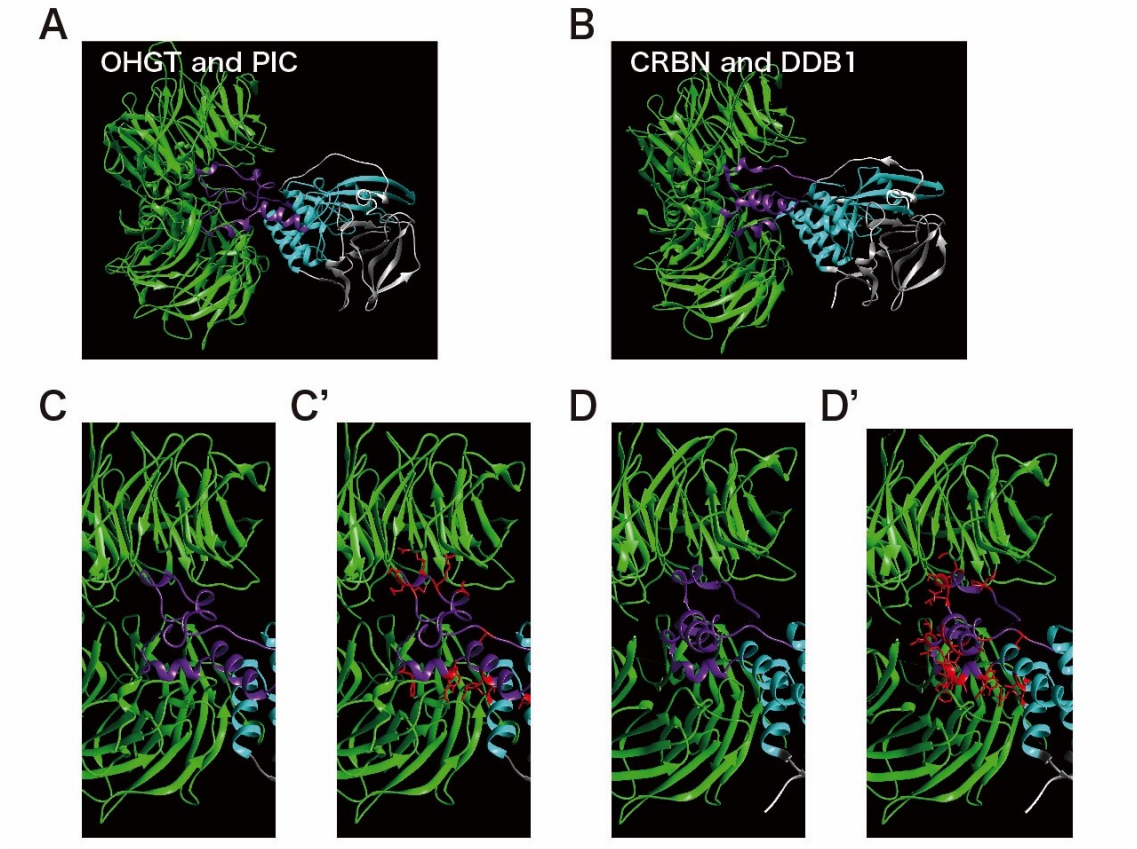

Figure 3.20. The 3D model of OHGT-PIC complex. (A) The 3D model of OHGT-PIC complex was created and aligned to respective positions in 4TZ4. (B) The structure of the human CRBN-DDB1 complex (PDB 4TZ4)[2]. (C,D) The close-up views of the OHGT-PIC/CRBN-DDB1 interaction interfaces. (C',D') Amino acid side chains of OHGT/CRBN that point towards the PIC/DDB1 interface are shown in red. The figures are modified from the Figure 7A-D of Wakabayashi *et al.,* 2016[65]. 3D modeling of OHGT-PIC complex was conducted in collaboration with A. Voelzmann.

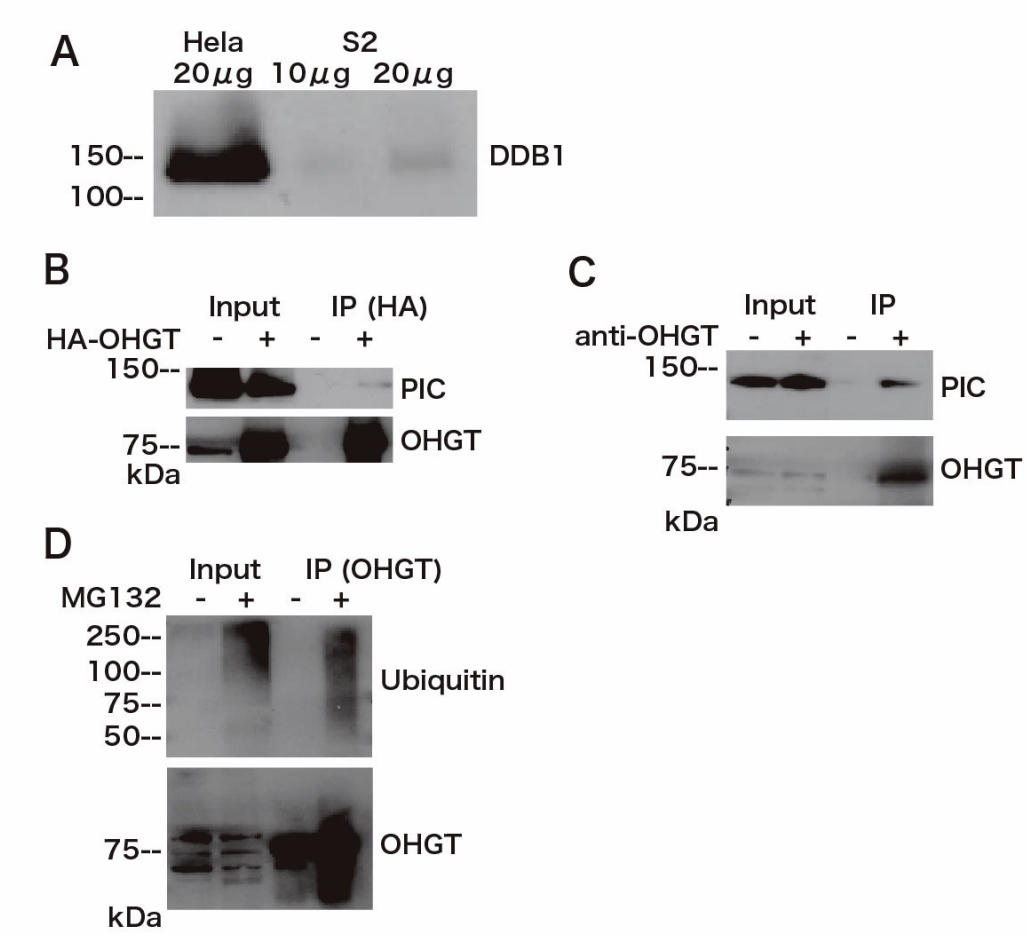

Figure 3.21. OHGT binds to PIC and may be a substrate receptor of the *Drosophila* CRL4 complex. (A) Total S2 cells lysate was subjected to western blotting with human DDB1-specific antibody. Total Hela cells lysate was used as the positive control. (B) S2 cells were co-transfected with pUASTattB-HA-OHGT and pAct-Gal4, and protein complex containing HA-OHGT was immunopurified using HA-specific antibody. Total lysates (Input) and immunoprecipitates (IP) were subjected to western blotting with antibodies to the indicated proteins (for detecting OHGT, guinea pig anti-OHGT(15-33) was used). (C) Protein complex containing endogenous OHGT was immunopurified using rabbit anti-OHGT(1-187). Total lysates (Input) and immunoprecipitates (IP) were subjected to western blotting with antibodies

to the indicated proteins (for detecting OHGT, guinea pig anti-OHGT(15-33) was used). (D) S2 cells were treated with MG132, subsequently endogenous OHGT was immunopurified using using rabbit anti-OHGT(1-187). Total lysates (Input) and immunoprecipitates (IP) were subjected to western blotting with antibodies to the indicated proteins (for detecting OHGT, guinea pig anti-OHGT(15-33) was used). The figures are reprinted from the Figure 7E-G of Wakabayashi *et al.,* 2016[65].

3.4. Discussion

Growth regulation in multicellular organisms is controlled by paracrine and endocrine mechanisms, which coordinate organ size with extrinsic cues to determine size and proportions of the body. In particular, nutrient abundance during growth period has a strong influence on organismal growth, and the genetic programs underlying growth must be able to adapt their growth and metabolic programs to altered nutrient conditions. The conserved IIS/ILS cascade is the key growth regulatory pathway. Circulating ligands including insulin, IGF or insulin-like peptides initiates the signal cascade regulating metabolism, cell proliferation and cell growth in peripheral organs. Utilization of this humoral system enables organisms to control growth in orchestrated manner.

The present work unveiled that OHGT is a novel growth regulator in *Drosophila*. OHGT in the fat body negatively regulates ILS. In the *ohgt* mutants generated by CRISPR-Cas9 mediated targeted mutagenesis, increased level of phospho-dAkt, reduced level of dFOXO target genes and reduced level of genes encoding DILPs' cofactors were associated with overgrowth phenotype. To the author's knowledge, this is the first evidence arguing that a CRBN family member regulates growth via IIS/ILS.

In vertebrates, IGFs are the major player to regulate growth. IGF-1 is synthesized in the liver and they accumulates in body fluids as a heterotrimeric complex with ALS and IGFBP3/5[118]. Formation of the complex improves stability of IGF-1, thereby promoting its half-life in circulation[118]. A similar ternary complex have been identified in *Drosophila*, as DILP2 forms a complex with dALS and IMP-L2 in haemolymph[75]. Knockdown of *dALS* in the

fat body increases final body weight[75], whereas overexpression of *Imp-L2* ameliorates hyperplasia caused by *dInR* misexpression[104].

Downregulation of *dALS* and *Imp-L2* was associated with the *ohgt* mutants. This result implicates that OHGT in the fat body may play a role in a feedback loop (Figure 3.21). In physiological condition, circulating DILPs promotes ILS in periphery including fat body cells. The ILS may alter OHGT's functions, which in turn activates transcription of some genes including *dALS* (and also *Imp-L2* to a minor extent). The fat body subsequently releases dALS into haemolymph, suppressing DILPs activity. In the absence of functional OHGT, on the other hand, fat body cells may not be able to properly activate transcription of *dALS*. Insufficient amount of dALS increases active DILPs in circulation, promoting overgrowth in periphery. Of note, upregulation of *dilp6*, a gene encoding the functional homolog of vertebrate IGF-1, was also observed (data not shown). Previous studies have reported that *dilp6* deletion mutants show a growth defect phenotype resulting in smaller body size[99,100]. Elevation of *dilp6* in the *ohgt* mutants may also contribute to enhance the overgrowth phenotype.

Intriguingly, *dALS* was reduced in both total and fat body specific fractions, whereas *Imp-L2* was only reduced in total fraction but not in fat body specific fraction. These results suggest that OHGT in other organs may be responsible for the *Imp-L2* downregulation. Larval muscle was previously shown to non-autonomously regulate ILS via producing IMP-L2[119], therefore OHGT in muscle might function in similar manner with that in the fat body.

Vertebrate CRBN is a substrate receptor of the CRL4 complex that mediates ubiquitin-dependent degradation of specific substrates[4]. Previous studies demonstrated that the

$CRL4^{CRBN}$ complex regulates transcription by two distinct mechanisms: by directly targeting and degrading transcription factors[1,8,10] and by targeting histones at a specific regulatory region[13]. Through an unbiased biochemical screen, a homeobox protein MEIS2 was identified as an endogenous substrate of the $CRL4^{CRBN}$ complex[1]. Also, in the presence of lenalidomide, the complex targets two lymphoid-specific transcription factors Ikaros and Aiolos for polyubiquitination and degradation[8,10]. A recent publication demonstrated that in mammalian T cells, CRBN directly binds to a regulatory region of *Kcna3* gene[13], in turn recruits other CRL4 components and a histone methyltransferase EZH1 to promote histone modification, resulting in altered expression of the gene[13].

All the components of the CRL4 complex are conserved in *Drosophila*[113]. Functional null mutations of *dCullin4* or *pic* leads to growth arrest during larval stage and are lethal[113]. Consistent with the conservation of the CRL4 complex, the modeling of the OHGT-PIC complex according to the human CRBN-DDB1 crystallization data revealed that the interaction interface between the *Drosophila* proteins may share structural properties with the human proteins. This modeling was further supported with co-immunoprecipitation studies in S2 tissue culture cells in the present work. Unfortunately, the presence of the $CRL4^{OHGT}$ *in vivo* could not be confirmed either genetically or biochemically in this work. Therefore, further investigations are required to address whether the $CRL4^{OHGT}$ complex is present and regulates growth *in vivo*.

If $CRL4^{OHGT}$ is indeed present, whether the complex plays a role in growth regulation via interacting with unknown proteins is an interesting question left unanswered. One potential substrate could be dFOXO, the major downstream transcription factor of ILS. Of note, several

studies have demonstrated that mammalian FOXO proteins and another Cullin family member, the Skp1-Cullin1-Skp2 complex, negatively regulates their functions to each other. The Skp1-Cullin1-Skp2 complex targets phosphorylated FOXO1 for ubiquitination and subsequent degradation under high IIS activity[120]. Another FOXO protein, FOXO3A was shown to directly binds to Skp2, negatively regulating the complex formation and its E3 ubiquitin ligase activity[121]. Thus similar functional regulatory mechanism between the $CRL4^{OHGT}$ and dFOXO could exist in *Drosophila*.

The transheterozygous $ohgt^{Ex2}$ over deficiency mutants showed slightly stronger phenotypes compared to the homozygous $ohgt^{Ex2}$ mutants in body and organ size quantification (Figure 3.9), indicating that the $ohgt^{Ex2}$ allele may not be a null allele. This mutant allele is expected to express a mutant protein consists of amino acids 1 to 84 of the endogenous OHGT protein plus extra seven amino acid residues induced by a frameshift mutation. The only potential sequence motif found in this region through *in silico* analyses was a non-covalent SUMO-interacting motif (amino acids 34-38; VDVIE) (Figure 3.1D). As roles of non-covalent SUMO-interaction in E3 ubiquitin ligase activity regulation have been identified in other species[122–124], the potential SUMO-interacting motif in the N-terminal region could have biological significance.

One unique aspect of CRBN family members is that certain class of small molecules can modulate their functions. Thalidomide and its analogs was shown to modulate interaction between CRBN and a number of substrates[1,6,8,10,11,36]. CRBN homologs across the animal and plant kingdoms exhibit 100% sequence conservation in three tryptophan residues that form a

hydrophobic pocket occupied by the small molecules, implicating that endogenous modulators of these proteins may exist[2]. Future investigations will be required to elucidate whether functions of OHGT can be regulated by such still unidentified modulators.

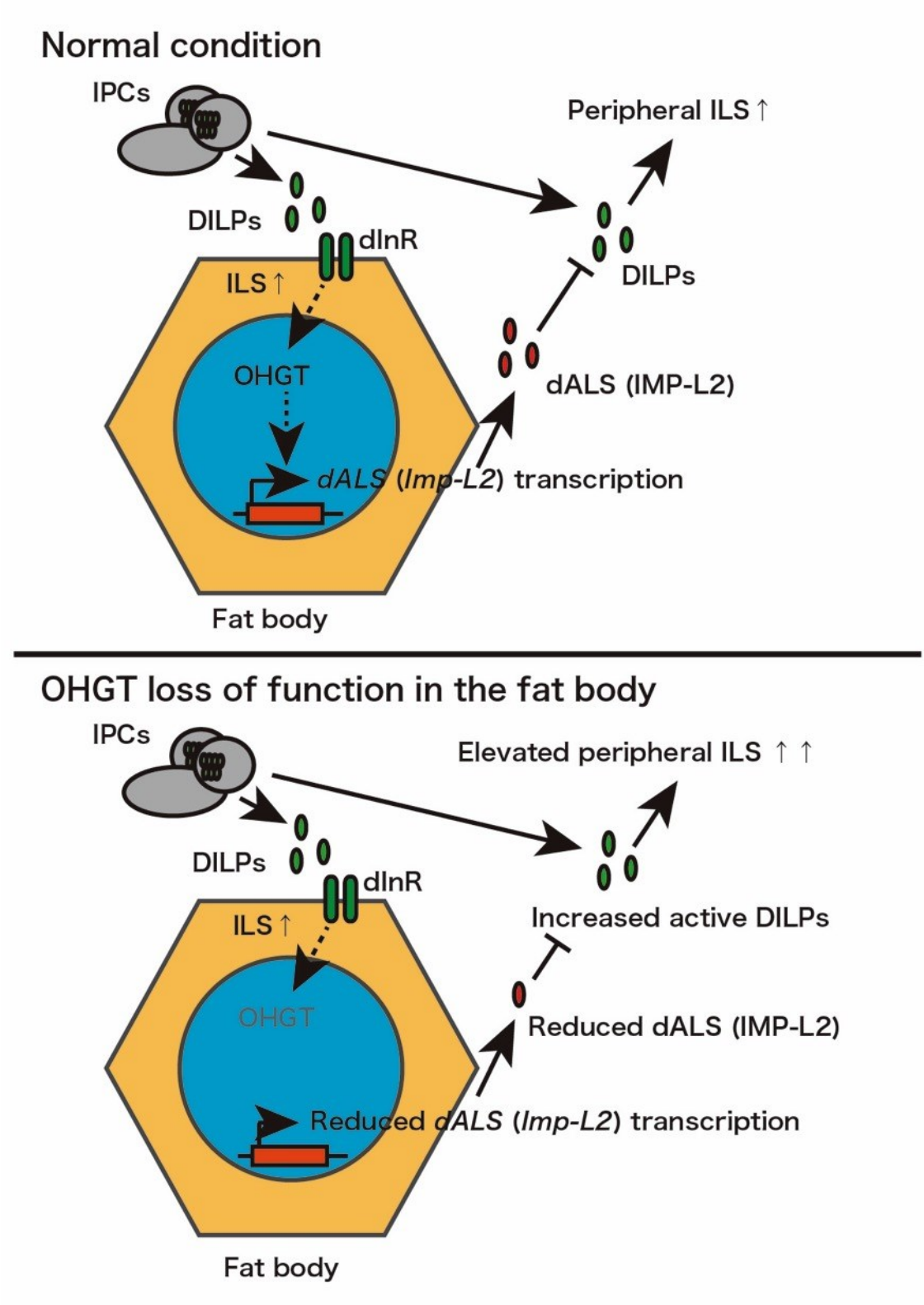

Figure 3.22. A hypothetical model of the overgrowth phenotype. (Top) In normal condition,

dInR initiates ILS that is transduced to nuclear OHGT, which in turn activates transcription of genes including *dALS* by unknown mechanism. The fat body secretes dALS into circulation, suppressing activity of DILPs. (Bottom) When functional OHGT is missing or reduced, transcription of *dALS* is not properly activated in response to ILS. Reduction of secreted dALS enhances activity of circulating DILPs, promoting ILS in peripheral tissues.

Chapter 4. Conclusion and future prospect

In this thesis, functions of human CRBN and OHGT, its *Drosophila* ortholog, was described. In the chapter 2, cytoprotective function of CRBN against misfolded proteins accumulation induced by proteasomal dysfunction was described. In the chapter 3, OHGT was demonstrated as a novel regulator of ILS-mediated growth of *Drosophila*. These studies provide insights for pleiotropic functions of CRBN family members.

The genetic clinical studies have suggested that altered expression and/or functions of CRBN are linked to onset of IDs[9,12]. Although expression of *CRBN* family members have been confirmed in the vertebrate central nervous systems[4,125], functions of their products still remain unknown. *Drosophila* is a suitable model to study functions of CRBN family member in the central nervous system, with accessibility to numerous genetic tools including a collection of Gal4 driver lines that enables expression of exogenous genes in small subsets of neurons[126–128].

In addition to growth and metabolic regulation, ILS is linked to other biological phenomenon. Of note, roles of *Drosophila* ILS have been well described in the context of life span determination and the innate immune response.

A great amount of literatures proved that altered IIS/ILS influences aging in eumetazoans[129,130]. In *Drosophila*, various genetic conditions that mimic systemic or tissue-specific reduction of ILS, including mutation of the pathway component[131], ablation of the IPCs[132] and overexpressing dFOXO[133–137], have been reported to prolong lifespan.

Combating pathogens is an energy demanding process; hence it is reasonable that

ILS is linked to immune response mechanisms. Studies identified that elevated innate immune response by bacterial infection or genetic manipulation can alter systemic ILS, leading to changes in energy storage[138,139]. Furthermore, a direct role for dFOXO in the innate immune response has been described. Becker and colleagues showed that dFOXO upregulates genes encoding antimicrobial peptides independently from the canonical innate immunity pathways[140].

Along with the physiological processes, *Drosophila* ILS has been implicated in some pathological conditions including cancer. Recently, two groups independently identified that the tumor cells in adult *Drosophila* secrete IMP-L2 to downregulate ILS in periphery, hence inducing robust wasting phenotypes that resemble cachexia condition observed in human cancer patients[76,111].

Whether OHGT is involved in these ILS-related biological phenomenon and/or pathological conditions, and whether these functions are evolutionary conserved, in particular in mammals, are the intriguing questions that require further investigations to address in the future.

Finally, *Drosophila* may be a useful model for discovery of therapeutic drugs targeting CRBN. In the last decade, *Drosophila* became increasingly popular as an *in vivo* cancer model, mainly due to high conservation of tumorigenesis-relevant signal pathways between human and *Drosophila*, and its powerful genetic tools[141,142]. Recently, it has been considered that *Drosophila* may be a suitable alternative to tissue culture cells for selecting potential antitumor compounds before conducting rodent assays[143].

In the past few years, CRBN has gained attention as the primary target of IMiDs for therapeutic effects against hematological cancers[8,10]. Several groups have succeeded to generate

novel thalidomide derivatives with functional moieties that promote $CRL4^{CRBN}$ to target specific substrates for ubiquitination and degradation[36,144,145]. Because the human CRBN-DDB1 complex and the *Drosophila* counterpart share structural similarity within the interaction interface as shown in this work, human CRBN therefore may function as a substrate receptor of the *Drosophila* CRL4 complex *in vivo*. Humanized *Drosophila* expressing human CRBN may be an excellent screening model for discovering novel thalidomide analogs with therapeutic effects.

References

1. Fischer, E. S. *et al.* Structure of the DDB1-CRBN E3 ubiquitin ligase in complex with thalidomide. *Nature* **512,** 49–53 (2014).

2. Chamberlain, P. P. *et al.* Structure of the human Cereblon-DDB1-lenalidomide complex reveals basis for responsiveness to thalidomide analogs. *Nat. Struct. Mol. Biol.* **21,** 803–809 (2014).

3. Lupas, A. N., Zhu, H. & Korycinski, M. The Thalidomide-Binding Domain of Cereblon Defines the CULT Domain Family and Is a New Member of the β-Tent Fold. *PLoS Comput. Biol.* **11,** e1004023 (2015).

4. Ito, T. *et al.* Identification of a primary target of thalidomide teratogenicity. *Science* **327,** 1345–1350 (2010).

5. Lee, K. M. *et al.* Disruption of the cereblon gene enhances hepatic AMPK activity and prevents high-fat diet-induced obesity and insulin resistance in mice. *Diabetes* **62,** 1855–1864 (2013).

6. Nguyen, T. Van *et al.* Glutamine Triggers Acetylation-Dependent Degradation of Glutamine Synthetase via the Thalidomide Receptor Cereblon. *Mol. Cell* **61,** 809–820 (2016).

7. Min, Y. *et al.* Cereblon negatively regulates TLR4 signaling through the attenuation of ubiquitination of TRAF6. *Cell Death Dis.* **7,** e2313 (2016).

8. Krönke, J. *et al.* Lenalidomide causes selective degradation of IKZF1 and IKZF3 in multiple myeloma cells. *Science* **343,** 301–305 (2014).

9. Higgins, J. J., Pucilowska, J., Lombardi, R. Q. & Rooney, J. P. A mutation in a novel ATP-dependent Lon protease gene in a kindred with mild mental retardation. *Neurology* **63,** 1927–1931 (2004).

10. Lu, G. *et al.* The Myeloma Drug Lenalidomide Promotes the Cereblon-Dependent Destruction of Ikaros Proteins. *Science (80-.).* **343,** 305–309 (2014).

11. Krönke, J. *et al.* Lenalidomide induces ubiquitination and degradation of CK1α in del(5q) MDS. *Nature* **523,** 183–188 (2015).

12. Papuc, S. M. *et al.* Microduplications of 3p26.3p26.2 containing CRBN gene in patients with intellectual disability and behavior abnormalities. *Eur. J. Med. Genet.* **58,** 319–323 (2015).

13. Kang, J. A. *et al.* Epigenetic regulation of Kcna3-encoding Kv1.3 potassium channel by cereblon contributes to regulation of CD4+ T-cell activation. *Proc. Natl. Acad. Sci. U. S. A.* **113,** 8771–8776 (2016).

14. Hershko, A. & Ciechanover, A. THE UBIQUITIN SYSTEM. *Annu. Rev. Biochem.* **67,** 425–479 (1998).

15. Thrower, J. S., Hoffman, L., Rechsteiner, M. & Pickart, C. M. Recognition of the polyubiquitin proteolytic signal. *EMBO J.* **19,** 94–102 (2000).

16. Chen, Z. J. & Sun, L. J. Nonproteolytic Functions of Ubiquitin in Cell Signaling. *Mol. Cell* **33,** 275–286 (2009).

17. Petroski, M. D. & Deshaies, R. J. Function and regulation of cullin-RING ubiquitin ligases. *Nat Rev Mol Cell Biol* **6,** 9–20 (2005).

18. Sarikas, A. *et al.* The cullin protein family. *Genome Biol.* **12,** 220 (2011).

19. Jackson, S. & Xiong, Y. CRL4s: the CUL4-RING E3 ubiquitin ligases. *Trends Biochem. Sci.* **34,** 562–570 (2009).

20. Zou, Y. *et al.* Characterization of nuclear localization signal in the N terminus of CUL4B and its essential role in cyclin E degradation and cell cycle progression. *J. Biol. Chem.* **284,** 33320–33332 (2009).

21. Liu, L. *et al.* CUL4A Abrogation Augments DNA Damage Response and Protection against Skin Carcinogenesis. *Mol. Cell* **34,** 451–460 (2009).

22. Jiang, B. *et al.* Lack of Cul4b, an E3 ubiquitin ligase component, leads to embryonic lethality and abnormal placental development. *PLoS One* **7,** e37070 (2012).

23. Angers, S. *et al.* Molecular architecture and assembly of the DDB1-CUL4A ubiquitin ligase machinery. *Nature* **443,** 590–593 (2006).

24. Lee, J. & Zhou, P. DCAFs, the Missing Link of the CUL4-DDB1 Ubiquitin Ligase. *Mol. Cell* **26,** 775–780 (2007).

25. Petzold, G., Fischer, E. S. & Thomä, N. H. Structural basis of lenalidomide-induced CK1α degradation by the CRL4CRBN ubiquitin ligase. *Nature* **532,** 127–130 (2016).

26. Liu, J. *et al.* CRL4ACRBN E3 ubiquitin ligase restricts BK channel activity and prevents epileptogenesis. *Nat Commun* **5,** 3924 (2014).

27. Jo, S., Lee, K. H., Song, S., Jung, Y. K. & Park, C. S. Identification and functional characterization of cereblon as a binding protein for large-conductance calcium-activated potassium channel in rat brain. *J. Neurochem.* **94,** 1212–1224 (2005).

28. Chen, Y.-A. A. *et al.* The Cullin 4A/B-DDB1-Cereblon E3 Ubiquitin Ligase Complex Mediates the Degradation of CLC-1 Chloride Channels. *Sci. Rep.* **5,** 10667 (2015).

29. Weiger, T. M., Hermann, A. & Levitan, I. B. Modulation of calcium-activated potassium channels. *J. Comp. Physiol. A. Neuroethol. Sens. Neural. Behav. Physiol.* **188,** 79–87 (2002).

30. Jentsch, T. J., Friedrich, T., Schriever, A. & Yamada, H. The CLC chloride channel family. *Pflugers Arch. Eur. J. Physiol.* **437,** 783–795 (1999).

31. Capdevila, J., Tsukui, T., Esteban, C. R., Zappavigna, V. & Belmonte, J. C. I. Control of Vertebrate Limb Outgrowth by the Proximal Factor Meis2 and Distal Antagonism of BMPs by Gremlin. *Mol. Cell* **4,** 839–849 (1999).

32. Louw, J. J. *et al.* MEIS2 involvement in cardiac development, cleft palate, and intellectual disability. *Am. J. Med. Genet. Part A* **167,** 1142–1146 (2015).

33. Chen, C. P. *et al.* A 5.6-Mb deletion in 15q14 in a boy with speech and language disorder, cleft palate, epilepsy, a ventricular septal defect, mental retardation and developmental delay. *Eur. J. Med. Genet.* **51,** 368–372 (2008).

34. Lopez-Girona, A. *et al.* Cereblon is a direct protein target for immunomodulatory and antiproliferative activities of lenalidomide and pomalidomide. *Leukemia* **26,** 2326–2335 (2012).

35. Zhu, Y. X. *et al.* Cereblon expression is required for the antimyeloma activity of lenalidomide and pomalidomide. *Blood* **118,** 4771–4779 (2011).

36. Matyskiela, M. E. *et al.* A novel cereblon modulator recruits GSPT1 to the CRL4 CRBN

ubiquitin ligase. *Nature* **535,** 252–257 (2016).

37. Lenz, W., Pfeiffer, R. A., Kosenow, W. & Hayman, D. J. Thalidomide and congenital abnormalities. *Lancet* **279,** 45–46 (1962).

38. Sheskin, J. Thalidomide in the treatment of lepra reactions. *Clin. Pharmacol. Ther.* **6,** 303–306 (1965).

39. D'Amato, R. J., Loughnan, M. S., Flynn, E. & Folkman, J. Thalidomide is an inhibitor of angiogenesis. *Proc. Natl. Acad. Sci. U. S. A.* **91,** 4082–4085 (1994).

40. Bartlett, J. B., Dredge, K. & Dalgleish, A. G. The evolution of thalidomide and its IMiD derivatives as anticancer agents. *Nat. Rev. Cancer* **4,** 314–322 (2004).

41. Sampaio, E. P., Sarno, E. N., Galilly, R., Cohn, Z. A. & Kaplan, G. Thalidomide selectively inhibits tumor necrosis factor alpha production by stimulated human monocytes. *J. Exp. Med.* **173,** 699–703 (1991).

42. Martiniani, R. *et al.* Biological Activity of Lenalidomide and Its Underlying Therapeutic Effects in Multiple Myeloma. *Adv. Hematol.* **2012,** 842945 (2012).

43. List, A. *et al.* Lenalidomide in the Myelodysplastic Syndrome with Chromosome 5q Deletion. *N. Engl. J. Med.* **355,** 1456–1465 (2006).

44. Hardie, D. G., Ross, F. a & Hawley, S. a. AMPK: a nutrient and energy sensor that maintains energy homeostasis. *Nat. Rev. Mol. Cell Biol.* **13,** 251–262 (2012).

45. Lee, K. M., Jo, S., Kim, H., Lee, J. & Park, C.-S. Functional modulation of AMP-activated protein kinase by cereblon. *Biochim. Biophys. Acta - Mol. Cell Res.* **1813,** 448–455 (2011).

46. Eichner, R. *et al.* Immunomodulatory drugs disrupt the cereblon-CD147-MCT1 axis to exert antitumor activity and teratogenicity. *Nat Med* **22,** 735–743 (2016).

47. Kataoka, K., Nakamura, C., Asahi, T. & Sawamura, N. Mitochondrial cereblon functions as a Lon-type protease. *Sci. Rep.* **6,** 29986 (2016).

48. Kaufman, L., Ayub, M. & Vincent, J. B. The genetic basis of non-syndromic intellectual disability: A review. *J. Neurodev. Disord.* **2,** 182–209 (2010).

49. Curry, C., Stevenson, R., Aughton, D., Byrne, J., Carey, J.C., Cassidy, S., Cunniff, C., Graham, J.M. Jr, Jones, M.C., Kaback, M.M., Moeschler, J., Schaefer, G.B., Schwartz, S., Tarleton, J., & Opitz, J. Evaluation of mental retardation: recommendations of a consensus conference. *Am. J. Med. Genet.* **72,** 468–477 (1997).

50. Kopito, R. R. Aggresomes, inclusion bodies and protein aggregation. *Trends Cell Biol.* **10,** 524–530 (2000).

51. Chin, L.-S., Olzmann, J. a & Li, L. Parkin-mediated ubiquitin signalling in aggresome formation and autophagy. *Biochem. Soc. Trans.* **38,** 144–149 (2010).

52. Kitada, T. *et al.* Mutations in the parkin gene cause autosomal recessive juvenile parkinsonism. *Nature* **392,** 605–608 (1998).

53. Lücking, C. B. *et al.* Association between Early-Onset Parkinson's Disease and Mutations in the Parkin Gene. *N. Engl. J. Med.* **342,** 1560–1567 (2000).

54. Olzmann, J. A. *et al.* Parkin-mediated K63-linked polyubiquitination targets misfolded DJ-1 to aggresomes via binding to HDAC6. *J. Cell Biol.* **178,** 1025–1038 (2007).

55. Fusco, C. *et al.* The E3-ubiquitin ligase TRIM50 interacts with HDAC6 and p62, and

promotes the sequestration and clearance of ubiquitinated proteins into the aggresome. *PLoS One* **7,** e40440 (2012).

56. Mishra, A., Godavarthi, S. K., Maheshwari, M., Goswami, A. & Jana, N. R. The ubiquitin ligase E6-AP is induced and recruited to aggresomes in response to proteasome inhibition and may be involved in the ubiquitination of Hsp70-bound misfolded proteins. *J. Biol. Chem.* **284,** 10537–10545 (2009).

57. Kawaguchi, Y. *et al.* The deacetylase HDAC6 regulates aggresome formation and cell viability in response to misfolded protein stress. *Cell* **115,** 727–738 (2003).

58. Sawamura, N., Wakabayashi, S., Matsumoto, K., Yamada, H. & Asahi, T. Cereblon is recruited to aggresome and shows cytoprotective effect against ubiquitin-proteasome system dysfunction. *Biochem. Biophys. Res. Commun.* **464,** 1054–1059 (2015).

59. Sha, Y., Pandit, L., Zeng, S. & Eissa, N. T. A Critical Role for CHIP in the Aggresome Pathway. *Mol. Cell. Biol.* **29,** 116–128 (2008).

60. Sarkar, S., Ravikumar, B., Floto, R. a & Rubinsztein, D. C. Rapamycin and mTOR-independent autophagy inducers ameliorate toxicity of polyglutamine-expanded huntingtin and related proteinopathies. *Cell Death Differ.* **16,** 46–56 (2009).

61. Ravikumar, B. *et al.* Inhibition of mTOR induces autophagy and reduces toxicity of polyglutamine expansions in fly and mouse models of Huntington disease. *Nat. Genet.* **36,** 585–595 (2004).

62. van der Vos, K. E. *et al.* Modulation of glutamine metabolism by the PI(3)K-PKB-FOXO network regulates autophagy. *Nat Cell Biol* **14,** 829–837 (2012).

63. Zhao, J. *et al.* FoxO3 Coordinately Activates Protein Degradation by the Autophagic/Lysosomal and Proteasomal Pathways in Atrophying Muscle Cells. *Cell Metab.* **6,** 472–483 (2007).

64. Mammucari, C. *et al.* FoxO3 Controls Autophagy in Skeletal Muscle In Vivo. *Cell Metab.* **6,** 458–471 (2007).

65. Wakabayashi, S. *et al.* Ohgata, the Single Drosophila Ortholog of Human Cereblon, Regulates Insulin Signaling-Dependent Organismic Growth. *J. Biol. Chem.* **291,** 25120–25132 (2016).

66. Bader, R. *et al.* The IGFBP7 homolog Imp-L2 promotes insulin signaling in distinct neurons of the Drosophila brain. *J. Cell Sci.* **126,** 2571–2576 (2013).

67. Grönke, S. *et al.* Control of Fat Storage by a Drosophila PAT Domain Protein. *Curr. Biol.* **13,** 603–606 (2003).

68. Pignoni, F. & Zipursky, S. L. Induction of Drosophila eye development by decapentaplegic. *Development* **124,** 271–278 (1997).

69. Bassett, A. R., Tibbit, C., Ponting, C. P. & Liu, J. L. Highly Efficient Targeted Mutagenesis of Drosophila with the CRISPR/Cas9 System. *Cell Rep.* **4,** 220–228 (2013).

70. Gratz, S. J. *et al.* Genome engineering of Drosophila with the CRISPR RNA-guided Cas9 nuclease. *Genetics* **194,** 1029–1035 (2013).

71. Gratz, S. J. *et al.* Highly specific and efficient CRISPR/Cas9-catalyzed homology-directed repair in Drosophila. *Genetics* **196,** 961–971 (2014).

72. Dahlem, T. J. *et al.* Simple Methods for Generating and Detecting Locus-Specific

Mutations Induced with TALENs in the Zebrafish Genome. *PLoS Genet.* **8,** e1002861 (2012).

73. Rodenfels, J. *et al.* Production of systemically circulating Hedgehog by the intestine couples nutrition to growth and development. *Genes Dev.* **28,** 2636–2651 (2014).

74. Fuss, B., Becker, T., Zinke, I. & Hoch, M. The cytohesin Steppke is essential for insulin signalling in Drosophila. *Nature* **444,** 945–948 (2006).

75. Arquier, N. *et al.* Drosophila ALS Regulates Growth and Metabolism through Functional Interaction with Insulin-Like Peptides. *Cell Metab.* **7,** 333–338 (2008).

76. Kwon, Y. *et al.* Systemic organ wasting induced by localized expression of the secreted Insulin/IGF antagonist ImpL2. *Dev. Cell* **33,** 36–47 (2015).

77. Rajan, A. & Perrimon, N. Drosophila cytokine unpaired 2 regulates physiological homeostasis by remotely controlling insulin secretion. *Cell* **151,** 123–137 (2012).

78. Biasini, M. *et al.* SWISS-MODEL: Modelling protein tertiary and quaternary structure using evolutionary information. *Nucleic Acids Res.* **42,** 252–258 (2014).

79. Pettersen, E. F. *et al.* UCSF Chimera - A visualization system for exploratory research and analysis. *J. Comput. Chem.* **25,** 1605–1612 (2004).

80. Ronquist, F. & Huelsenbeck, J. P. MrBayes 3: Bayesian phylogenetic inference under mixed models. *Bioinformatics* **19,** 1572–1574 (2003).

81. Huelsenbeck, J. P. & Ronquist, F. MrBayes: Bayesian inference of phylogenetic trees. *Bioinformatics* **17,** 754–755 (2001).

82. Altekar, G., Dwarkadas, S., Huelsenbeck, J. P. & Ronquist, F. Parallel Metropolis coupled

Markov chain Monte Carlo for Bayesian phylogenetic inference. *Bioinformatics* **20,** 407–415 (2004).

83. Sigrist, C. J. A. *et al.* New and continuing developments at PROSITE. *Nucleic Acids Res.* **41,** D344-347 (2013).

84. de Castro, E. *et al.* ScanProsite: Detection of PROSITE signature matches and ProRule-associated functional and structural residues in proteins. *Nucleic Acids Res.* **34,** 362–365 (2006).

85. Qiu, W.-R., Xiao, X., Lin, W.-Z. & Chou, K.-C. iUbiq-Lys: prediction of lysine ubiquitination sites in proteins by extracting sequence evolution information via a gray system model. *J. Biomol. Struct. Dyn.* **33,** 1731–1742 (2015).

86. Wang, P., Xiao, X. & Chou, K. C. NR-2l: A two-level predictor for identifying nuclear receptor subfamilies based on sequence-derived features. *PLoS One* **6,** e23505 (2011).

87. Zhao, Q. *et al.* GPS-SUMO: A tool for the prediction of sumoylation sites and SUMO-interaction motifs. *Nucleic Acids Res.* **42,** 325–330 (2014).

88. Ren, J. *et al.* Systematic study of protein sumoylation: Development of a site-specific predictor of SUMOsp 2.0. *Proteomics* **9,** 3409–3412 (2009).

89. Brameier, M., Krings, A. & MacCallum, R. M. NucPred - Predicting nuclear localization of proteins. *Bioinformatics* **23,** 1159–1160 (2007).

90. Hsu, P. D., Lander, E. S. & Zhang, F. Development and applications of CRISPR-Cas9 for genome engineering. *Cell* **157,** 1262–1278 (2014).

91. Cong, L. *et al.* Multiplex Genome Engineering Using CRISPR/Cas Systems. *Science*

(80-.). **339,** 819–823 (2013).

92. Hafen, E. Cancer, type 2 diabetes, and ageing: News from flies and worms. *Swiss Med. Wkly.* **134,** 711–719 (2004).

93. Garofalo, R. S. Genetic analysis of insulin signaling in Drosophila. *Trends Endocrinol. Metab.* **13,** 156–162 (2002).

94. Edgar, B. A. How flies get their size: genetics meets physiology. *Nat. Rev. Genet.* **7,** 907–916 (2006).

95. Brogiolo, W. *et al.* An evolutionarily conserved function of the drosophila insulin receptor and insulin-like peptides in growth control. *Curr. Biol.* **11,** 213–221 (2001).

96. Ikeya, T., Galic, M., Belawat, P., Nairz, K. & Hafen, E. Nutrient-dependent expression of insulin-like peptides from neuroendocrine cells in the CNS contributes to growth regulation in Drosophila. *Curr. Biol.* **12,** 1293–1300 (2002).

97. Puig, O., Marr, M. T. M., Ruhf, M. L. & Tjian, R. Control of cell number by Drosophila FOXO : downstream and feedback regulation of the insulin receptor pathway. *Genes Dev.* **17,** 2006–2020 (2003).

98. Rulifson, E. J., Kim, S. K. & Nusse, R. Ablation of Insulin-Producing Neurons in Flies: Growth and Diabetic Phenotypes. *Science (80-.).* **296,** 1118–1120 (2002).

99. Okamoto, N. *et al.* A Fat Body-Derived IGF-like Peptide Regulates Postfeeding Growth in Drosophila. *Dev. Cell* **17,** 885–891 (2009).

100. Slaidina, M., Delanoue, R., Gronke, S., Partridge, L. & Léopold, P. A Drosophila Insulin-like Peptide Promotes Growth during Nonfeeding States. *Dev. Cell* **17,** 874–884

(2009).

101. Géminard, C., Rulifson, E. J. & Léopold, P. Remote Control of Insulin Secretion by Fat Cells in Drosophila. *Cell Metab.* **10,** 199–207 (2009).

102. Colombani, J. *et al.* A nutrient sensor mechanism controls Drosophila growth. *Cell* **114,** 739–749 (2003).

103. Sano, H. *et al.* The Nutrient-Responsive Hormone CCHamide-2 Controls Growth by Regulating Insulin-like Peptides in the Brain of Drosophila melanogaster. *PLoS Genet.* **11,** e1005481 (2015).

104. Honegger, B. *et al.* Imp-L2, a putative homolog of vertebrate IGF-binding protein 7, counteracts insulin signaling in Drosophila and is essential for starvation resistance. *J. Biol.* **7,** 10 (2008).

105. Koyama, T. & Mirth, C. K. Growth-Blocking Peptides As Nutrition-Sensitive Signals for Insulin Secretion and Body Size Regulation. *PLOS Biol.* **14,** e1002392 (2016).

106. Agrawal, N. *et al.* The Drosophila TNF Eiger Is an Adipokine that Acts on Insulin-Producing Cells to Mediate Nutrient Response. *Cell Metab.* **23,** 675–684 (2016).

107. Delanoue, R. *et al.* Drosophila insulin release is triggered by adipose Stunted ligand to brain Methuselah receptor. *Science (80-.).* **353,** 1553–1556 (2016).

108. Scanga, S. E. *et al.* The conserved PI3'K / PTEN / Akt signaling pathway regulates both cell size and survival in Drosophila. *Oncogene* **19,** 3971–3977 (2000).

109. Brunet, A. *et al.* Akt promotes cell survival by phosphorylating and inhibiting a Forkhead transcription factor. *Cell* **96,** 857–868 (1999).

110. Garbe, J. C., Yang, E. & Fristrom, J. W. IMP-L2: an essential secreted immunoglobulin family member implicated in neural and ectodermal development in Drosophila. *Development* **119,** 1237–1250 (1993).

111. Figueroa-Clarevega, A. & Bilder, D. Malignant drosophila tumors interrupt insulin signaling to induce cachexia-like wasting. *Dev. Cell* **33,** 47–56 (2015).

112. Takata, K., Ishikawa, G., Hirose, F. & Sakaguchi, K. Drosophila damage-specific DNA-binding protein 1 (D-DDB1) is controlled by the DRE/DREF system. *Nucleic Acids Res.* **30,** 3795–3808 (2002).

113. Hu, J. *et al.* WD40 protein FBW5 promotes ubiquitination of tumor suppressor TSC2 by DDB1 − CUL4 − ROC1 ligase service WD40 protein FBW5 promotes ubiquitination of tumor suppressor TSC2 by DDB1 – CUL4 – ROC1 ligase. *Genes Dev.* **22,** 866–871 (2008).

114. Takata, K., Yoshida, H., Yamaguchi, M. & Sakaguchi, K. Drosophila Damaged DNA-Binding Protein 1 Is an Essential Factor for Development. *Genetics* **168,** 855–865 (2004).

115. Shimanouchi, K. *et al.* Drosophila Damaged DNA Binding Protein 1 Contributes to Genome Stability in Somatic Cells. *J. Biochem.* **139,** 51–58 (2006).

116. Groisman, R. *et al.* The ubiquitin ligase activity in the DDB2 and CSA complexes is differentially regulated by the COP9 signalosome in response to DNA damage. *Cell* **113,** 357–367 (2003).

117. Sugasawa, K. *et al.* UV-induced ubiquitylation of XPC protein mediated by

UV-DDB-ubiquitin ligase complex. *Cell* **121,** 387–400 (2005).

118. Boisclair, Y. R., Rhoads, R. P., Ueki, I., Wang, J. & Ooi, G. T. The acid-labile subunit (ALS) of the 150 kDa IGF-binding protein complex: An important but forgotten component of the circulating IGF system. *J. Endocrinol.* **170,** 63–70 (2001).

119. Ghosh, A., Rideout, E. J. & Grewal, S. S. TIF-IA-Dependent Regulation of Ribosome Synthesis in Drosophila Muscle Is Required to Maintain Systemic Insulin Signaling and Larval Growth. *PLoS Genet.* **10,** e1004750 (2014).

120. Huang, H. *et al.* Skp2 inhibits FOXO1 in tumor suppression through ubiquitin-mediated degradation. *Proc. Natl. Acad. Sci. U. S. A.* **102,** 1649–1654 (2005).

121. Wu, J. *et al.* Foxo3a transcription factor is a negative regulator of Skp2 and Skp2 SCF complex. *Oncogene* **32,** 78–85 (2013).

122. Parker, J. L. & Ulrich, H. D. A SUMO-interacting motif activates budding yeast ubiquitin ligase Rad18 towards SUMO-modified PCNA. *Nucleic Acids Res.* **40,** 11380–11388 (2012).

123. Keusekotten, K. *et al.* Multivalent interactions of the SUMO-interaction motifs in RING finger protein 4 determine the specificity for chains of the SUMO. *Biochem. J.* **457,** 207–14 (2014).

124. Merrill, J. C. *et al.* A role for non-covalent SUMO interaction motifs in Pc2/CBX4 E3 activity. *PLoS One* **5,** (2010).

125. Aizawa, M., Abe, Y., Ito, T., Handa, H. & Nawa, H. MRNA distribution of the thalidomide binding protein cereblon in adult mouse brain. *Neurosci. Res.* **69,** 343–347

(2011).

126. Bellen, H. J., Tong, C. & Tsuda, H. 100 years of Drosophila research and its impact on vertebrate neuroscience: a history lesson for the future. *Nat. Rev. Neurosci.* **11,** 514–522 (2010).

127. Jenett, A. *et al.* A GAL4-Driver Line Resource for Drosophila Neurobiology. *Cell Rep.* **2,** 991–1001 (2012).

128. Pfeiffer, B. D. *et al.* Tools for neuroanatomy and neurogenetics in Drosophila. *Proc. Natl. Acad. Sci. U. S. A.* **105,** 9715–9720 (2008).

129. Kenyon, C. J. The genetics of ageing. *Nature* **464,** 504–512 (2010).

130. Tatar, M., Post, S. & Yu, K. Nutrient control of Drosophila longevity. *Trends Endocrinol. Metab.* **25,** 509–517 (2014).

131. Clancy, D. J. Extension of Life-Span by Loss of CHICO, a Drosophila Insulin Receptor Substrate Protein. *Science (80-.).* **292,** 104–106 (2001).

132. Broughton, S. J. *et al.* Longer lifespan, altered metabolism, and stress resistance in Drosophila from ablation of cells making insulin-like ligands. *Proc. Natl. Acad. Sci. U. S. A.* **102,** 3105–3110 (2005).

133. Giannakou, M. E. *et al.* Long-Lived Drosophila with Overexpressed dFOXO in Adult Fat Body. *Science (80-.).* **305,** 361–361 (2004).

134. Hwangbo, D. S., Gershman, B., Tu, M.-P., Palmer, M. & Tatar, M. Drosophila dFOXO controls lifespan and regulates insulin signalling in brain and fat body. *Nature* **429,** 562–566 (2004).

135. Bai, H., Kang, P. & Tatar, M. Drosophila insulin-like peptide-6 (dilp6) expression from fat body extends lifespan and represses secretion of Drosophila insulin-like peptide-2 from the brain. *Aging Cell* **11,** 978–985 (2012).

136. Demontis, F. & Perrimon, N. FOXO/4E-BP signaling in Drosophila muscles regulates organism-wide proteostasis during aging. *Cell* **143,** 813–825 (2010).

137. Alic, N. *et al.* Cell-Nonautonomous Effects of dFOXO/DAF-16 in Aging. *Cell Rep.* **6,** 608–616 (2014).

138. Dionne, M. S., Pham, L. N., Shirasu-Hiza, M. & Schneider, D. S. Akt and foxo Dysregulation Contribute to Infection-Induced Wasting in Drosophila. *Curr. Biol.* **16,** 1977–1985 (2006).

139. DiAngelo, J. R., Bland, M. L., Bambina, S., Cherry, S. & Birnbaum, M. J. The immune response attenuates growth and nutrient storage in Drosophila by reducing insulin signaling. *Proc. Natl. Acad. Sci.* **106,** 20853–20858 (2009).

140. Becker, T. *et al.* FOXO-dependent regulation of innate immune homeostasis. *Nature* **463,** 369–373 (2010).

141. Brumby, A. M. & Richardson, H. E. Using Drosophila melanogaster to map human cancer pathways. *Nat. Rev. Cancer* **5,** 626–639 (2005).

142. Rudrapatna, V. A., Cagan, R. L. & Das, T. K. Drosophila Cancer Models. *Dev. Dyn.* **241,** 107–118 (2012).

143. Gladstone, M. & Su, T. T. Chemical genetics and drug screening in Drosophila cancer models. *J. Genet. Genomics* **38,** 497–504 (2011).

144. Lu, J. *et al.* Hijacking the E3 Ubiquitin Ligase Cereblon to Efficiently Target BRD4. *Chem. Biol.* **22,** 755–763 (2015).

145. Winter, G. E. *et al.* Phthalimide conjugation as a strategy for in vivo target protein degradation. *Science* **348,** 1376–81 (2015).

Acknowledgement

First of all, I would like to express my immeasurable appreciation and deepest gratitude to my three supervisors, **Professor Toru Asahi, Professor Michael Hoch and Associate Professor Naoya Sawamura,** for generously offering me an opportunity to conduct the exciting doctoral project, as well as guiding me through the doctoral program. It was an irreplaceable experience for me to play major roles in an international collaboration, from starting the project from scratch to publishing an article in the end. I would also appreciate referees for my doctoral dissertation, **Professor Toshio Ohshima, and Mr. Masashi Mita** in Shiseido Company, Ltd., for their critical feedbacks and warm encouragement during doctoral exams.

I am grateful to **all members and staffs of Hoch lab and Asahi/Sawamura lab.** I would like to mention a special thanks to **Dr. Pilar Carrera Santaliestra, Dr. Dominic Gosejacob, Dr. Mirco Brondolin, Ms. Melanie Thielisch and Ms. Sabine Büttner** in Hoch lab and **Dr. Takeyoshi Wada and Ms. Haruka Yamamoto-Yamada,** former members of Asahi/Sawamura lab, for their technical advice and helpful discussions.

I would like to thank my co-authors, **Dr. Meike Brömer** in the German Center for Neurodegenerative Diseases (DZNE) and **Dr. André Völzmann** in University of Manchester, for always being kind to share their experience and expertise for my project.

I would like to express my deep gratitude to **Dr. Hiroshi Ohki,** who has been mentoring me since 2013. His warm and encouraging words were essential for me to overcome the toughest moment during my doctoral program.

I would also like to appreciate **Dr. Chihiro Nozaki** in the Institute of Molecular Psychiatry, University of Bonn, for being very thoughtful, caring and inspiring during my stay in Bonn. She was very kind to share her knowledge and experience that always motivated me.

I would like thank following people for generously supporting my stay in Bonn: **Dr. Hideomi Tanaka**, a former member of Hoch lab; **Mr. Hidetoshi Takahashi,** husband of Dr. Nozaki; **Ms. Anne-Marie Springmann and Ms. Tomoko Shimizu**, former administrative officers in Waseda University European Center in Bonn.

Last, but not least, I would like to express my deep appreciation to **my parents Takashi and Naoko, my family members and Ms. Yukari Asou**, for always offering me unconditional supports.

S.W. was financially supported by the Leading Graduate Program of Science and Engineering, Waseda University from MEXT, Japan and the European Union Institute in Japan at Waseda University (EUIJ Waseda) during the doctoral program.

早稲田大学　博士（理学）　学位申請　研究業績書

氏 名　若林　慧　　印

（2017 年 2 月 1 現在）

種 類 別	題名、表・発行掲載誌名、発表・発行年月、連名者（申請者含む）
論文○	Wakabayashi S., Sawamura N., Voelzmann A., Broemer M., Asahi T., Hoch M. "Ohgata, the Single *Drosophila* Ortholog of Human Cereblon, Regulates Insulin Signaling-Dependent Organismic Growth", *The Journal of Biological Chemistry* **291**(48), 25120-25132 (2016).
論文○	Sawamura N., Wakabayashi S., Matsumoto K., Yamada H., Asahi T. "Cereblon is recruited to aggresome and shows cytoprotective effect against ubiquitin-proteasome system dysfunction", *Biochemical and Biophysical Research Communications* **464**, 1054-1059 (2015).
講演 （以下同）	Wakabayashi S., Sawamura N., Voelzmann A., Broemer M., Asahi T., Hoch M. "Ohgata, the Single *Drosophila* Member of Cereblon Protein Family, is a Novel Regulator of Insulin Signaling-Dependent Organismal Growth", The 39th Annual Meeting of the Molecular Biology Society of Japan, LJ0281, Yokohama, November 2016. 若林慧、澤村直哉、朝日透、ミヒャエル・ホッホ、“セレブロンタンパク質ショウジョウバエ相同体の機能解析”、早稲田大学ナノテクノロジーフォーラム第 1 回分科会ワークショップ「健康・医療分野」、東京、2016 年 3 月。 若林慧、澤村直哉、朝日透、ミヒャエル・ホッホ、“セレブロンタンパク質ショウジョウバエ相同体の機能解析”、早稲田大学博士課程教育リーディングプログラム 1st 合同シンポジウム、東京、2016 年 3 月。

早稲田大学　博士（理学）　学位申請　研究業績書

種 類 別	題名、表・発行掲載誌名、発表・発行年月、連名者（申請者含む）
講演 （以下同）	Wakabayashi S., Sawamura N., Asahi T., Hoch M. "Functional analysis of the *Drosophila* homologue of CRBN", German-Japanese Joint Symposium between the University of Bonn and Waseda University, Bonn, Germany, September 2015. Wakabayashi S. "Functional analysis of the *Drosophila* homologue of human *Cereblon* gene", The 7th HOPE meeting, Tokyo, March 2015. Wakabayashi S., Sawamura N., Asahi T., Hoch M. "Functional analysis of *dCRBN*, the *Drosophila* homologue of human *Cereblon* gene", German-Japanese Joint Symposium between the University of Bonn and Waseda University, Tokyo, February 2015. Wakabayashi S., Sawamura N., Asahi T., Hoch M. "Functional analysis of the *Drosophila* homologue of human *Cereblon* gene", The 1st International Conference on Three Dimensional Development of Lab-Exchange Type Biomedical Science Research Consortium, Chiba, September 2014. Wakabayashi S. "Generating *dCRBN* knockout *Drosophila* lines using CRISPR-Cas9 system", German-Japanese Joint Symposium Metabolic Sensing: Biology and Nano-medicine, Bonn, Germany, August 2014. Wakabayashi, S., Asahi T., Sawamura N. "The E3 ubiquitin ligase component cereblon is recruited to aggresome by proteasome stress", Neuroscience 2013, San Diego CA, USA, November 2013.

早稲田大学　博士（理学）　学位申請　研究業績書

種 類 別	題名、表・発行掲載誌名、発表・発行年月、連名者（申請者含む）
講演 （以下同）	Wakabayashi S. "Functional analysis of *Drosophila* homologue of Cereblon protein", German-Japanese Joint Symposium Metabolic Sensing: Biology and Nano-medicine, Bonn, Germany, September 2013. Wakabayashi S., Yamada H., Asahi T., Sawamura N. "Functional analysis of a mental retardation related gene *Cereblon*", The 1st Mini-symposium between Monash University and Waseda University, Melbourne, Australia, January 2013. 若林慧、山田春佳、朝日透、澤村直哉、″Cereblon localizes at aggresomes through its E3 ubiquitin ligase activity″、第 85 回日本生化学会大会、福岡、2012 年 12 月。 Wakabayashi S., Yamada H., Asahi T., Sawamura N. "Cereblon accumulates in aggresomes due to proteasome impairment", The 11th Biennial Meeting of the Asian Pacific Society for Neurochemistry and The 55th Annual Meeting of the Japanese Society for Neurochemistry, Hyogo, October 2012. 若林慧、山田春佳、朝日透、澤村直哉、"Cereblon is a component of aggresome″、第 45 回日本発生生物学会・第 64 回日本細胞生物学会 合同大会、兵庫、2012 年 5 月。 Wakabayashi S., Yamada H., Asahi T., Sawamura N. "Cereblon is a component of aggresome", The 2nd Workshop for Diamond Researchers between the University of Bonn and Waseda University, Tokyo, February 2012.